FINAL REPORT

Ion Rings for Magnetic Fusion

DOE Grant #DE-FG02-93ER54221

Principal Investigator, Dr. John B. Greenly
Laboratory of Plasma Studies
369 Upson Hall
Cornell University
Ithaca, NY 14853

July 2005

Ion Rings for Magnetic Fusion

USDOE grant # DE-FG02-93ER54221

Final Technical Report

June 2005

I. Introduction

This Final Technical Report presents the results of the program, Ion Rings for Magnetic Fusion, which was carried out under Department of Energy funding during the period August, 1993 to January, 2005. The central objective of the program was to study the properties of field-reversed configurations formed by ion rings. In order to reach this objective, our experimental program, called the Field-reversed Ion Ring Experiment, FIREX, undertook to develop an efficient, economical technology for the production of field-reversed ion rings.

A field-reversed configuration (FRC) in which the azimuthal (field-reversing) current is carried by ions with gyro-radius comparable to the magnetic separatrix radius is called a field-reversed ion ring. A background plasma is required for charge neutralization of the ring, and this plasma will be confined within the ring's closed magnetic flux. Ion rings have long been of interest as the basis of compact magnetic fusion reactors [1,2,3], as the basis for a high-power accelerator for an inertial fusion driver [4], and for other applications of high power ion beams or plasmas of high energy density. Specifically, the FIREX program was intended to address the longstanding question of the contribution of large-orbit ions to the observed stability of experimental FRCs to the MHD tilt mode. Typical experimental FRCs with $s \sim 2$-4, where s is the ratio of separatrix radius to ion gyro-radius, have been stable to tilting, but desired values for a fusion reactor, $s > 20$, should be unstable [5,6,7,8,9]. The FIREX ring would consist of a plasma with large s for the background ions, but with $s \sim 1$ for the ring ions. By varying the proportions of these two populations, the minimum proportion of large-orbit ions necessary for stability could be determined. The incorporation of large-orbit ions, perhaps by neutral-beam injection, into an FRC has been advanced for the purpose of stabilizing, heating, controlling angular momentum, and aiding the formation of a reactor-scale FRC, and the FIREX program was intended to test the ideas behind this approach.

We will describe in this report the technological development path and advances in physics understanding that allowed FIREX to reach a regime in which ion rings were reproducibly created with up to about half the current necessary to produce field reversal. Unfortunately, the experiments were limited to this level by a fundamental, unanticipated aspect of the physics of strong ion rings in plasma. The FIREX ring is a strongly anisotropic, current-carrying population of ions moving faster than the Alfven speed in the background plasma. The rapidly changing ring current excites very large-amplitude Alfven waves in the plasma, and these waves strongly affect the ring, causing rapid energy loss in a way that is not compatible with the success of the ring trapping scenario around which FIREX was designed. The result was that FIREX rings were always very short-lived. We will discuss the implication of these results for possible future use of large-orbit ions in FRCs. In short, it appears that a certain range of the parameters characterizing the ring Alfven mach number and distribution function must be avoided to allow the existence of a long-lived energetic ion component in an FRC. This report will explain why FIREX experimental results cannot be directly scaled to quantitatively predict this range for a particular FRC configuration. This will require accurate, three-dimensional simulations. FIREX results do constitute a very good dataset for validating such a code, and simulations already carried out during this program provide a guide to the important physics involved.

II. Summary of results

We give in this section an overview of the primary results of the FIREX program. These results will be presented in detail in section III. Appendix A presents detailed results of radial injection experiments. Appendix B presents a brief review of ion ring stability theory, and detailed results of our simulations of the ion ring-Alfven instability.

The basic design of the FIREX experiment was a direct scaling up of the axial cusp-injection method used in the previous Cornell program of the 1980's called IREX[1]. The

new experiment succeeded in producing ion rings with an order of magnitude stronger diamagnetic field. The result has been that FIREX has entered a completely different regime of ring-plasma interaction, in which collective effects mediated by Alfven waves dominate the ring and plasma response.

The FIREX ring formation scheme injects a proton beam, in an annulus between 10 and 15 cm radius, axially across a magnetic cusp into a solenoidal magnetic field. The beam is deflected in crossing the cusp, forming a rotating ring of about the same 10-15 cm radial dimension, in the 0.6 T magnetic field. The beam density in FIREX is high enough so that very nearly complete charge neutralization must be enforced at every point along the ring trajectory to avoid severe disruption of the ring by electrostatic fields. The first result of FIREX is that a suitably chosen background plasma distribution in the cusp and solenoid, formed from neutral gas either by the ring itself or by a separate preionizing discharge, is adequate to reduce electrostatic perturbation of the ring to an acceptably low level. FIREX ring experiments were not at all limited by ring space-charge effects, and rings could be formed successfully in background plasma in the density range of 10^{20} /m^3 to 10^{21} /m^3. This is the desired density range for FRC plasmas of interest for fusion energy application. As we will discuss, it is also found that rings are able to cross the separatrix and enter the closed flux of an FRC-like reversed field region without disruption by space-charge fields.

FIREX is able to reproducibly form ion rings with diamagnetic field up to almost half of the 0.6 T confining solenoid magnetic field. Since the vacuum chamber wall is flux-conserving, the ring diamagnetism appears as a peak field reduction of up to 0.2 T on axis, accompanied by an increase of 0.1 T at the wall. These are by far the strongest ion rings ever produced. This strong field is more than enough to produce ring dynamics dominated by very strongly collective, nonlinear interactions between the ring and the background plasma. With the optimized axial cusp-injection configuration in FIREX, the ~0.1 MA, 0.5 MeV proton beam is converted into a rotating ring that initially has about 80% of its energy in rotation. The remaining axial velocity carries the ring into the confining magnetic solenoid.

The FIREX experiment was designed based on the previous experience in ion ring experiments [10], and on advances in the state of the art of intense ion beam generation, mainly driven by inertial fusion research in the early '90's. In addition, a fundamental aspect of the FIREX design was based upon results of two-dimensional simulations of ring injection into plasma [11]. These simulations were made with the code FIRE that was built at the beginning of the FIREX program. FIRE is a 2D axisymmetric code using fluid electrons and particle-in-cell ions both for the ring and the background.

The FIRE simulations [11] showed that a favorable regime should exist for the experiment as a result of the strong rings it can create. In this regime collective effects emerge which cause rings to be slowed down and stopped axially after crossing the cusp. This slowing is caused by axial energy loss due to the generation of Alfven waves by the ring current as it travels through the plasma. The axial slowing was an essential element of the design for trapping the rotating beam into a tightly confined ring. In the previous IREX experiments, rings were axially trapped by a fast gated magnetic mirror field, but the weak rings continued to bounce back and forth in the mirror. In FIREX, the simulations showed that the collective slowing should rapidly damp out axial motion and allow the ring to relax into a stationary, axially self-confined equilibrium. Alfven wave generation had been previously observed with weak rings [10] with negligible effect on the ring, but in FIREX the much greater ring current would cause this nonlinear interaction to become a very strong axial damping mechanism.

This mechanism is indeed observed in FIREX. Strong FIREX rings come to a stop in the solenoid, whereas weak rings (attenuated by injecting the beam through a partially transparent screen) pass on through the solenoid without stopping.

Despite the achievement of efficient transport of beam through the cusp and into the solenoid, and despite the effectiveness of the axial trapping mechanism, FIREX rings have not achieved field reversal. The FIREX pulsed power generator that supplies the electrical pulse to generate the beam, designed and constructed at Cornell for the

experiment, reached its design specifications and performed reliably throughout the experimental program. The magnetically-insulated ion diode that transforms the pulser output into a proton beam was continuously refined and improved throughout the program. It reached the level of producing about half the total charge in the proton beam necessary for field reversal. The limitations of this diode design are now well understood, and new designs that promise to further increase this output by more than the needed factor of two were proposed. One of them, an entirely new configuration for radial injection, was tried in a brief exploratory campaign and indeed attained more than a factor of two increase in proton output. However, the new designs were not pursued further during the FIREX program.

The primary reason the new diode designs were not further developed is that a serious limitation on the lifetime of strong rings was discovered. It was recognized that unless this limitation could be understood and circumvented, field-reversed rings in FIREX could not be properly formed or live long enough to study usefully. The experimental observations and simulation results that lead to this main conclusion of the FIREX program are summarized here and discussed in detail in Section IV.

Injection of rings into preionized plasma, or into neutral gas that is rapidly ionized by the ring, results in the generation of very large amplitude (>kG) compressional Alfven waves that propagate dominantly in the radial direction from the ring annulus. These waves are the response of the plasma to the injected diamagnetic ring current, which rises in a time shorter than the Alfven transit time across the plasma column. The waves are launched from the annular region occupied by the ring as a rarefaction inward toward the magnetic axis, and as a compression outward toward the wall. The generation of these waves produces forces on the ring protons that cause them to lose both axial and rotational energy.

Two fundamental features of the ring dynamics result from this interaction. First, as we have already described, the ring is slowed axially. It is stopped and reflected in a magnetic field that does not stop or reflect a weak ring whose dynamics are governed by

single-particle conservation of magnetic moment. Second, the loss of rotational energy causes the ring radius to decrease as the proton gyro-radius decreases. This rotational energy loss is so rapid that despite the slowing of the axial motion, the pitch angle of the protons tends to decrease (their velocity is more axially directed) so they are quickly lost from the self-field diamagnetic well of the ring and leave both ends of the solenoid. The loss is roughly equal in the original downstream direction and back toward the diode in the reflected upstream direction. The result is that the FIREX rings are always observed to have a lifetime of only about six gyroperiods in the solenoid, that is about 0.7 μs. This behavior does not agree with axisymmetric, two-dimensional (r-z) FIRE simulations. Those simulations give the axial slowing, stopping and reflection, but show much longer ring lifetime because they do not include the (r, θ) dynamics that causes rotational energy loss and dispersal of the ring. A three dimensional code, FLAME [12], was also constructed for the program, but early computations were done with inadequate resolution in the azimuthal (θ) direction to discover the rotational energy loss.

FIREX rings always have shown considerable nonuniformity. The nonuniformity starts at the diode, which produces a beam with perturbations of a factor of two in current density on spatial scale of the less than 1 cm, and with temporal fluctuations on a 10 ns scale. These are inherent features of all intense beam ion diodes using surface-flashover ion sources as employed in FIREX. Thus, FIREX rings from their very birth, have large-amplitude nonuniformity of charge and current density on short spatial and temporal scales. This nonuniformity is observed to grow during the lifetime of the ring, and is accompanied by short-wavelength (cm scale) fluctuations in self-magnetic field that are observed to propagate as Alfven waves.

When two-dimensional (r, θ) simulations of the ion ring rotational dynamics were carried out with the FIRE code, they revealed a severe instability in this plane, again caused by the interaction of the ring current with Alfven waves of the background plasma. This instability, growing exponentially from noise in the simulations, generates very large amplitude waves, dominantly of short wavelength compared to the ring radius. The instability causes rapid loss of ring rotational energy within a few ion gyroperiods. In the

experiment, the initial small-scale nonuniformity should be expected to drive this instability very strongly.

Clearly, the dynamics of FIREX ion rings can only be correctly described by fully three-dimensional physics. The 3D FLAME code proved not to be a practical tool for simulating the experiment because its spectral representation of the azimuthal dimension, within computational limits, did not allow adequate resolution of the short-wavelength modes that apparently dominate the experiment. A major open issue remaining is to come to a fully three-dimensional understanding of FIREX ring dynamics, particularly with a view toward predicting the importance of unstable collective Alfven interactions in other systems with fast ions. This issue will be further discussed in section IV of this report.

The energy lost by the ring that so severely limits its lifetime is rapidly dissipated in the background plasma. The total wave energy reaches ~ 0.5 kJ in the experiment, so very substantial heating power is supplied as the waves dissipate in the plasma. Plasma heating is observed by spectroscopy, looking at Doppler linewidths. Microsecond heating of the plasma to above 100 eV ion temperature is observed. Because there is no lasting strong mirror or reversed field region formed by the ring for axial confinement of the hot plasma, and because the FIREX plasma is heavily contaminated by carbon and high-Z impurities from the wall and immersed diagnostics, the hot plasma lifetime due to particle loss and radiative cooling is of order 10-30 μs in FIREX. In the experiment, the short-wavelength modes that take rotational energy from the ring are very heavily damped, and do not propagate far from the ring annulus. To match this damping in simulations, effective resistivity at least two orders of magnitude above classical is required. The induced plasma current density may be high enough to reach such values based on current-driven turbulence; the spatial scale of the wave gradients is short enough that two-fluid effects may be important in this dissipation. Furthermore, the Alfven wave frequencies are near the ion cyclotron frequency for protons, and there is evidence that ion-cyclotron modes may be involved in the energy dissipation.

A detailed study of the ring Alfven instability was made in 2D FIRE simulations, and it was found that the growth rate and saturated amplitude of the unstable fluctuations vary with the ring strength, with stronger rings more unstable as expected. The Alfven Mach number M_a, the ratio of ring ion velocity to Alfven speed in the plasma, is also an important parameter, with $1< M_a <10$ being the range of maximum growth rate. FIREX rings are in this range. It is also found that rings with more spread-out radial distributions are less unstable than the tightly organized annular FIREX rings. As ion gyro-radius is reduced to simulate rings with s>2, the instability grows more slowly, saturates at lower amplitude, and results in longer ring lifetime.

The final task of the FIREX program was to investigate the injection of an ion ring below field reversal into a preexisting FRC. If future studies identify a distribution of large-orbit ions in an FRC that is adequately Alfven-stable and can provide the desirable features of a large-orbit ion population, an experimental method of injection is needed. Axial injection of a high-current ring has long been considered for this purpose [2]. To test this concept, an internal coil was designed and constructed to mock up the field of an FRC within the FIREX solenoid. The coil has very small cross-section to avoid intercepting ring ions, and successfully produces a field-reversed region in the preionized plasma in the experimental chamber. The FIREX ring is injected in the standard way, and encounters the "FRC" in its axial motion along the solenoid. The result is favorable, in that the ring protons cross the separatrix and pass into the FRC region with no observable disruption due to space charge. The pitch angle of the protons decreases as expected on crossing the flux at the end of the FRC. The protons pass through the FRC and exit the far end, their pitch angle increasing back toward the original value as they exit the FRC flux. However, 2D FIRE (r,z) simulations show the ring becoming trapped in the FRC due to axial energy loss, while in the experiment, as in ordinary injection experiments without the FRC, the ring is not trapped, but rather it is lost axially on the same rapid time scale as in the standard injection scenario into the plain solenoid field.

III. Detailed presentation of results

The FIREX experiment was designed to produce field-reversed rings of ~500 keV protons confined by a 0.6 T magnetic field, and to study the dynamics of this ring and its confined plasma in a 2 m long, 0.5 m diameter chamber. An overall view of the facility is shown in Figure 1.

The facility consists of the following major components. A pulsed power generator produces a 0.7 MV, 0.5 MA, 150 ns pulse. This pulse is applied to a magnetically-insulated ion diode that converts the electrical pulse into a proton beam. The diode is integrated into a magnetic field coil system with three basic regions. First, the diode insulating magnetic field controls electron flow in the diode and allows efficient production of protons. Second, the magnetic cusp just outside the diode's accelerating gap converts the axially directed velocity of the proton beam to rotation. Third, the solenoid region, with axial ramp and downstream mirror field, confines the resulting ion ring.

The cusp and solenoid regions are prefilled with a plasma, usually hydrogen. The plasma has a strong axial density gradient, with high density ($>10^{21}$ /m^3) in the cusp, and lower density (10^{20} /m^3) in the solenoid. The high density in the cusp gives efficient injection of the proton ring from the diode through the cusp and into the solenoid, and the resulting rings show almost no perturbation that could be attributed to incomplete charge neutralization in the cusp injection process. The lower density in the solenoid provides the density range of most interest for study of the interaction of ring and plasma in the solenoid. With this density the lifetime of the ring protons due to classical collisions with the background is ~ 1 ms, far longer than the duration of the experiment.

A notable success of The FIREX system has been its optimization to give highly reproducible operation. A change of 1% in the ratio between diode and solenoid fields, which provides a sensitive adjustment for maximum injection efficiency, has observable, reproducible effects. This level of control is a considerable advance in the state of the art in pulsed high-power beam experiments. The major practical limitation in this facility is that a polyethylene sheet in the ion diode and a 2 μm mylar foil separating the diode from the cusp and solenoid are destroyed and must be replaced after each pulse.

In summary, the FIREX system operates as follows. In routine, reproducible operation, > 75% of the proton beam from the diode is formed into a ring with > 80% of its energy in rotation and the remainder in axial motion along the solenoid axis. The protons occupy an annular ring between 9 and 15 cm radius in the solenoid. The ring charge is 6 mC. The ring current peaks at about 0.4 MA/m (current per unit axial length). The ring is about 0.3 m long at its best axial compression. The diamagnetic field on axis is up to 0.2 T in a 0.6 T solenoid field. Thus the strongest ion rings produced by FIREX have only about a third of the current necessary to reverse the field on axis and form a field-reversed ring.

The FIREX program was funded beginning in August 1993. The program began with theory and simulation code development, and used the resulting FIRE code to help define the basic experimental design. Over the next three years, the system was designed, constructed and brought into operation. This was accomplished at a funding level about the same in real dollars as the much smaller ion ring experiment funded at Cornell in the 1980's only because equipment was already on hand from that previous program, because pulsed-power and data acquisition facilities originally supplied to Cornell by Sandia National Laboratories for a different project were allowed to be transferred to the new ion ring program, and because the work was accomplished by a staff no larger than that of the earlier program. The result is the largest and most complex experimental facility our laboratory has operated. FIREX generates by far the highest power pulsed ion beam in any university facility, and has been exceeded only by installations at Sandia

National Laboratories, the Naval Research Laboratory, and at Forschungszentrum Karlsruhe in Germany with more powerful generators and much larger staffs. Over the duration of the program we have operated and developed our facility, which comprises the pulsed beam generator, the ring formation apparatus including the ion diode, the 8 kG, 2.5 m long, 50 cm diameter solenoid, the cusp-forming field coils powered by 200 kJ of capacitor banks, and most recently a pulsed, locally distributed gas fill and fast preionizing discharge for the background plasma. We have also developed diagnostics for the ion ring particles and magnetic field, and for the background plasma. A computer-based data acquisition and analysis system has been continuously developed along with the diagnostics. Theoretical and simulation work closely coupled with the experiment has also been carried forward. The 2D and 3D hybrid codes FIRE and FLAME were built, and have generated illuminating results. We now describe in more detail the results of all these activities.

A. FIREX systems

1. Experimental facility

The design of the pulsed power generator that drives the ion diode in FIREX follows principles brought to a high state of development in the 1980's for large accelerators at Sandia National Laboratories. The design output of the FIREX pulse at the diode is nominally 800 kV, 600 kA, 150 ns. The pulser consists of a 300 kJ Marx generator whose output charges an intermediate store in the form of a triaxial water capacitor. The intermediate store is discharged by a self-breaking gas switch into a 1.4 ohm triaxial transmission line, which is switched out to the load by two stages of low-inductance multi-gap water switches separated by a short output transmission line segment to supress capacitively coupled prepulse. The output pulse is delivered into vacuum through an axial stacked insulator, to a short magnetically-insulated transmission line which terminates at the ion diode.

The pulser was designed with circuit simulations which employed predicted ion diode impedance characteristics derived from previous experiments in our laboratory at the same voltage and ion current density. This work was done on the LION accelerator supported by Sandia National Laboratories. Sandia support was indispensible to the realization of FIREX. Sandia personnel conducted (at no cost) a thorough design review of the FIREX pulser, and made a number of important recommendations about construction details, as well as checking design calculations, and running particle-in-cell simulations of the magnetically-insulated vacuum feed section to confirm our design. Also, the LION accelerator itself was replaced in the Sandia program by a new accelerator, and LION was transferred to Cornell to use as the basis of the new FIREX pulser. The large tank containing the oil-insulated marx generator was reused (improved capacitor technology allowed the increase from 100 to 300 kJ in the same volume) and the water tank was enlarged to hold the larger FIREX water section. Many other parts of the LION installation were used in FIREX, including all the gas switches, controls, charging supplies, gas and water purifying systems, oil and water storage tanks, the overhead crane, cable conduits and screen room for data acquisition.

The FIREX magnetic field system uses a large solenoid and thyristor power supply from the previous DOE program, procured in 1978.
The solenoid was modified by boring some of its turns to larger radius, and a new larger coil section for the FIREX diode region was fabricated. The FIREX magnetic field is shown in Figure 1. The field design was validated and refined using FIRE simulations to produce optimally symmetrical axis-encircling ion orbits. A new cart and rail mechanical support system was designed and fabricated for the solenoid. The FIREX vacuum system uses oil diffusion pumping systems and other components from the previous DOE program.

The FIREX experimental systems shown in Figure 1 have been entirely reliable in operation over the last four years of the program, with no field coil failures and only normal downtime for pulsed power maintenance. The 300 kJ FIREX marx generator and

water pulse forming system is used routinely at 90% of full design charge. The output charge is limited by the main gas switch in the water following the intermediate storage capacitor. This switch is a 1980 Sandia PBFA I switch from our LION generator which (along with many other parts) was used in constructing FIREX. This switch is operated beyond its original design parameters. A new switch designed to the desired performance would have been a significant expense, and the difference was not important to our research path.

The 1 MJ TRANSREX thyristor supply for the FIREX solenoid, purchased by DOE in 1977, is still performing well. The two 100 kJ capacitor banks for diode pulsed field coils are also reliable, as is the fast bank used for a preionizing z-discharge in the solenoid volume. One of these banks was built for FIREX using existing capacitors; the other two banks were pre-existing.

Over the course of the FIREX project, we acquired a total of twelve Tektronix TDS210 two-channel 1 GS/s digital oscilloscopes. These, incidentally, were extremely inexpensive at ~$600/channel with GPIB interface, and totally satisfactory for our needs. Together with two more TDS210's and a 16-channel Analytek/Tektronix digitizer unit from our laboratory, we acquire up to 44 channels of data on each experimental pulse. All of the data are acquired and analyzed using software routines which are continuously updated as diagnostic setups are modified from pulse to pulse. The added data channels and automated analysis allowed us to use extensive arrays of ring particle diagnostics and magnetic field diagnostics which have revealed the complex perturbations in azimuthal structure of FIREX ion rings.

The experimental data rate on FIREX is determined mainly by the time needed to replace the anode plasma source in the diode, which is destroyed by each pulse. This routine work, along with the installation of a new 2μm mylar foil between the diode and cusp, plus the pump-down time to the desired vacuum of below 1×10^{-4} Torr in the diode, limit the experiment to one pulse per day. Viewing and analyzing the data typically occupies

several hours after each pulse. Often, changes in the diagnostic setup or plasma conditions were made for every pulse.

Computing resources included our Laboratory of Plasma Studies SPARC workstation network, used for experimental data analysis, an HP workstation (supplied by Sandia) used to run the FIRE and FLAME simulation codes, and several PC's also used for data acquisition and analysis.

2. Ion ring diagnostics

Diagnostics for the ring protons are based on Faraday cup- type collectors with variously chosen collimated collection solid angles defined by shields with apertures. Collectors were implemented to measure independently the axial and azimuthal components of ion current density. Arrays of these collectors measured radial, azimuthal and axial distributions of current. One of the most useful configurations was the "Faraday wand" which consisted of a single long collector inside a 3mm diameter stainless tube with a row of 0.5 mm diameter apertures along its length. These "wands" are mounted at the chamber wall and projected radially inward so that their array of apertures is positioned from 9 cm radius to 21 cm radius. They therefore measure the ring azimuthal current density radially integrated (measured in A/cm). The wands were deployed in arrays distributed in azimuth and in the axial direction. Figure 2 shows data from an array of 24 of these faraday wands, at four azimuths in six axial locations.

All of the ion collectors are operated without bias voltage. Instead of using a negative bias to exclude electron current collection, the collectors and their collimating shields are oriented in such a way that the path from the entrance aperture to the cup is transverse to the applied magnetic field. The distance from the aperture to the collector across the field (usually a few mm) deflects electrons of energy up to several keV from reaching the collector. These "magnetically-insulated" ion collectors are conservative diagnostics in

that there is essentially no way they can overestimate ion current density. Secondary electrons generated at the collector surface by ion bombardment see no electric field to accelerate them to the shield and generate spurious current. If very high-energy electrons are able to cross the magnetic insulation and be collected, they will reduce the measured current. It was found experimentally that there were circumstances in which electron current did partially cancel the ion current in some of these collectors, but suitable modifications of shields and collimation were effective in eliminating this. One way of testing the effectiveness of the magnetic insulation was to add a negative bias to the collector. The bias should not give an increase in measured current density if the magnetic insulation is effective.

Figure 3 illustrates the worst case of corruption of ion current denstiy measurement by electron currents in FIREX. The positive ion current signals from the wands began to be badly corrupted by negative-going swings just after passage of the main ring proton current. It was determined that these negative swings were occurring at the time when the phase of the magnetosonic wave launched by the ring current was such as to drive electrons toward the wand apertures. Although the magnetic insulation of the wands should have been adequate to suppress collection of even many-keV electrons, nevertheless a substantial current was able to reach the collector and cause the negative signal. The explanation is not clear, but probably involves the following factors. Ring protons strike the outside of the wands. The proton ring current density is large enough to ablate the stainles steel shield. There is direct evidence, described below, that a high density of rather cold, partially ionized material is ablated, and expands out to a few mm from the wand surface during the time in which the ring passes. The large-amplitude magnetosonic waves produce a changing magnetic flux which makes a substantial inductive electric field (in the lab frame, not the moving plasma frame) of several hundred V/cm. This field acting on the cold, dense, collisional ablated plasma at the wand surface is able to drive negative (electron) current across the magnetic field and to the collector.

This problem was solved by adding an external shield to the wands consisting of two metal strips on both sides of the wand tube, extending 2.5 mm in front of the wand apertures. The effect of this shield should be to short out electric fields out to this distance in front of the wand surface. Signals with the added shields are shown in Figure 3. The negative swings are essentially eliminated.

A second problem also results from the ablation of material from the wands. This material can be dense enough after some time in the pulse to actually stop 500keV ring protons from getting to the collector and effectively ends the measurement of ring current density. This "hole-closure" effect has been seen before with very high-power ion beams, and it certainly occurs with the strong FIREX rings. The effect is seen clearly in the data of Figure 4, in which signals from standard wands are compared with those from wands with an added collimator which prevents the main incoming ring from striking the apertures, but allows collection of later, higher pitch-angle protons in the nearly stationary ring. The signals on the collimated wands persist substantially longer than the uncollimated ones, because the reduced ablation retards hole closure. It is clear that we are approaching the limits of direct proton-collecting diagnostics in FIREX. New diagnostics were designed for FIREX in which Rutherford scattering is used to greatly reduce proton current density before collection. Such diagnostics have been used in the most intense beam experiments for inertial-confinement fusion. These were not implemented on the experiment however, because the collectors are much more expensive, and because the short life of FIREX rings did not require them.

Another type of ring proton diagnostic is a set of small time-integrating pinhole cameras with various configurations of collimators. Protons on orbits that passed near the axis, inconsistent with 2D simulations, were first detected, and their larmor radii were measured, with these cameras. The cameras use CR-39 nuclear track detecting plastic sheet to register the time-integrated spatial distribution of proton density at a detection plane. The typical energy-analyzing configuration uses a pinhole followed by a slit parallel to the magnetic field, followed by the CR-39. The pinhole-slit-detector plane combination gives three points defining a circle which is the larmor radius of the

particles. The slit allows particles to pass through at different axial (pitch) angles, so the larmor radius or proton energy is found as a function of pitch angle.

Pinhole cameras placed near the outer chamber wall were oriented to collect ring ions that charge-exchange on background neutrals to become fast neutral hydrogen atoms and leave on a tangent to their ion orbits. Some of these atoms re-strip before collection, so both neutrals and ions are seen. In general, the cameras found far fewer neutrals and re-stripped ions in the low-density fills than in the 200 mTorr fill, as would be expected. With this lower overall collection in low-density, the cameras were able to clearly resolve an excess of both charge-exchange neutrals and of protons with extra energy loss that had passed within a few mm of a faraday wand. This confirms the existence of dense, cold material around the wand that both slowed the ions passing through and produced enhanced charge-exchange. An estimated $10^{23}/m^3$ neutral density of ablated neutrals in a cloud extending 3mm from the wand is inferred from the pinhole camera data.

Spectroscopic diagnostics for the background plasma on FIREX have been developed to measure background ion temperature by Doppler broadening of emission lines. A 1 m spectrometer was coupled to a streak camera, followoed by an additional MCP image intensifier to allow μs time resolution of linewidth. These data will be discussed below.

3. Development of the FIREX ion diode

The magnetically-insulated ion diode that generates the FIREX proton beam was continuously developed to its optimized configuration of the last three years of the program. Early in the program the experiments were limited by mechanical failures of the highly-stressed field coil built into the anode of the ion diode. The final configuration that eliminated this problem is shown in figure 1. The anode coil design was changed so that part of the reversed flux that forms the radial insulating field for the diode and the magnetic cusp is now produced by a separate coil mounted at the chamber wall. The stress is shared between the two coils, and the result has been no failures for the

last four years of the program. Furthermore, an improved anode field coil design was developed which gives better performance than the original design in total proton output, voltage pulse flatness, and azimuthal beam uniformity. This has been accomplished by a change in construction which moves the coil windings farther from the anode surface, making the field at the surface less sensitive to error in the positions of the turns and to their current feed connections. The construction has also been made stronger and more accurate by embedding these turns in machined G-10 epoxy-glass material, a very tough material well-suited to taking the impulse loads of the pulsed diode fields. The improved accuracy in aligning the magnetic field to the anode surface results in better electron confinement in the diode gap, which is the key to producing high, uniform ion current density with low electron current loss.

A major part of the success in producing strong rings in FIREX was the control of the time history of diode impedance. Impedance collapse toward the end of the pulse has long been a characteristic of magnetically-insulated ion diodes with solid anode surfaces. FIREX contributed to the understanding of the mechanism of this collapse, by demonstrating an effective method of impedance control. The impedance collapse results from flooding of the diode gap with neutral gas ablated from the solid anode surface during the pulse. The gas is able to expand a few mm into the gap late in the pulse because it is partially ionized. The ions are accelerated, but there is a high probability of charge-exchange in the dense gas, so fast neutrals are produced that stream out into the gap. The gas breaks doiwn very rapidly late in the pulse by an avalanching mechanism that is enhanced by the confinement of electrons in the insulating magnetic field. The ions produced by this breakdown are extracted into the beam, but the electron space charge left behind causes steadily increasing enhancement of the space-charge limit to ion current density in the gap. The ion current rises rapidly, and the diode impedance falls.

As a consequence of this mechanism, in the first years of the program FIREX diode pulses exhibited rapid impedance collapse, causing the voltage to droop and resulting in a

large proton velocity spread. This made the production of strong, axially slow-moving rings impossible.

This mechanism has been very effectively controlled in FIREX by the addition of an electron "limiter" on the anode of the diode. The limiter is a circular strip of 0.25 mm thick, silver-painted mylar, projecting 1.5 mm above the surface of the polyethylene anode, and located at the inner radial edge of the polyethylene. The limiter operates by providing a loss path along the insulating field lines for electrons confined in this first 1.5 mm above the anode surface. Bleeding off this charge greatly inhibits the accumulation of negative charge there, and consequently inhibits the enhancement of ion current and collapse of impedance. Limiters had been developed in our laboratory and shown effectiveness in shorter (40 ns) pulses, but the FIREX result with a 150 ns pulse is a much more severe test of the concept. Its success was crucial to enabling the production of strong rings in FIREX.

The polyethylene surface discharge produces anode plasma promptly, thus loading the beginning of the power pulse and holding the early voltage peak down more effectively than the epoxy anode used at the beginning of FIREX. Before the limiter was developed, this copious plasma production with polyethylene was found to produce a very rapidly expanding anode plasma, which caused the diode impedance to decline rapidly later in the pulse and give unacceptable voltage droop. The limiter therefore enables use of polyethylene. The result is the flattest voltage pulses yet achieved in magnetically-insulated ion diodes of the FIREX type. This makes more of the pulse length fall within the voltage range for good cusp transmission of the protons into an axially slow-moving ring. Figure 5 shows a comparison of diode voltage, currents and impedance with the new and old coils and plasma sources.

Other options for further ion diode development were investigated during the program, including a novel radial diode that was briefly tested in FIREX. These new possibilities will be discussed in Section IV. A report on the radial diode is given in Appendix A.

4. Background plasma formation

At the beginning of experiments, a neutral gas fill in the cusp and solenoid was used. As in the previous Cornell experiments, it was found that at least 50 mTorr of hydrogen gas is required to produce enough plasma density by ion beam bombardment to give effective charge neutralization in the cusp. This density results in background plasma in the $10^{21}/m^3$ range throughout the solenoid. It was desired for axial slowing and trapping to use lower density, giving a higher Alfven speed closer to the ring ion velocity and producing stronger ring-plasma interaction. This is accomplished by using an axial gradient in the gas fill pressure profile and a pre-ionizing discharge in the ring propagation region. A fast gas valve with a radial nozzle is located on axis in the cusp region. The valve opens in less than 100μs and fills the cusp within 20 cm of the diode with about 50 mtorr of hydrogen gas. This allows the downstream solenoid volume to be operated at much lower pressure, typically 1-4 mtorr static fill of hydrogen, rather than the 50-200 mtorr previously used.

This lower pressure gas fill is preionized by a discharge driven by a capacitor bank between two electrodes at about z=20 and z=110 cm axial distance from the diode. The upstream (20 cm) electrode is a highly transparent array of thin wires to allow nearly unhindered ring passage. The downstream (negative) electrode is an array of axially pointed rods to encourage radially and azimuthally uniform initiation of the 10 kV, 50 μs risetime, 40 kA peak current discharge, which flows along the solenoidal field in the axial direction. The uniformity of this discharge in (r, theta) was studied with a fast framing camera looking along the axis from the downstream end. The discharge was found to have very poor uniformity and reproducibility. It was improved substantially by adding a "flashboard" to the negative electrode. This flashboard consists of a 15 cm radius azimuthal hoop of copper tape on an insulating substrate, mounted concentrically on the negative electrode rods. The tape is interrupted with a series of 0.5 mm gaps, bridged by graphite paint. One end of the string of gaps is connected to the negative electrode while the other end is capacitively coupled with 50 nF to the positive electrode. When the 10

kV capacitor bank is fired, before the gas breaks down the voltage appears across the string of gaps and causes surface arcs across the graphite. The plasma from these very fast-risetime, low-energy arcs provides electrons and ultraviolet light to help initiate the discharge. Framing images of the discharge show much improved uniformity and reproducibility with the flashboard.

The neutral gas distribution produced by the puff plus static fill does not give good cusp transmission and ring formation by itself, but when it is preionized by the discharge, the ring formation region is at least as good as in the best previous standard regime of injection into 200 mtorr neutral gas. The lower downstream pressure gives substantially lower background plasma density in the solenoid than the 200 mtorr case, giving a higher Alfven speed which interacts more strongly with the ring. In the low-density case the ring essentially stops at 50-70 cm in the solenoid, while in the high-density case, most of the ring exits the downstream end of the observation region. The ring diamagnetic field is also much stronger in the low-density case. These results are discussed in detail in the next section.

B. Experimental results

We will present here the most important features of the FIREX results, especially those obtained with the optimized system during the last three years of experiments. First, we show the observations of collective axial ring slowing and stopping. Second, we discuss the ring diamagnetism and wave activity associated with the interaction. Third, we present the evidence for instability seen in the detailed azimuthal and axial structure of rings. Fourth, we analyze the overall effectiveness of the FIREX system in forming rings. Fifth, we present measurements of plasma heating, and finally we discuss the results of "FRC" injection experiments.

1. Axial stopping of rings

The current density of the strongest FIREX rings reaches peaks of up to 0.4 MA/m of axial length. In the most tightly axially compressed rings there is about 60 kA total ring current, concentrated into about 30 cm length. The total proton charge in these compact

rings is about 6 mC. Figures 6 and 7 show data from two FIREX pulses with nearly identical diode voltage shapes, and identical magnetic field strength. In one pulse the background was the 200 mTorr hydrogen gas which has been our standard background until this year. In the other, the puff was used in the cusp, with a 2 mTorr preionized fill downstream. The base pressure in the solenoid was 0.5 mTorr for this shot, so this fill is 25% heavier species, and 75% hydrogen. In Figures 6 and 7 we see data from the Faraday wand arrays showing that in the low-density fill the ring essentially stops at the 50-70 cm axial location, and most of the ring current density is concentrated in a 20-30 cm axial length. As the nearly stationary concentrated ring peak evolves, some of it escapes downstream, and some is reflected back upstream (toward the diode). We return to an examination of this evolution in part 3 below. By contrast, in the high-density fill with lower Alfven speed and weaker interaction, most of the ring current travels further axially, with a substantial fraction exiting downstream and little reflection. The ring is never as concentrated in as short an axial length. This difference is similar to the results of simulations, as will be shown in the next section. Though we show only a single pair of pulses here, this behavior is quite reproducible. The most important point is that both the low and high-density ring pulses are very different from weak rings without collective interaction, as shown in Figure 12 and discussed in the next section. Weak rings travel through the system essentially without axial slowing or concentration.

2. Ring diamagnetism

Figure 8 shows the changes in axial magnetic field on axis and at the outer wall for pulses in low and high-density backgrounds. The most salient feature is the nearly sinusoidal ringing of the signals. This is the signature of a radial magnetosonic oscillatory mode of the background plasma column. This type of oscillation was seen at low amplitude (a few gauss) with weak rings in a previous experiment; in FIREX, the total amplitude is now up to half of the 5.75 kG applied field. With simple assumptions, the frequency of these oscillations gives the magnetosonic speed, and hence the background plasma

density. The results are shown in the table 1. The speed comes from the condition that this is the lowest radial mode of the plasma, in which one-half cycle of oscillation corresponds to wave propagation across the 25 cm from the axis to the wall. The second column of the table is the mass density (ion density n_i times effective mass m_{eff}) in the 5.75 kG field to give this speed (this is the Alfven speed V_a- the plasma pressure is assumed negligible). We assume here that this density is radially uniform. The third column gives m_{eff} (in units of proton mass) assuming that hydrogen and background gas (nitrogen, assumed singly ionized) are in the plasma in the same proportions as the initial fill and base pressure. The final columns give the resulting inferred ion number density, and the fraction of the fill density that is thereby inferred to be ionized.

Table 1

	V_A (cm/s)	(n_i m_{eff}) (/cm3)	m_{eff}	n_i (/cm3)	fraction of fill
2 mTorr (preionized)	$4.6x10^7$	4.8x1014	4.25	$1.1x10^{14}$	0.8
200 mTorr (neutral)	$2.4x10^7$	1.8x1015	2	$8.8x10^{14}$	0.06

Figure 8 shows representative waveforms for the magnetic fields produced by the ring on axis and at the wall for these two cases.

Given the uncertainty in composition of the low-density plasma, this is consistent with full ionization of the fill. In the high-density case, the 6% ionization fraction is much higher than can be accounted for by direct ionizing collisions by ring protons. However, we are now in a regime where other processes can be expected to dominate. The electric field associated with the magnetic oscillation will be discussed further below, but here we point out that though the electric field vanishes in the moving frame of the plasma tied to magnetic flux in the ideal MHD alfven wave, in the lab frame there is an inductive loop

voltage produced by the changing magnetic flux. With the amplitudes observed, the peak loop voltage at the ring radius is now quite large, roughly 50 kV, or 600 V/cm. This field would cause rapid breakdown of the high-pressure gas fill, and probably is the main factor in the higher ionization inferred from the data.

With this Alfven speed information, we can better understand the ring axial interaction data shown in Figures 6 and 7. In simulation studies, the basic parameter found to determine the strength of the interaction is the ratio of the ring axial velocity to the background Alfven speed, which we denote M_A. From the table, we infer that in the preionized low-density case, M_A is about ten, while in the 200 mTorr case M_A is about twenty. In simulations the strongest interaction occurs for $1<M_a<10$. The difference in interaction between M_A =10 and M_A =20 is consistent with the results shown in the Figures.

The wave amplitude of 1.5 kG in the 5.75 kG applied field is in a regime which raises many questions about how correctly to model the wave excitation and propagation. At this large amplitude there is substantial energy interchange between the ring, the wave fields and the plasma.

We mention here some basic considerations of the important effects in this regime. Not only does the ring transfer axial momentum to the wave which stops it near z=60 cm, but the >50 kV inductive loop voltage due to the field perturbation inside the ring radius will be felt by the ring protons. If the protons feel this field for one cyclotron period (about equal to the risetime of the ring current), they would lose 50 keV of their rotational energy, which goes into the magnetic energy of the wave field. As the field oscillates, cyclic exchange of energy between the ring and the field can occur, but if the wave is damped by other dissipation, there should be a net loss of energy by the ring protons. If a ring is stable for long enough in the solenoid, the ring and field should come to an equilibrium. This final configuration will have lost energy to heating of the background plasma by the wave fields during the relaxation. Indeed, energy-analyzing pinhole cameras at z=50 cm show that ring protons under these conditions in the experiment (e.g., the pulse of Figure 2) have lost almost 100 keV rotational energy, which would give

about 0.6 kJ total energy lost by the ring. The increase in magnetic field energy obtained by radially integrating the field at the time of the wave peak amplitude is about 0.5 kJ. Most of the energy invested by the ring in generating the waves is being lost by the waves to the plasma.

The energy loss by the wave to the background plasma may be dominated by turbulent resistivity due to high wave current densities. Using Spitzer resistivity, currents associated with the peak wave amplitudes would generate a resistive loop voltage of order 100 V, which would dissipate only a few joules of energy. The ideal MHD character of the wave would be negligibly perturbed. The current density in the wave at a given amplitude depends of course on the wavelength of the wave, which in turn depends on the Alfven speed and the risetime. For the experimental conditions, namely a ring current risetime of about 100 ns and an Alfven speed as inferred in the table, this gives a 2-4 cm scale for the wavefront. The resulting plasma current density implies an electron drift speed in excess of the initial electron thermal speed, so the resistivity is expected to be substantially enhanced above classical. On the other hand, if the wave scale is 25 cm, the lowest radial mode in the chamber, the current density for this amplitude might fall below thresholds for strongly anomalous resistivity.

In any case, in order to dissipate the wave field energy on the observed time scale, the resistivity would need to be enhanced by a factor of order 100 over Spitzer. In this case, the resistive loop voltage is above 10 kV, and the plasma begins to be significantly decoupled from the field. Thus the ideal MHD magnetosonic wave is expected to become highly diffusive when the wavelength is short and the current density is high. This may explain why the magnetic signals in the experiment tend to be so smoothly sinusoidal at the longest possible wavelength (lowest order radial mode): the wave is launched with a sharper front, but diffuses rapidly until the current density falls substantially. We will return to this point in discussing comparison of these results to simulations.

Another basic feature of the observations is that the observed amplitude of the wave depends strongly on the background plasma density. In the high density case of table 1, the peak magnetic signal on axis is 0.9 kG, while in the low-density case it is 1.5 kG, with very similar injected rings current. This effect was predicted long ago [13], by looking at the way the wave is excited by the ring current. If the ring current duration at a given axial location is short compared to the radial Alfven transit time across the ring radial width, then the full magnetic field of the ring current cannot appear. The flux and plasma simply can't move fast enough to respond fully to the ring current, or, in other words, the ring current is partially cancelled by induced plasma current. We are in exactly this regime with these pulses, but the observed amplitudes do not agree with simple estimates based on the above argument. In both high and low density, a larger magnetic field amplitude appears than this simple picture would give, and this probably is another indication of the strongly diffusive response to fast-risetime, large-amplitude excitation. A special 1D (radial) code was built to investigate this issue, and it was found that no simple time-independent model of diffusivity in the axisymmetric model suffices to match the experimental behavior. We comment further on this issue in Section IV.

There are still other factors complicating the physics in this regime. The risetime of the wave field is on the order of the proton cyclotron frequency in the unperturbed field, placing this interaction in a complex regime for Alfven wave dynamics even for linear waves. Under our conditions, where the wave field duration is short compared to the cyclotron period for all ions heavier than protons, those background ions can be accelerated by the wave and absorb energy directly. In a series of pulses, the effect of the mass, and cyclotron frequency, of the background ions was investigated by using a variable ratio of hydrogen to Nitrogen in the solenoid. Figure 8 shows the behavior of the magnetic field on axis at 60 cm in the solenoid. It is seen that shots into pure nitrogen have low wave damping, and that the wave decay rate increases strongly with increasing hydrogen fraction in the plasma. The protons in the background plasma clearly are able to absorb wave energy much more efficiently than the heavier nitrogen ions, and this must be related to the ratio of cyclotron frequency to wave frequency. The protons are much nearer the ion cyclotron resonance than the heavier species.

In any case, irrespective of the details of all the possible mechanisms by which energy is coupled from the waves to the plasma, it appears that 0.5 kJ is dissipated in a time of about 1 μs. This 500 MW of heating power, if it is deposited in the plasma over the full chamber radius and mostly within the 30 cm ring length (we see very little axial wave propagation), would heat the $10^{20}/m^3$ plasma by 250 eV, assuming electron-ion equilibration. The spectroscopic measurements show ions well above 100 eV as we will show.

3. Ring stability and lifetime

FIREX always produces rings with a significant amount of azimuthal nonuniformity. With the early diode field coil versions, the injected perturbation was quite strong on large spatial scales, and the nonuniformity appeared to grow in a coherent way as the rings traveled axially into the ramped solenoid. The rings were very strongly azimuthally structured after 1m of travel.

As we were able to produce more slowly moving rings, we observed this structure progressively more clearly. Figure 10 shows the signals on three azimuthally displaced radial faraday cup arrays. The azimuthal propagation of clearly defined, separated lumps of ring charge is clearly seen, especially near the center of the ring annulus at 15 cm radius.

Similar modulation in time had been observed with much weaker rings in the original IREX experiment in the 1980's, and was assumed to be an axial breakup of the ring into axisymmetric "ringlets", a benign instability of a ring with very little axial velocity spread. The diagnostics in that experiment did not look for azimuthal structure. This presumed ringlet structure did not appear to cause the trapped IREX rings to disperse or reduce their lifetime significantly, and would be expected to be stabilized in stronger rings with stronger axial betatron motion of the ion orbits. However, with the much

stronger FIREX rings, this type of time modulation of ring current does still appear, and reaches nearly 100% modulation of the collector signals in the slow-moving rings.

The basic picture is as follows. By z=100 cm in the solenoid, reached in about three cyclotron periods by the ring protons in transit from the diode, the ring in those early FIREX shots was completely formed into a nonaxisymmetric spiral shape. The modulations in the collector signals are not due to axisymmetric ringlets passing by, but rather are due to the rotation of the spiral. The spiral, composed of the ring protons in their orbits, of course rotates at the cyclotron frequency. The ring protons are concentrated into only about one half of the circumference at any axial position. The radial extent of the spiral is concentrated between about 13 cm to 17 cm radius. A snapshot in time would show about one and one-half turns of the spiral about the axis, and it is about 90 cm long axially, thus its pitch is about 60 cm/turn. The spiral is also translating axially, and the superposition of rotation and translation is somewhat like a screw thread advancing. However, the spiral translates axially only about 30 cm in each rotation (cyclotron time). Thus, the rate of translation is slower than would give a true screw-like advance (the "thread" would be stripped!). Another way to understand the structure is to remember that the orbits of single protons are also spirals, which advance screw-like with a certain pitch angle. The pitch angle of the spiral envelope containing the individual proton orbits is lower (elongated axially) compared to the individual orbits, so it advances less than one spiral turn in each cyclotron rotation. The frequency of the modulation on a probe array at a given axial and azimuthal position is therefore somewhat lower than the cyclotron frequency.

The structure inferred from the collector arrays is supported by magnetic probe measurements of the ring self-magnetic field. While on-axis B_z probes see fairly smooth signals that do not follow the collector array modulations, Off-axis B_z probes are more modulated, giving evidence of the asymmetry. B_{theta} oscillations are also seen, which can only be generated by broken azimuthal symmetry, or by strong radial oscillations which are not seen with the collector arrays.

One of the many questions generated by these observations is whether initial azimuthal nonuniformity of the proton beam from injected by the ion diode can explain the structure. This is certainly not true in a direct sense, since if for instance the diode were only producing beam in one half of its circumference and the protons followed single-particle orbits into the solenoid, a spiral would indeed result, but it would be a true screw-like spiral, advancing one turn per cyclotron period, as do the single-particle orbits. In fact, the twelve diode collectors, located in four radial arrays around the diode azimuth, do not show any such severe nonuniformity. Rather, they do show considerable scatter, and individual collectors vary by 50% on any one pulse, and among different pulses. This is characteristic of current density variations in this type of diode when viewed by small-area collectors (0.5 mm diameter). So, the beam is quite nonuniform on small spatial scales, and nonuniform by perhaps 30% from one quadrant to another, but does not show anything approaching the nearly complete void covering half of the circumference seen at 100 cm. The collector arrays have also been placed at 50 cm axial position, and see significant nonuniformity, but not the clear spiral structure. The conclusion is that this structure grows by a collective interaction as the ring propagates 1m into the solenoid, and the growth is probably faster than linear.

The injected nonuniformity from the diode is probably the initial perturbation that drives the growth. There is reproducibility in the orientation of the spiral at 100 cm, and there is also reproducibility in the overall nonuniformity in the diode. Whether these are truly correlated is not absolutely clear. To address this question, we intentionally blocked one quadrant of the diode and observed with the collector arrays arranged azimuthally at the 50 cm location. We did observe perturbations that are inconsistent with single-particle orbits, in particular, protons arriving later than expected at azimuths near the “hole” in the beam. These data do therefore indicate collective modification of the single-particle orbits.

During the last three years of the program, with improved large-scale axisymmetry of the injected beam from the new coil, we have not seen these large-scale coherent azimuthal ring structures. It appears that the spiral growth was indeed initiated by a large

perturbation to axisymmetry in the injected beam from the earlier diode. However, the rings are still far from symmetric. As seen in the faraday wand data of Figures 2 and 4, especially the collimated set which, as we have discussed, viewed the ring current more accurately later in time, there are substantial modulations seen in the stopped ring.

The most difficult issue in characterizing FIREX ring dynamics is to identify how the observed nonuniformity downstream is related to the ring nonuniformity injected from the diode. The question is whether nonuniformity is a manifestation of instability, or simply the propagated lumpiness of the injected beam. We have concluded that the nonuniformity observed downstream is not the simple propagation of perturbations from the diode, but is the result of collective ring-plasma Alfven interaction. We present here the evidence that leads to this conclusion.

First, ring ion scattering and energy loss grows in time as the ring propagates. We have used the CR-39 energy and pitch-angle resolving pinhole cameras (described in the diagnostics section to measure this. These cameras found protons within 4 cm of the axis, where 2D (r,z) simulations show no protons should be. Both there and near the chamber wall, the cameras showed protons with a very wide range of pitch angles, far beyond the range seen in the 2D simulations. Some dynamical process in the experiment is scattering proton orbits much more strongly than in the simulations (which, being axisymmetric, have no azimuthal instabilities). This scattering is observed to grow as the ring moves downstream, so cannot be accounted for by perturbations local to the diode or cusp. The larmor radius of the protons collected by the cameras indicates substantial energy loss as well, up to half of the original energy.

Because the CR-39 cameras detected ring protons near the axis, a special wide acceptance-angle magnetically-insulated faraday cup was deployed there, and time-resolved proton current density on these orbits was indeed detected. Proton current reaches this location, 4 cm off axis, coincident with the arrival of the ring current at larger radii on the faraday wands. The near-axis signal peaks at about 10 A/cm^2 early during the risetime of the ring current, and persists at a low level through most of the time the

ring is in the system. This peak near-axis current density is only about one percent of the ring current density, but its presence at any level indicates strongly perturbed proton orbits are occurring, especially early, near the head of the ring. This could be evidence of incomplete space-charge neutralization and consequent scattering of protons by electric fields, or it could be a manifestation of instability active at the head of the ring.

In FIREX, the ring lifetime in the solenoid is of course far below the millisecond classical slowing-down time for the high-energy protons on the low-density plasma. The lifetime is determined by loss of the protons before any significant classical collisional energy loss can occur. Almost all of the particle loss is axial, both downstream due to residual axial energy from injection, and upstream after reflection in the ramped solenoid. This evolution can be seen in the time histories of Figures 6 and 7.

To fully track the ring dynamics, we have developed new magnetically-insulated proton collector arrays which have brought us to a quantitative accounting of the ring from injection to loss from the system. We observe the transverse rotational (azimuthal and radial) current density of the ring protons, and the axial component of ion current at both ends of the solenoid. Figure 11 illustrates these results by comparing the radial distribution of the charge of the incoming proton ring as it enters the solenoid with the radial distribution downstream, after the ring has interacted with the plasma. The figure compares data for normal "full beam" rings with "attenuated beam" cases in which the ring is reduced in current by more than a factor of five, by placing a semitransparent mesh between the diode and cusp, to suppress the strong ring-plasma nonlinear interaction. Each of the profiles is normalized to a total of 1 mC charge so that the differences in distribution can be easily compared. The figure shows that though the incoming ring has essentially the same radial distribution for the full-strength and attenuated cases, the downstream profiles are different: the strong rings have moved radially inward compared with the weak rings. The mean radius of the ring charge distribution is at 13.2 cm for the weak rings, in agreement with single-particle r-z simulations, while for the strong rings it is 11.4 cm. It can be seen that a significant population of protons in the strong rings appear at radius less than about 8 cm, which is

well inside the inner ring radius of 10 cm predicted by axisymmetric (r-z) simulations, but is consistent with the (r-theta) simulations which predict rotational energy loss. Analysis of these measurements indicates that up to 40% of the rotational energy of the ring has been lost by the time it reaches the downstream measurement point.

Since these protons actually lose more rotational than axial velocity, their pitch angle decreases, and they can exit through the loss cone of the downstream magnetic mirror field in FIREX. The table below summarizes measurements using radial arrays of magnetically-insulated proton collectors measuring the z (axial) component of the ring current, located to measure the ring charge exiting downstream as well as back upstream toward the diode after reflection in the mirrored solenoid. Data are shown for two different fill pressures for the preionized background plasma. Figure 12 shows characteristic data from the collector arrays used to make these measurements.

Comparison of Fraction of Beam Exiting
Upstream Versus Downstream

Shot #	P (mTorr)	US (%)	DS (%)
425	1	78	22
426	1	44	56
427	1	87	13
428	1	58	42
437	1	58	42
Avg.		<65>	<35>
432	8	81	19
434	8	57	43
435	8	37	63
441	8	59	41
442	8	43	57
Avg.		<55>	<45>

The fraction of beam reflected is a very sensitive function of the diode voltage pulse shape (higher voltage, higher proton energy, means less ring is reflected). This sensitivity accounts for the large scatter in the data, but on average half to two-thirds of the beam is reflected while the remainder exits out the downstream mirror. At the diode voltages measured for these shots, both strong-ring FIRE simulations and single-particle orbit calculations would predict that nearly all of the beam should be reflected. The fact that much of the beam exits downstream through the mirror is due to rotational energy loss, which drops the particle pitch angles into the loss cone for the mirror. The two pressures shown, 1 and 8 mTorr, are the hydrogen fill pressures for the preionized plasma discharge into which the ring is injected. There is clearly measurable dependence of ring dynamics on fill pressure, and therefore on plasma density and Alfven speed in the background plasma. This dependence agrees with simulations which show that the strength of the ring-plasma interaction is sensitive to the ratio of ring ion speed to the Alfven speed. As this ratio, the Alfven mach number, increases above unity, simulations show that the interaction becomes stronger up to a broad maximum at 3-10, and then decreases above that as the ring and wave speeds become widely separated. This interaction with many cavity modes of this bounded system is not a very narrowly peaked resonance, and cannot be easily avoided by "detuning" the ring speed from the waves.

The azimuthal dynamics of the ring is characterized by the ion-collecting diagnostics and by Bdot probe arrays that measure magnetic field changes due to the ring current and wave generation. The basic picture of instability in the r-theta plane has been shown by these diagnostics. Strong coherent azimuthal modulation of the ring current and magnetic field develops as the ring moves downstream in the plasma. Figures 13 and 14 show that there are intense high-frequency field fluctuations in the ring annulus, which are not seen at the wall or on axis. These very intense field fluctuations are waves generated by the collective interaction of the ring protons with the plasma. Figure 15 shows a visualization of the data from radial and azimuthal arrays of Bdot loops that clearly shows propagating waves of short wavelength in the ring annulus. The Alfven speed can be measured from these data, and agrees with other measures that the plasma density is $\sim 10^{20}/m^3$.

Finally, a measure of the ring ion pitch angle was made using arrays of pairs of collectors viewing the axial and azimuthal component of ring current density. The ratio of the two components provides a measure of the mean pitch angle of the particles being collected at a given location. It is found that though mean pitch angle at the position of the stopped ring can be above 80 degrees, particles exiting the ends of the solenoid have much lower pitch angles, below 60 degrees. Thus the stopped ring is made up of a population of particles that are not confined in its diamagnetic well and are rapidly lost axially.

The magnetic data show strong localization of the short-wavelength modes in the immediate vicinity of the ring annulus. These modes are heavily damped and decay before they propagate far away from the annulus. On te other hand, the lowest order mode that propagates the basic ring diamagnetism is damped on the whole plasma column. Background plasma diagnostics have investigated the resulting heating. It was at first believed that stronger heating could be observed in the ring annulus. Figures 13 and 16 show magnetic data demonstrating persistent diamagnetism in the ring annulus after the ring is gone. This was initially attributed to plasma diamagnetic pressure resulting from heating of the low-density plasma volume, most strongly in the ring due to the damping of high-frequency modes there.

After careful investigation it has been concluded that this diamagnetic signal is indeed due to plasma, but is closely localized to the locations of the probes themselves, and does not correctly represent an overall plasma pressure. The plasma ablated from the probes themselves is believed to be responsible for most of the magnitude of these signals, and their time duration is the time for these local plasma clouds to disperse into the general background. The ablated plasma around the probes is two orders of magnitude denser than the general background, so the ~0.05 T diamagnetism in the 0.6 T field represents temperature of ~ 10 eV. If this signal were due to the low-density bulk plasma, ~keV temperature would be needed. In the case of the mock-FRC injection are there diamagnetic signals that may represent bulk plasma pressure generated as these localized high-pressure sources disperse. These signals occur only when the FRC coil current is

large enough to form closed reversed flux and confine the plasma better than in the open solenoid. These signals persist for 20-40 μs, and have spatial dependence consistent with plasma diamagnetism: the plasma pressure is seen to flow along gradients of the reversed field to accumulate in low-field regions.

4. Background plasma diagnostics

A spectroscopic system based on a Hamamatsu streak camera with an MCP amplifier has been implemented on FIREX to view narrow spectral regions. It consists of an 18-m quartz optical fiber which collects plasma light from the drift region within a 25° solid angle at a distance of 80 cm from the diode anode. The output end of the fiber is imaged with two-fold magnification at the input slit of a VM-500 1-m grating monochromator with 16.6 Å/mm linear dispersion. The vertical output slit of the monochromator is imaged with an achromatic lens on the horizontal input slit of the streak camera. The streak is imaged with a recording system consisting of an MCP amplifier and a gated CCD video camera with PC-based frame grabber. Total wavelength region recorded by the system is about 100 Å at an instrumental width of 1.85 Å. Experimental data are processed by means of several programs written in Mathcad.

This system is used to record line intensities and widths both in the preionized low-density plasma, and in ring pulses. For the plasma discharge alone, widths of several Balmer lines give estimates of ion temperatures in the neighborhood of 5 eV, and electron densities of 1-3 x 10^{14} /cm^3, consistent with the density inferred from wave frequencies during ring injection.

In FIREX pulses with injection of rings into both neutral gas and pre-ionized plasma, Balmer series lines from H_α up to H_ε have been recorded, as well as nitrogen and oxygen lines. We observe strongly broadened lines. Table 2 summarizes some of the lines observed and widths measured.

Conditions in the drift chamber	Spectral line	Observation time	Total line width, A
Pre-filled gas, 4 mTorr	H_β	After injection of the beam	3.0
Pre-filled gas, 50 mTorr	H_β	After injection of the beam	4.3
		At the afterglow, 20 μs	3.5
Pre-filled gas, 200 mTorr	H_δ	After injection of the beam	1.9
		At the afterglow, 28 μs	6.5
Pre-ionized plasma, 1 mTorr	H_α	Before the beam injection	3.2
		After injection of the beam	7.0
		At the afterglow, 20 μs	5.0
Pre-ionized plasma, 2 mTorr	H_β	Before the beam injection	(2.5)
		After injection of the beam	3.5
		At the afterglow, 28 μs	5.0
Pre-ionized plasma, 2 mTorr	H_γ	Before the beam injection	3.5
Pre-ionized plasma, 2 mTorr	H_δ	Before the beam injection	--
		After injection of the beam	3 –4.5
		At the afterglow, 28 μs	5.5
Pre-ionized plasma, 1 mTorr	H_ε	Before the beam injection	(5.3)
		After injection of the beam	-
		At the afterglow, 30 μs	11.4
	NII, λ=3995	After injection of the beam	2.85
		At the afterglow, 8 μs	1.8

TABLE 2

It is seen that, first, the three lines, H_α, H_β and NII, observed immediately after the ring injection have widths consistent with Doppler broadening by ion temperatures above 100 eV. Second, the higher Balmer lines are not visible until 20-30μs after ring injection when their intensities increase greatly. At these later times they have substantial widths.

As an example of these data, a streak of the H_β line with a 37 μs total length, and the analyzed line width are shown in Figure 17. A proton ring was injected in the drift chamber pre-filled with 50 mTorr hydrogen (atomic density $3.5 \cdot 10^{15}$ cm^{-3}). In this pulse most of the ring passed through the chamber without stopping. The line intensity as a function of time is shown in Fig. 17b. The full width at half maximum (FWHM) is shown with circles. Taking into account the instrumental width, the real line width is shown with the diamonds. If all the width were determined by Stark broadening, the density of the radiating region would be $1.3 \cdot 10^{15}$ cm^{-3} just after ring injection. This would be about 35% ionization of the gas fill, a factor of five higher than inferred from the wave frequency (as in table 1). If all the width were Doppler, ~200 eV "temperature" would be implied. The detected line must then be dominated by charge-exchange neutrals from a strongly heated or possibly nonthermal plasma ion distribution. Clearly, energy is being rapidly deposited in the background by the ring, and data from multiple lines must be consistently interpreted to reach any degree of confidence in inferences of ionization and heating, especially on the fast ~1 μs time of the ring injection.

The low-density preionized background case is easier to analyze. The density is known and Stark broadening is a negligible contributor to the linewidth. Figure 18 shows typical results of ring injection into preionized, 1 mTorr hydrogen. The inferred temperature from Ha is about 100 eV, while CII gives almost 150 eV at the earliest time the line appears.

The hydrogen line, of course, comes from neutrals that should not exist in plasma in thermal equilibrium at this elevated temperature. The light collection of the diagnostic is from a volume that extends all the way across the plasma radius. The neutrals probably come from charge-exchange of hot background ions on cold material ablated from the

wall and from immersed probes. When the field of view does not include any immersed probes, the line intensity is reduced, but the width is similar. CII likewise should be burned through at these temperatures. The very short duration of the signal and the very rapid decrease in linewidth indicate very rapidly changing, nonequilibrium radiating population of this species.

The spectroscopic diagnostic is the subject of a student thesis that is still in progress; further analysis will be presented when this work is completed.
It is clear that very rapid heating, in a time comparable to the wave damping time, occurs in FIREX, and the inferred heating power is comparable to the wave energy being dissipated during that time. The lifetime of the hot plasma is short. It is probably dominated by radiative cooling due to the carbon and other heavy contaminants, as well as by quenching due to the intrusion of cold ablated material into the plasma column.

5. Overall FIREX ring formation efficiency.

FIREX reached about half the current in an axially compact ring to begin to reverse the field on axis. Examining the various losses in transforming the FIREX current pulse into ring current indicates what could be gained by further changes. The FIREX generator supplies about 60 mC to the water-vacuum interface. About 25-30 mC are lost in the self-magnetically insulated vacuum feed from the interface to the diode, mainly in electron current across the applied field lines linking anode to cathode just before the diode. Thus 30-35 mC are available at the diode. The electron loss current in the diode gap is about 50% of the total, leaving 15 mC in the ion beam. About half of the ion beam, 8mC, is in protons which penetrate the output foil and enter the cusp, and the remainder is composed of heavier ion species, dominantly carbon. Of this 8 mC injected, 6 mC is formed into a compact ring which can be stopped in the solenoid. Thus the total efficiency from the pulsed power to the ring is about 10%.

Taking these losses in sequence and examining them in more detail, first, the efficiency of delivering current to the diode structure by the self-magnetically insulated vacuum feed probably is near optimum. Only about 5 mC are lost in the feed between the interface and a current monitor on the feed just upstream of the diode structure. Loss between this point and the diode accelerating gap is dominated by electron loss across the applied magnetic field lines which connect the anode and cathode just upstream of the diode. This field line connection is an unavoidable consequence of the magnetic topology of the FIREX design, since the coil embedded in the anode is used to produce the magnetic flux that forms a balanced cusp for axis-encircling ring orbits.

The electrons lost to the anode structure upstream of the anode coil come from two sources. First, the vacuum electron flow in the self-magnetically insulated feed is diverted to the anode by this applied field. Second, electrons are emitted locally from the cathode wall in the region where the applied magnetic field intersects the wall near the "ground coil". These electrons can cross to the anode structure and are lost. The experimental diagnostics do not distinguish between these two electron loss sources, which total about 25-30 mC. The self-magnetically insulated feed is expected to be operating near theoretical efficiency, and this vacuum flow, calculated to be about 5 mC, is in any case not expected to be available to couple into diode current, as has been established in other work on self-magnetically insulated flows in pulsed-power devices. Thus, the bulk of the 25-30 mC loss, and the portion that can be reduced, comes from electrons emitted near the ground coil.

Electrons emitted from the cathode edge at the diode gap can follow the applied field around to the upstream side of the anode coil and be lost. This loss cannot be distinguished from electrons lost directly across the gap to the anode ion source. The total of these losses from the cathode edge is measured, and gives the 50% diode efficiency number quoted above, which means another 15-20 mC lost to electrons. Thus most of the loss in the system is due to electron flow to the anode structure in the diode applied magnetic field.

In the diode gap itself, about 8 mC is lost in the ions other than protons which are produced by the anode plasma source and accelerated in the gap. This number is typical for surface-discharge hydrocarbon sources such as the polyethylene used on FIREX. Finally, the 75% of the 8mC proton charge injected into the cusp which is successfully organized into a compact ring is determined by all the details of cusp propagation and ring dynamics which have been our primary study in FIREX up to now. A possible way to improve this final fraction somewhat would be to produce a truly flat or even a rising voltage pulse in the diode, something that has been done in special diodes using sophisticated anode plasma sources developed in our laboratory. This type of source, known as a MAP diode, was investigated at the start of the program for FIREX, but was determined to be impractical to implement in the FIREX configuration.

This overall accounting of charge losses identifies two strong possibilities for attaining substantial increases in ring charge. A decrease in electron loss to the diode structure would provide the largest gain; second would be an improvement in the proton fraction of the accelerated ions.

First, with regard to electron loss, the present FIREX diode, integrated into the full-cusp injection scheme, has inherent features which prevent it from achieving the required performance to put out enough charge in the proton beam for field reversal.

There are three features of the FIREX configuration which result in its limitation. The first is the applied magnetic field connection from anode to cathode upstream of the anode coil, as already described. The loss by this path has turned out to be more severe than was estimated before the experiment was built, and we believe that no further minor changes of details of the configuration would significantly reduce it.

The second feature was also recognized from the beginning of the project, and is inherent to the full-cusp magnetic topology which requires the magnetic flux which insulates the diode accelerating gap to connect to the inside radius of the anode structure rather than to the cathode, as in the best-performing diodes in other experiments. Within the constraints of available capacitor bank energy and the chosen magnetic configuration, the

field design was shaped to minimize electron losses from the gap to the anode by this path, but the result is still a substantial loss to the inside radius of the anode structure. With the present configuration, we see no way to materially reduce this loss further.

The third feature relates to field errors, and although also considered from the beginning, was less well understood from previous experiments. FIREX has contributed a useful advance in this understanding. It is this understanding that led to the final improvements in the performance of the diode. Within the constraints of available capacitor bank energy, the field coil within the FIREX anode must be located very close behind the anode surface to produce the desired cusp and insulating field. It is impossible to completely avoid field perturbations due to the feed for this coil and its discreet turns. This is an important source of performance limitation, because the field perturbations encourage electron loss to the ion-emitting anode surface itself. These losses were manifested by localized damage to the anode surface in the feed region.

With differences in the details of coil construction over the course of FIREX experiments, we have observed that coils with worse field perturbations showed more anode damage, and produced slower rising and lower peak proton current. Although the electron losses causing this damage are probably only a small fraction of the total loss to the anode structure, they preferentially drain from the gap the most important part of the electron population, those which move closest to the anode and have the strongest influence on the ion current density that can be transported across the diode gap. The result is that the range of ion current density produced from the best to worst coils is over 50%. The final FIREX diode coil design we are now using is by far the best we have yet achieved in this respect, and probably is as good as is practically achievable. With the new coil, the damage to the anode is much more uniform than with previous coils, and shows no particular feature in the area of the coil current feed. We believe this is why thd diode with this coil produces a more intense and more uniform beam, and forms more azimuthally uniform rings.

With this coil, it is possible that we may have reached a level where further reduction of field errors would not further enhance performance. However, we are still significantly below the level of current density achieved in the best diodes with smoothly machined flux-excluding anodes that give essentially perfect magnetic field alignment to the anode surface.

The electron limiter in the FIREX diode reduces the rate of decline of diode impedance through the pulse, giving a flatter voltage pulse has proven to be crucial to the performance attained this year. Before FIREX, the first ideas of the mode of operation of limiters, which we had introduced in previous experiments at Cornell, attributed their effect to collecting and thus removing high-energy (cathode-emitted) electrons from the gap near the anode surface. If these electrons are drained away, the current divergence is eliminated. This however is a relativistic effect, and is predicted to vanish below about 575 kV; thus the FIREX diode, as we are now operating it with lower voltage, should not be in this divergent regime and the limiter should not have a strong effect. In fact, we find that the limiter is even more crucial in controlling the impedance with the new polyethylene anode than with the previous epoxy anodes. We have developed a new model of limiter operation from a different assumption, that it is mostly low-energy electrons, generated by avalanche breakdown of neutrals near the anode in the expanding, partially ionized anode plasma layer, that are removed by collection to the limiter. Draining off these electrons in this controlled way inhibits the avalanche and slows the plasma expansion across the gap, controlling the impedance. The polyethylene anode produces more plasma sooner in the pulse than the epoxy anode, as evidenced by the earlier and faster rise of ion current with polyethylene, and the limiter has an even stronger effect by controlling the later expansion of that plasma. This is the only model consistent with a wide range of data from FIREX and other experiments, and is a significant new contribution to understanding of diode dynamics and achievement of improved ion diode performance.

The radial diode that was invented during the FIREX program and tested briefly is described in Appendix A. The radial injection scheme is very promising, with the

increase on ring charge of more than a factor of two anda substantial improvement in current density uniformity. In the first tests the energy and gyroradius of the protons were too large to be confined in the solenoid, because the voltage was comparable to the standard diode voltage, so the decentered orbits of the radial injection configuration intersected the wall. There was no indication, however, that the ions would not be confined and form a ring if the voltage and field were matched to give the proper gyroradius. As we now discuss, simulation results indicate that the rings formed by radial injection could be more stable than standard FIREX rings because of their greater radial spread.

C. Simulation and theoretical results

Theory and simulation were well integrated with experimental work on FIREX, to the extent that it is somewhat artificial to separate them in this report. Simulations have become an important tool for interpreting experimental data and planning new experiments. Appendix B presents detailed results of simulations of the ion ring-Alfven instability in the (r,θ) plane.

FIRE 2D code simulations are used to make detailed comparisons with the experimental measurements of proton current density and ring self-magnetic field. The simulations use experimental diode voltage and current waveforms as inputs to simulate the proton orbits in a very accurate representation of the FIREX magnetic fields. Accuracy of these inputs is very important as we simulate axially slow-moving rings: as the diode voltage and proton energy are reduced to near the threshold for transmission through the cusp, there is extreme sensitivity to the voltage and field parameters in determining the propagation of the ring. Five percent change in the voltage or field leads to substantial difference in the fraction of the ring charge that reaches 1m in the solenoid. Great effort has been expended on both the experimental and simulation sides to reach a trustworthy comparison of experimental and simulation results. This work has resulted in the realization that due to the extreme sensitivity of radial distribution to input parameters,

and the small-scale nonuniformity of the real injected beam, some spatial integration is advantageous in collecting the experimental beam current density data. As a result, the radially integrating faraday wands give the best data for comparison of simulations and experimental data.

Simulations allowed us to understand the role of the background plasma parameters in controlling axial formation of our present experimental rings and their azimuthal stability. In the formation stage, the ring axial motion is desired to be well coupled to Alfven waves, to dissipate the ring axial energy. Once the ring is formed, its azimuthal stability requires minimization of such coupling to the ring rotational energy. These two opposite requirements determine the optimal background plasma parameters in the ion ring experiment and will be discussed below in more detail. The simulations suggested that it would be advantageous to use a preformed plasma with optimal parameters rather than to let the parameters vary rapidly as the neutral gas becomes ionized by the passing ring. That suggestion proved to be very fruitful for accurate control of the ring dynamics in the experiment.

1. Ring axial dynamics

In the ring formation stage, it is important for the leading edge of the ring to encounter plasma, rather than to have plasma formed only further back in the ring with zero density at the leading edge. This is because ∂Br due to the ring current is the dominant component coupling to Alfven modes carrying axial momentum, and this component peaks near the leading edge of the ring. Plasma must therefore be present at the leading edge to provide the Alfven dynamics. For the waves to propagate outside the ring radius, a preformed plasma must exist there. With preformed plasma, a density in the low $10^{19}/m^3$ range in the code, which gives the ion speed/Alfven speed ratio M_A around unity, produces the most rapid slowing (see the discussion below). However, M_A =10 still produces significant interaction. Figures 19 and 20 show a comparison of simulations in cases similar to those of the low- and high- density fills in Table 1 from the experiment, as well as a simulation of a very low-current ring in the low-density condition. It is seen that the ring stops in the low-density case, while propagating much

further in the high-density case, similar to experiment. The low-current case shows that in the absence of the strong ring current the collective interaction disappears, and the ring goes farther and faster through the solenoid with no axial bunching. Figure 21 shows snapshots of the ring distribution in the three simulations. The stopping and axial self-trapping of the ring in the low-density case is apparent.

To quantify these results, a set of simulations were carried out to look at the actual rate of axial slowing down of the ring by the Alfven interaction, as a function of background density, and in different magnetic configurations. First, it has been found that the axial momentum loss to waves is very complicated, and not quantitatively similar to the estimates in idealized unbounded geometries made in the past [8]. Cavity modes in the bounded, inhomogeneous system have strong effects. The maximum rate of momentum loss occurs when the ring axial speed is above the Alfven speed, and varies in a complex way with the speed ratio. Figure 22 shows these results, derived from the FIRE 2D simulations of the slowing process. The strength of the interaction is also certainly affected by the axial ring-current profile, which changes in response to the wave drag, thus producing a strongly nonlinear evolution. The code thus becomes a necessary tool for estimating the slowing down of rings in realistic situations.

2. Ring azimuthal dynamics

Once the ring is formed, it is important to maintain its azimuthal stability. The paper by Omelchenko and Sudan [11] analyzed stability of an infinite, uniform ion beam propagating in plasma with an arbitrarily oriented external magnetic field. Applied to the ion ring experiment, the analysis showed no azimuthal instability of the ring, but predicted beam axial instability leading to ring formation. Subsequent FLAME 3D code simulations by the same authors [12] seemed to have confirmed that conclusion, and for some time, we did neglect all deviations from axisymmetry in our ion ring dynamics analysis.

Accurate comparison of simulations and experiment has proven to be most important when the detected deviations in the experimental behavior from the quasi-neutral, axisymmetric FIRE code physics led us to a better understanding of the role of 3D effects in the ring behavior. One such deviation came from comparison with simulations of the experimental results showing strong beam current density modulations at 1m that could not be attributed to the axisymmetric radial beating of the beam at the ion cyclotron frequency observed in the simulations. Another important indication of nontrivial azimuthal structure of the beam was provided by comparison of simulations and experimental results for the ring self-magnetic field. Simulations were used to calculate expected ring magnetic field from experimental ring current density measured by a radial array of ion collectors. The simulations showed that if the measured current density modulations were axisymmetric, they would result in much larger oscillations in the self field than the ones observed in the experiment.

Stimulated by these results, we started to collect more information about azimuthal structure of the beam, and discovered the strong beam azimuthal modulations we have described.

These discoveries also stimulated us to adapt the 2D FIRE code from its standard (r,z) geometry to run in r-theta (actually x,y) geometry, to study beam azimuthal dynamics. These simulations immediately showed violent instability of radially thin rings with azimuthal velocity comparable to the Alfven velocity in the background plasma. As the instability develops, ring particles lose a large fraction of their energy and the ring spreads and fills in toward the axis as particle larmor radii decrease, as shown in Figure 23. For radially thick rings (the situation closer to the one analyzed by Omelchenko and Sudan [11]), simulations showed less strong instability. Rings with ion larmor radii less that the radius of the ring were also found more stable. These rings show only very little initial instability and reach a steady state that is only slightly spread from the initial state, with little ring energy loss. Figure 24 shows a comparison of rings under these different conditions. Another parameter found to control ring stability was the Alfven mach number M_A. Rings with orbital velocity much larger that the plasma Alfven velocity,

M_A>>1, were found to have much smaller growth rate and significantly less disruptive nonlinear stage of the azimuthal instability. Appendix B presents the detailed results of FIRE simulations of the unstable azimuthal ring dynamics.

The 3D code FLAME was used to investigate ring azimuthal stability in real 3D geometry, though with azimuthal resolution limited to low-order moeds of long wavelength. These simulations also show a rapidly growing thin-ring instability with a kink-like structure in three dimensions when the ring orbital velocity is comparable to the plasma Alfven velocity. Similar to our 2D modeling, the 3D simulations also show rapid growth and nonlinear evolution with substantial energy loss by ring protons, to a final nearly steady state in which the ring is broadened both radially and axially, as shown in Figure 25.

3. Anomalous plasma resistivity and plasma heating.

The effects of anomalous resistivity are a central issue in the physics of ring-plasma interaction. The local resistivity can affect the excitation and propagation of Alfven waves, thus affecting the magnetic perturbation felt by the ring and determining its dynamics. The resistivity of course also determines the details of energy deposition in the plasma.

To better understand the process of beam-formed background ionization and resistivity in the experiment, a new kinetic model of proton beam ionization of hydrogen gas was constructed, including all important collisional processes among the ring protons, plasma ions and neutrals, and electrons. The results showed that the actual ionization rate by ring protons is about a factor of three slower than previous estimates, taken from models previously constructed by other researchers [14], originally for other gasses which do not include all of the cross-sections which are important for hydrogen. This model would predict less than 1% ionization of the 200 mTorr fill by the ring protons directly. The experimental estimate of ionization of 6% (see table I) is much higher than either of these models and this is almost certainly due to a large contribution to the ionization rate by plasma electrons in the wave fields.

The classical Spitzer and collisional electron-neutral resistivity estimated for our plasma parameters is too low to result in significant dissipation during the ring formation time of less than 1 μs. Comparison of 2D simulations with experiment gives clear evidence that the experimental resistivity must be far higher than classical. The magnetic field signals in 2D simulations (with classical resistivity) and in the experiment show very different Alfven mode structure. In the experiment, only a low frequency, damped wave mode is observed outside of the ring annulus, while in the simulations a much broader spectrum of modes propagates away from the passing ring and stays in the system for a long time. It was suggested in earlier experiments by Schamiloglu [10] in our laboratory that anomalous resistivity due to cross-field current-driven-turbulence could damp Alfven modes significantly. Estimates have been made for our conditions of the anomalous resistivity resulting from two-fluid instabilities as analyzed by Gordeev and Gretchikha [15]. Enhancements in effective resistivity of two orders of magnitude were found possible. Values of this order strongly affect the characteristics of the waves in simulations. We have not found a single global value of resistivity that produces simulations matching the experimental waveforms. It appears likely that no global value will be adequate to model resisitivity for the time-and space-dependent wave current densities.

FIRE simulations were used to model the plasma heating to compare with experimental results. Figure 26 shows results of three simulations with differing background plasma conductivity. As the conductivity is reduced so that the damping of the short-wavelength modes is more localized to the ring annulus as in the experiment, the plasma heating is increased and localized to the ring annulus as well. Figure 27 shows simulation results for two resistivities, as a function of time up to 300 ns after the ring injection begins, showing the very high heating power transferred from ring to plasma by the waves. Figure 28 gives an accounting of energy flow in the simulations, showing that after about 500 ns, numerical dissipation becomes significant as the wave spectrum reaches the simulation grid scale.

4. Ion ring-FRC merging

The FIRE code was used to simulate axial injection and merging of a ring into a preformed FRC. This process has been investigated before with simpler codes, and it is of interest to look at this using the more complete physics in FIRE. A very striking result was found, as illustrated in Figure 16. When a ring of strength and axial velocity similar to present FIREX experiments was injected axially into a mockup FRC (using the current of a field coil inserted into the solenoid to produce the reversed field), the ring protons entered the closed field-line FRC region as expected for single-particle orbits. When the ring encountered the radial field at the far end of the FRC and the ring axial velocity slowed, a very strong interaction with the plasma occurred, coupling ring axial momentum to Alfven waves and removing enough axial momentum to trap the ring in the FRC when it bounced back to the end from which it had entered. Further axial velocity loss occurred on each subsequent end reflection, and the ring rapidly settled down into a stationary distribution in the FRC, as seen in Figure 29. This effect has not been previously pointed out. If this strong trapping could be produced experimentally, it would obviate previous conjectures that it is necessary to slow a ring to sub-Alfvenic axial speed to merge successfully with an FRC [1], and would make ring-FRC merging possible with our present FIREX rings.

Accordingly, this scheme was investigated experimentally. An internal coil for the mock-FRC field was designed and constructed. The coil construction is shown in Figure 30. It was located at 18 cm radius, and had small cross section so that the ring ion orbits, in simulation, pass inside the coil radius. Protons whose orbits would intersect the coil are deflected strongly by the high field just outside the coil, so very little loss to the coil surface occurs in simulation. Figure 31 shows as realistic a simulation as possible with FIRE of the injection of a FIREX ring into the field of this coil, using actual FIREX experimental voltage and current waveforms for the injected ring, and accurate representation of the magnetic fields. As in the idealized simulation, the ring is efficiently trapped in the reversed field of the coil. Note especially that the ring orbits pass through the region outside the coil radius, between the coil and the wall. Most of the

ring passes through this region after its first reflection from the downstream end of the coil field. These strong radial excursions of the ring orbits produce transient radial current that strongly launches torsional Alfven waves, and contributes to the dissipation of ring energy that leads to trapping.

The experiment did not show this trapping. The ring protons did cross the separatrix and traverse the FRC field with no observable disruption due to space charge. The experiment was designed so that the ring encountered the FRC before instability had a chance to scatter the proton orbits badly. The pitch angle of the protons goes from nearly 80 degrees before the FRC, down to less than 45 degrees in the FRC, and then back up to 80 degrees after exiting the FRC downstream, consistent with conservation of canonical momentum. Very little reflection off the downstream side of the FRC radial flux was seen in the experiment, and especially, very little ring current was seen outside the coil radius. These observations disagree with the 2D simulation. Clearly the 2D picture is not realistic, but it is not clear in detail what causes the true 3D dynamics to differ so strongly. Basically, the disagreement is apparently again the consequence of ignoring nonaxisymmetry and rotational energy loss in the simulations. It may not be possible to understand the ring propagation in complex fields like the FRC by trying to superpose the two complementary (r,z) and (r,θ) 2D pictures given by the simulations. An attempt to include the rotational energy loss in the (r,z) simulations by imposing a rotational energy loss rate based on the (r,θ) simulation results did not reproduce the experiment either. In fact, the dominant local force on a clump of ion charge is probably best approximated by a diffusive drag force directed basically against the instantaneous direction of motion. Figure 32 shows snapshots of a simulation of an initially compact, isolated clump of ring charge during its interaction with the background. The code is quasineutral, so space charge plays no role. Energy is being given up to Alfven waves, and the clump is spread out along its direction of motion. The force on the ions in the clump acts like a diffusive drag force along the direction of motion. In this approximation, the pitch angle of a propagating ring would not change significantly due to the wave interaction, but the energy decreases. Consequently, the orbits are similar to single-particle orbits in the applied field, but with continuous slowing down. Such orbits would not be reflected and

confined by the FRC field: if a particle can get in, it gets out again unless it actually comes to a stop before it exits. It may be that this clump-drag model gives a first approximation to a simple picture of nonuniform ring dynamics in complex fields. However, even in the case, relevant to the experiment, where the short-wavelength waves are heavily damped so that wave reflections from boundaries do not play an important role, the real situation is far more complex. The interaction of clumps of ring charge with waves launched by other clumps and the complex propagation of the waves in the strongly nonuniform magnetic field are likely to play important roles in the evolution of the ring as a whole. Clearly, fully 3D simulations are absolutely necessary to model the real situation.

IV. Discussion of results and recommendations for future investigations.

The FIREX program did not achieve its goal of studying field-reversed ion rings, despite several notable successes. The method of producing rings by axial cusp injection of a very high-current pulsed ion beam was successful in attaining high efficiency of injection of the beam into a tightly organized rotating ring. The FIREX ion diode, as it was developed with incremental modifications of the basic original design configuration, succeeded in producing a longer pulse with better control of impedance and beam energy over the duration of the pulse than any previous intense beam experiment. This good control enabled the efficient cusp injection. The efficient injection of rings with diamagnetism on axis of up to a third of the applied field was accomplished in a background plasma in the correct density range to be relevant to FRC physics. Collective slowing and stopping of the ring axial motion was observed. Rings were observed to cross the separatrix and enter the closed flux of an FRC-like magnetic field, demonstrating the first requirement of the axial merging scheme of incorporating large-orbit ions into a separately formed FRC. However, the usefulness of all these results was compromised by the very short life of the rings. The lifetime was only a few ion gyroperiods; during this time substantial energy loss and orbit scattering had taken place

that led to the failure of axial trapping, either in the solenoid or in an FRC-like field. Rapid dispersal and loss of the ring followed in all cases. The investigation of this rapid loss led to simulations that revealed a severely destructive instability of strong rings of super-Alfvenic ions in the background plasma.

In evaluating these results we have considered several avenues for further progress. We will discuss them here. They address the two basic issues on which FIREX was focussed: first, the physics and technology of beam generation for the production of FRCs with a large-orbit ion component, and second, the understanding of the dynamics of FIREX rings.

After FIREX, any discussion of desirable methods of ion beam generation and ring formation must start by considering the question of what distribution of large-orbit ions is desired. Indeed, the FIREX design started from such a consideration, namely that the most highly-organized, axially short and radially narrow ring should be the goal. The reason for this choice was primarily that this would maximize the diamagnetic field of a given total ring charge, and make the goal of field reversal easiest to attain. Additionally, and critical to the FIREX design, it was predicted that such a ring would be strongly slowed and easily trapped axially. We now have found that with ions of a good fraction of an MeV energy (required by the beam generation technology to produce enough total charge in a single pulse) and with a background plasma in the fusion-relevant range, such a ring is very short-lived. The large-amplitude Alfven activity that accompanies the injection of a $M_A>1$ high-current pulsed beam to form a ring on an ion gyroperiod time scale does give the collective interaction to slow and stop the ring, but the other side of this coin is the rapid loss of rotational energy. Several questions arise from this result.

Most importantly, it needs to be understood in what way the FIREX results, both experimental and simulation, apply to other situations, especially the case of a large-orbit component in a high-s FRC. The relationship is not at all clear. The 2D FIRE simulation results, while they do map out the behavior of the instability in the idealized 2D geometry

of an infinitely long, axially uniform ring, are certainly not quantitatively relevant to either FIREX rings or to a real FRC.

Perhaps the clearest support for this contention comes from the simulation results themselves. As the ring ion distribution becomes less tightly organized, so that the ring is radially thicker or the ions do not symmetrically encircle the axis, the instability grows more slowly and its saturated state is more benign in terms of ring lifetime and energy loss. The effect of the third (axial) dimension in real ion rings, or FRCs, would also be to spread the ion orbits due to axial betatron motion in the self-field. It might be that even FIREX-like rings, of narrow energy and canonical momentum spread and axis-encircling orbits, would be more stable than the 2D results suggest. However, the rapid loss of rings in the experiment, even though they do form a deep, axially short self-field well for a short time, argues that this effect is not likely to help significantly in the parameter range that FIREX occupied.

There is another issue involved with the 3D nature of the real rings that complicates the comparison to simulations. This is that the field lines of the solenoid in FIREX are tied to grounded conducting surfaces at both ends, at the cusp wall and at the downstream electrode of the plasma ionizing discharge. If the ring were perfectly azimuthally symmetric, its charge could be neutralized without any electric field in the (r,θ) plane, by a population of plasma electrons that accompany the axial motion of the ring but do not need to rotate with it. However, when the ring current density is nonuniform, as it always is in FIREX rings, maintaining charge neutralization requires more complex electron current paths in the plasma. This current could flow across the field coinciding with and neutralizing the "clumps" of ring ion current, but this requires an electric field, either in the azimuthal direction if the electrons act like a resistive fluid, or in the radial direction if ExB drift drives the electrons. Either of these fields tends to be shorted out by the line-tying to the ends of the solenoid, on the rapid whistler transit time, an effect that is not included in the 2D (r,θ) simulations.

This effect can be considered in idealized form in the (z,θ) plane: a clump of ring charge moves in the θ direction; the motion is parallel to a conducting wall that is separated from the ring in the z direction (along the field). If plasma conductivity along the field is high and the communication (whistler) time to the wall is short enough, any electrostatic field across the clump would be shorted out. Charge neutrality would be supplied by electron current flow in a loop from the wall to the head of the clump, and from the tail of the clump back to the wall. This moving current loop, closed by the ring ion current, would of course excite Alfven waves in the plasma, and this interaction mechanism is not included in the 2D simulations. The same point applies even if the current loop does not extend all the way to the wall, because of cross-field plasma conductivity. As soon as the ring axisymmetry is broken, the Alfven wave interaction becomes fundamentally three-dimensional.

A fundamental difference between the experiment and the 2D (r,θ) simulations is that in the experiment, the initial rise of the lowest-order radial Alfven mode of the cylindrical plasma column appears at all radii from axis to wall with almost no radial propagation delay from the time the ring arrives. In contrast, in the simulations the mode propagates at the Alfven speed radially away from the exciting ring current annulus, so it begins its rise on axis and at the wall only after the Alfven transit time. It appears that in the experiment the initial cancellation of the overall ring current by co-rotating electrons is partially inhibited. Even when the ring is injected into initially neutral gas, this inhibition cannot be attributed to inadequate electron density in the ring early in time, because the unperturbed propagation of the ring proves that its charge is very well neutralized by electrons. This disagreement between experiment and simulations is likely to be evidence of the fully 3D dynamics of fields and currents in the real ring. Consequently, the short-wavelength modes responsible for the rapid rotational energy loss in the experiments and simulations are also likely to be different in their quantitative details.

An FRC with an immersed ion ring component would be yet a different case, certainly also fully 3D in nature. The quantitative result of the experimental ring lifetime is not applicable to the FRC case, and the 2D simulations are certainly also not quantitatively

useful. However, the basic character of the Alfven instability seems clearly to be relevant to the FRC. That is, a beamlike component of ions with $M_A>1$ should be unstable to the generation of Alfven waves.

To quantify the relevance of the basic ring-plasma Alfven interaction, define Γ as the Alfven mach number $M_A = (v_i/v_A)$ of an ion in an FRC with outer turning point at the separatrix and s defined as the ion gyroradius r_i (using the external field), divided by the separatrix radius R_s. Then

$$\Gamma = (4\pi r_i)^{1/2} (n^{1/2} R_s/m_i^{1/2} s)$$

or, in practical units: $n(10^{20}/m^3)$, $R_s(m)$, $m_i(m_{deuteron})$

$$\Gamma \sim 30 (n^{1/2} R_s/m_i^{1/2} s)$$

so, for deuterons in a $10^{20}/m^3$, 1 m size FRC, $\Gamma = 1\sim10$ for ions with $s = 30\sim3$. This is the range for thermal ions, and this is exactly the range of maximum instability growth rate in the 2D simulations. On the other hand, for large-orbit, s~1 protons of a ring-like component in this same FRC,
$\Gamma > 40$, well above the range of maximum 2D instability. So it is possible that in a reactor-scale FRC, a ringlike component might not be as dangerous in terms of Alfven stability as the thermal ions, based on their Alfven mach number. With respect to their distribution, however, a beamlike, highly anisotropic distribution is more dangerous than the high-s, more nearly isotropic thermal ion distribution. To the extent that the 2D simulations can be a guide, it is clear that for the thermal super-Alfvenic ions, the plasma edge, near the separatrix where orbits turn and the distribution is most anisotropic, is the region of most concern for Alfven wave generation.

Using this relation for existing experimental FRCs, choosing a case with $R_s = 0.1$ m, $s = 3$, $n = 10^{21}/m^3$ gives $\Gamma \sim 3$, so the 2D prediction would be that instability would occur, but would be far less severe than in the s= 1 FIREX rings, and would saturate with moderate ion energy loss (see, for example, the difference between s~1 and s~2 shown in Figure 24, and also Appendix B).

It is clear that properly designed 3D simulations are the highest priority for progress in understanding the issues raised by the FIREX results, and applying them to new configurations.

It appears that FIREX-type rings, with nearly singular velocity distributions and s=1, are the worst case for instability and rotational energy loss at any given Alfven mach number, at least in simple 2D geometry. Such rings in a reactor-scale FRC plasma could have M_A so high that instability might not be a problem. However, at smaller scales the ring tends to fall into the range of severe instability, unless the background plasma density is increased well above the range used in FIREX.

FIREX was restricted to the most unfavorable regime because the strong axial Alfven interaction was needed to trap the axially-injected ring. The strong interaction was indeed produced, but along with it comes the interaction in the azimuthal plane that severely limits the ring lifetime. If rings were injected in a different way that did not depend on collective interaction for trapping, as in the radial injection scheme where the ring could be "born trapped" by being produced directly inside a magnetic mirror field with the radial diode, the constraint would be removed (see Appendix A). In such a case the background could be chosen with higher mass density to lower the Alfven speed and raise M_A well above the dangerous range. This would actually be a better case for understanding what would happen in a reactor-scale FRC where large-orbit ions would have large M_A, as we have explained above.

We conclude that the radial injection scheme described in Appendix A is the most promising avenue to producing an FRC with a strong ion ring component. The diode design is possible to integrate directly into a magnetic mirror field that could confine the FRC axially. The diode's simplicity and high ion efficiency should satisfy the requirements for injection of a substantial component of large-orbit ions into a separately formed FRC, or possibly to form the FRC itself. Again, reliable 3D simulations would be

greatly advantageous to evaluate stability, energy loss and lifetime in advance of any experiment. The final period of the FIREX experiment was devoted to testing the axial ring-FRC merging scenario suggested by 2D simulations, which was not borne out. In retrospect, a further development of the radial scheme might have pointed the way toward real progress.

References

1. J. M. Finn and R. N. Sudan, Nuclear Fusion **22**(11), 1143 (1982).

2. R.N. Sudan, "Particle Ring Fusion" in **Unconventional Approaches to Fusion**, Ettore Majorana International Science Series, B. Brunelli and G.G.Leotta, Eds. (Plenum, New York, 1982).

3. L. Steinhauer, et al., "FRC 2001: A White Paper on FRC Development in the Next Five Years", Fusion Technology 1996.

4. R.N. Sudan, Laser and Particle Beams **11**, 415 (1993).

5. A. Friedman, R.N. Sudan and J. Denavit, Phys. Fluids 29(10), 3317 (1986).

6. C.E. Seyler, J.F.Krall, L.Sparks and R.N. Sudan, Nucl. Fusion 24, 1013 (1984).

7. J. Krall, C.E. Seyler and R.N. Sudan, Phys Fluids B 3, 1015 (1991).

8. D. C. Barnes, J.L. Schwartzmeier, H.R. Lewis and C.E. Seyler, Phys. Fluids 29, 2617 (1986).

9. D. C. Barnes and R.D. Milroy, Phys. Fluids B 3, 2609 (1991).

10. E. Schamiloglu, J.B. Greenly, and D.A. Hammer, Applied Physics Letters **55**(26) 2727 (1989).

11. Yu.A. Omelchenko and R.N. Sudan, Phys. Plasmas **2**(7), 2773 (1995)

12. Yu.A. Omelchenko and R.N. Sudan, J. Computational Physics 133, 146 (1997).

13. H.L. Berk and L.D. Pearlstein, Phys. Fluids 19, 1831 (1976).

14. B.V. Oliver, P.F. Ottinger, D.V. Rose, D.D. Hinshelwood, J.M. Neri and F.C.Young, Phys. Plasmas 6 (2) 582 (1999).

15. A.V. Gordeev and A.V. Gretchikha, Sov.J. Plasma Physics 18(1) 1 (1992).

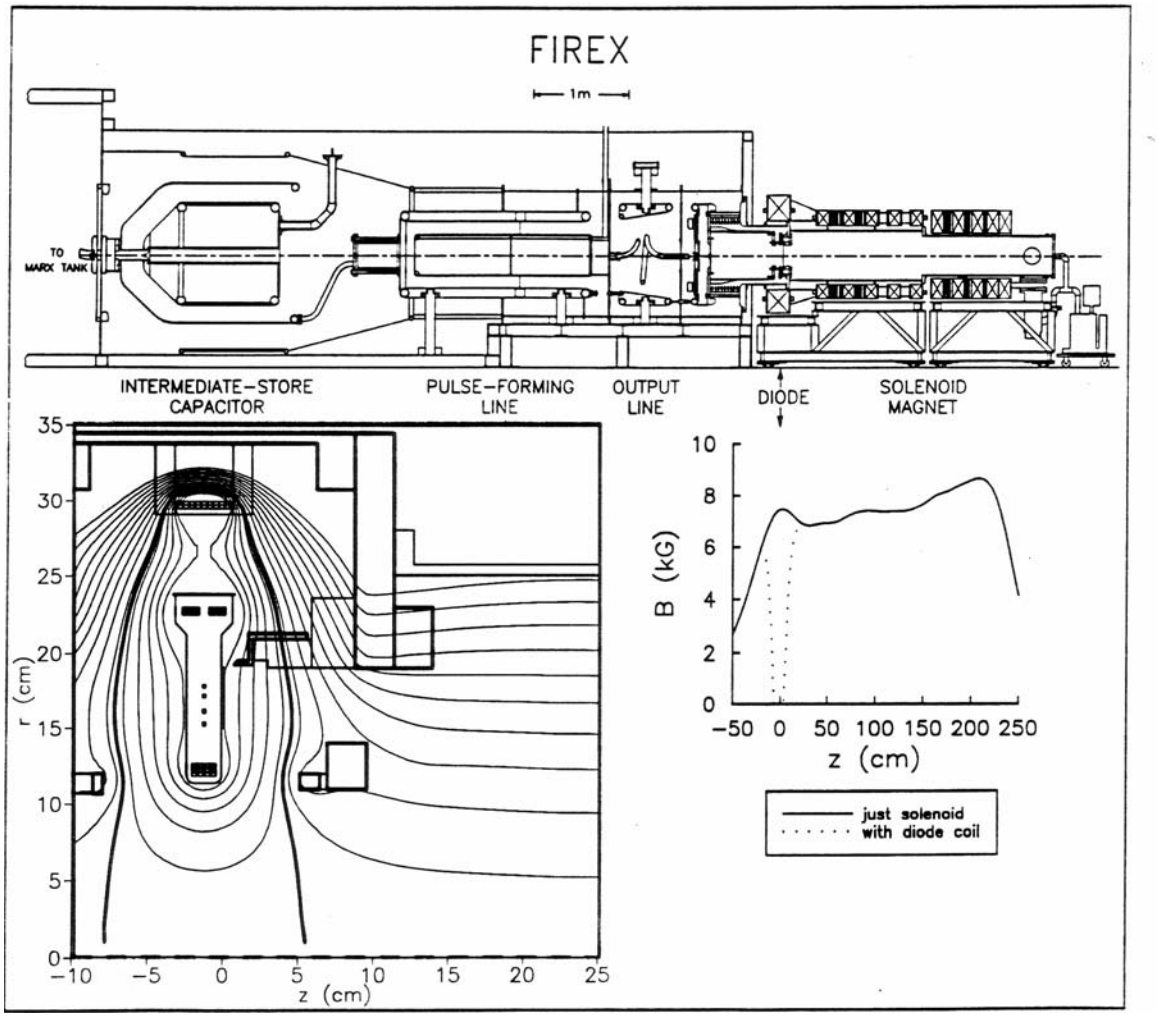

Figure 1. Above, schematic of FIREX system, from left to right showing Marx generator (off picture to left), water pulse-forming section, water-vacuum interface (between output line and diode), ion diode, vacuum vessel and solenoid.
Below left: final FIREX diode configuration with separate coils in anode and at wall, as well as partially penetrable flux-shaping elements. Below right: FIREX magnetic field profile on axis, showing diode, cusp and solenoid field regions.

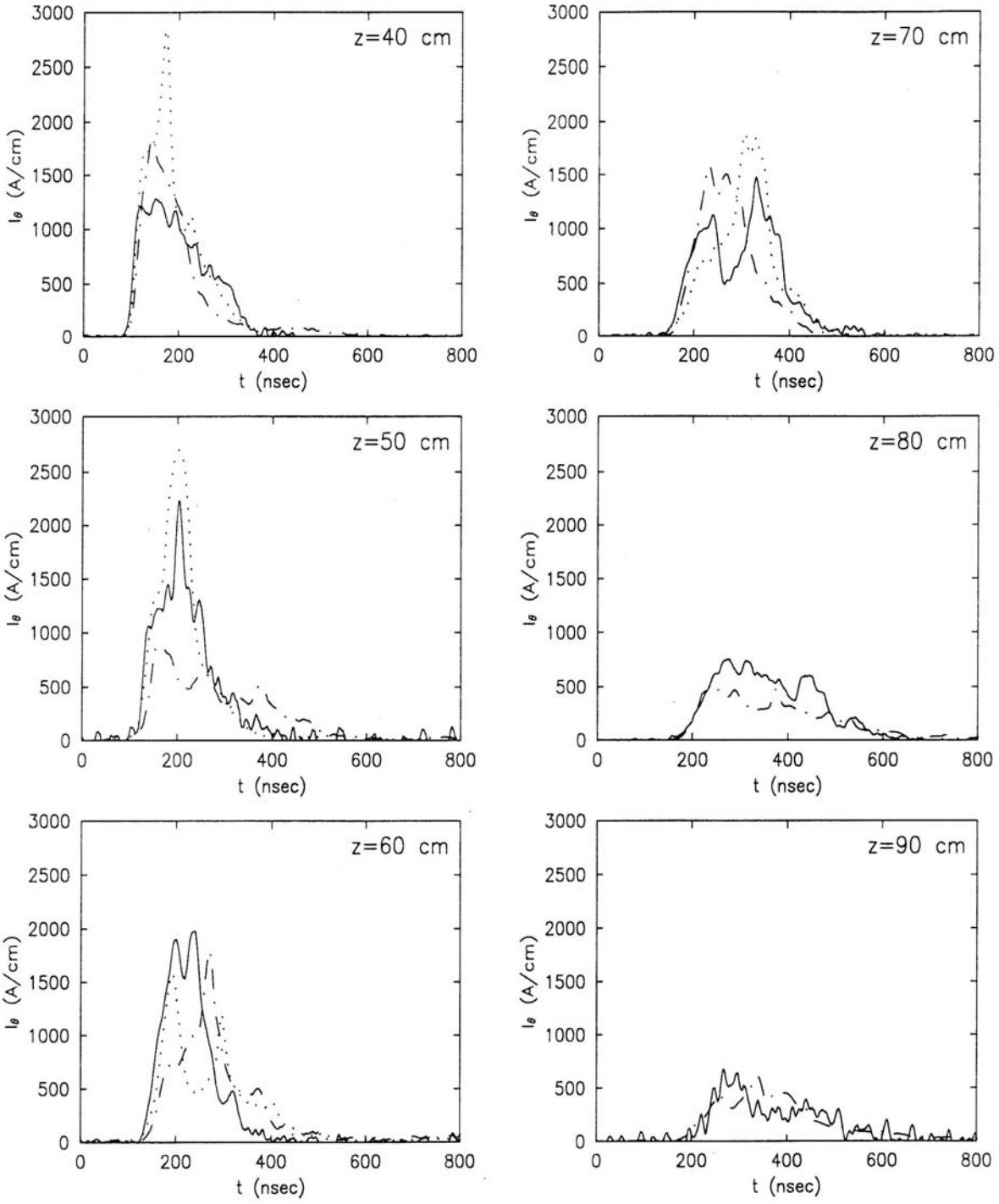

Figure 2. Faraday wand data for a pulse into low-density plasma from three of the four azimuthal locations where wands are located. Data from the fourth location are not shown here because they are collimated as described in the text. See Figure 4 for a comparison of data from collimated and uncollimated wands.

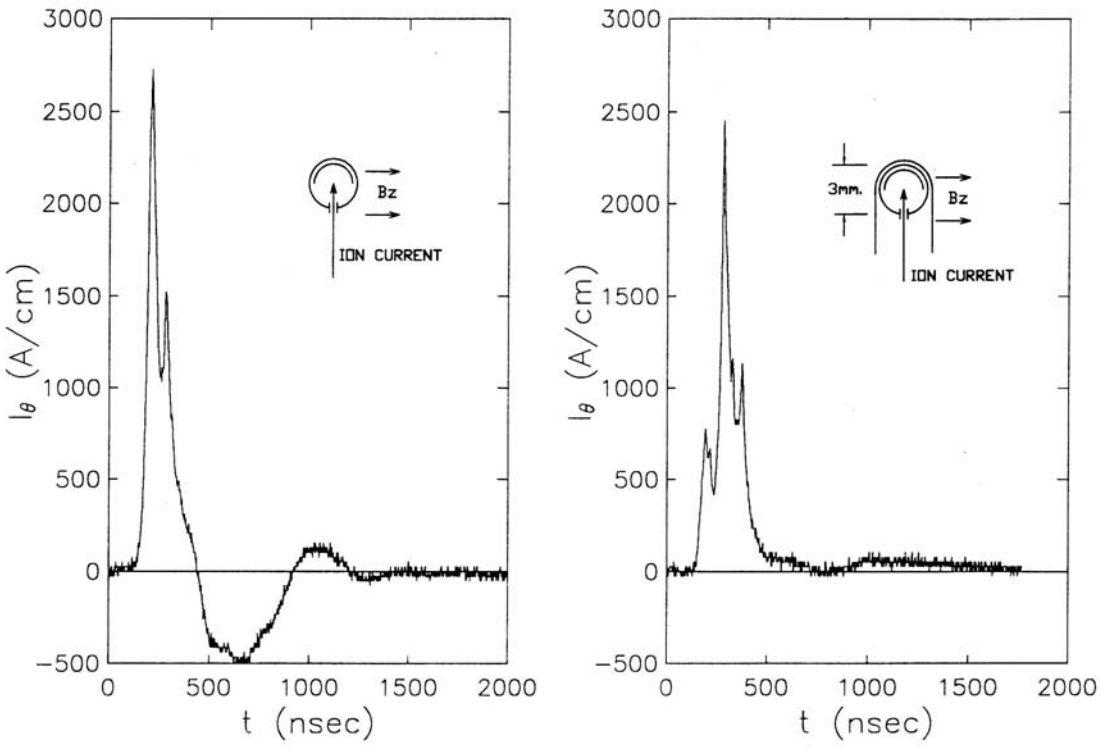

Figure 3. Data from Faraday wands without (left) and with (right) additional shielding from electric fields. The sketches show the configurations, with the direction of the applied solenoid field (axial), and the direction of ion ring current (azimuthal). It is seen that the shield nearly eliminates as the oscillations after the ring current peak. These oscillations correspond to the Alfven wave in the plasma.

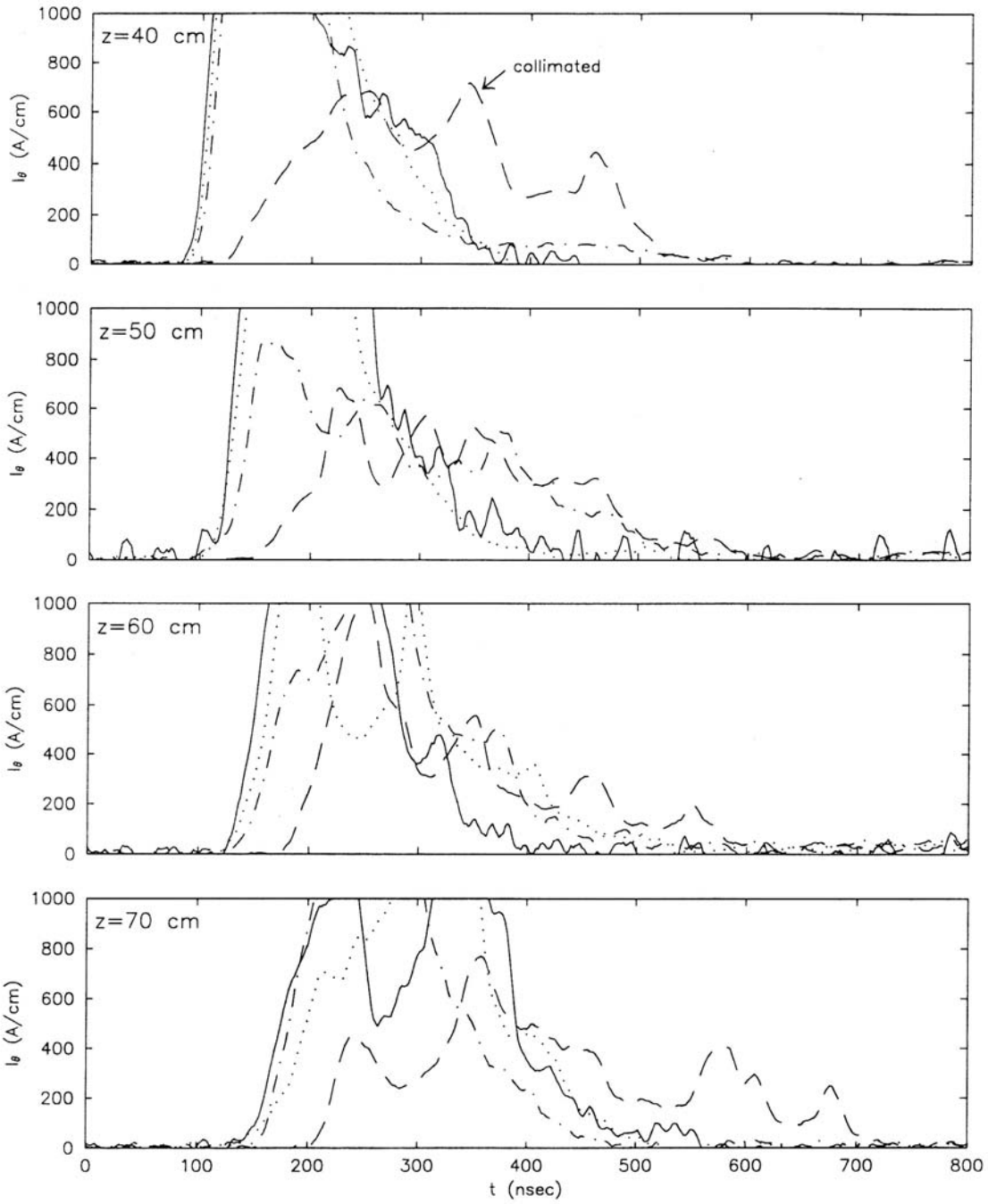

Figure 4. The effect of hole closure on Faraday wand signals. The dashed curves are the signals from wands collimated to eliminate the early part of the incoming ring; the other curves are from three uncollimated wands at the same axial but different azimuthal locations. The collimated signals in some cases have significantly longer duration.

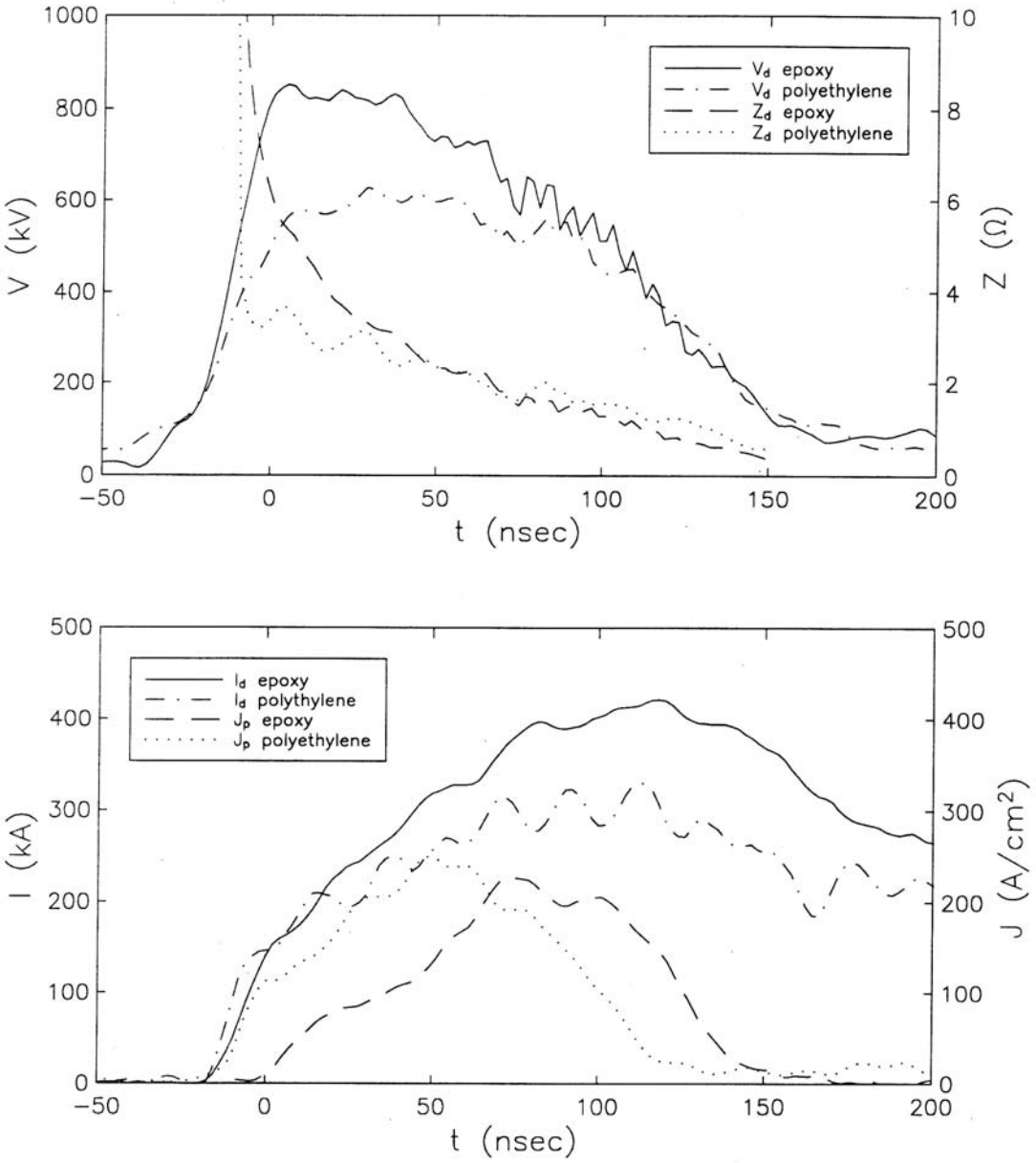

Figure 5. Comparison of epoxy and polyethylene anode ion sources. Bottom: Id is total diode current, Jp is ion current density from the diode. Ion current begins more promptly with polyethylene. Top: Vd is diode voltage, Zd is diode impedance. Impedance drops to good working level faster with polyethylene, holding the early voltage down and producing a much flatter voltage pulse shape.

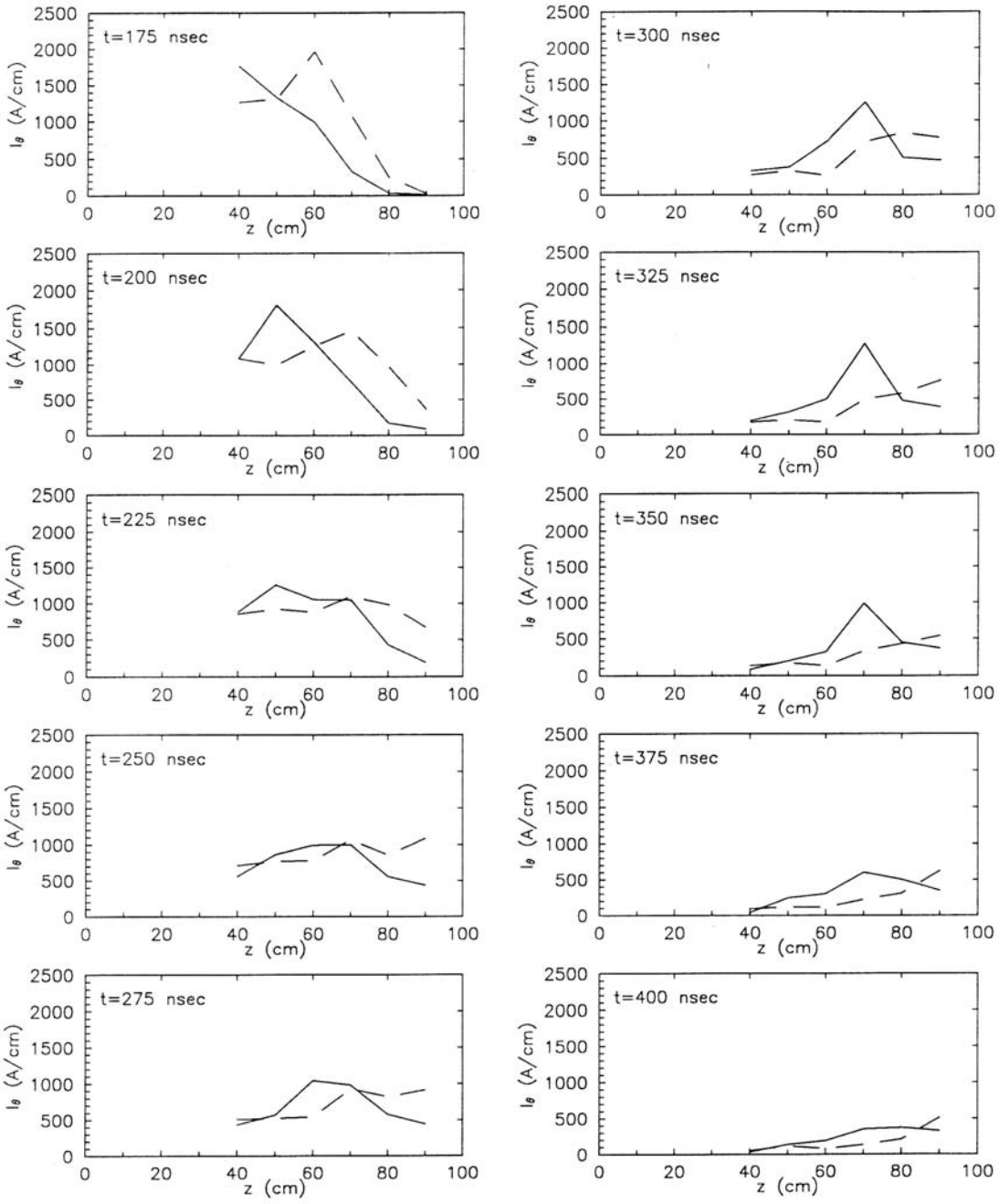

Figure 6. Comparison of ring stopping in different background plasma conditions. Dashed curves are Faraday wand data from injection into 200 mTorr hydrogen gas. Solid curves are injection into the puff plus 2 mTorr preionized hydrogen. Axial slowing is evident in the 2 mTorr case, with a significant fraction of the ring stopping in an axially compact distribution near z=70 cm.

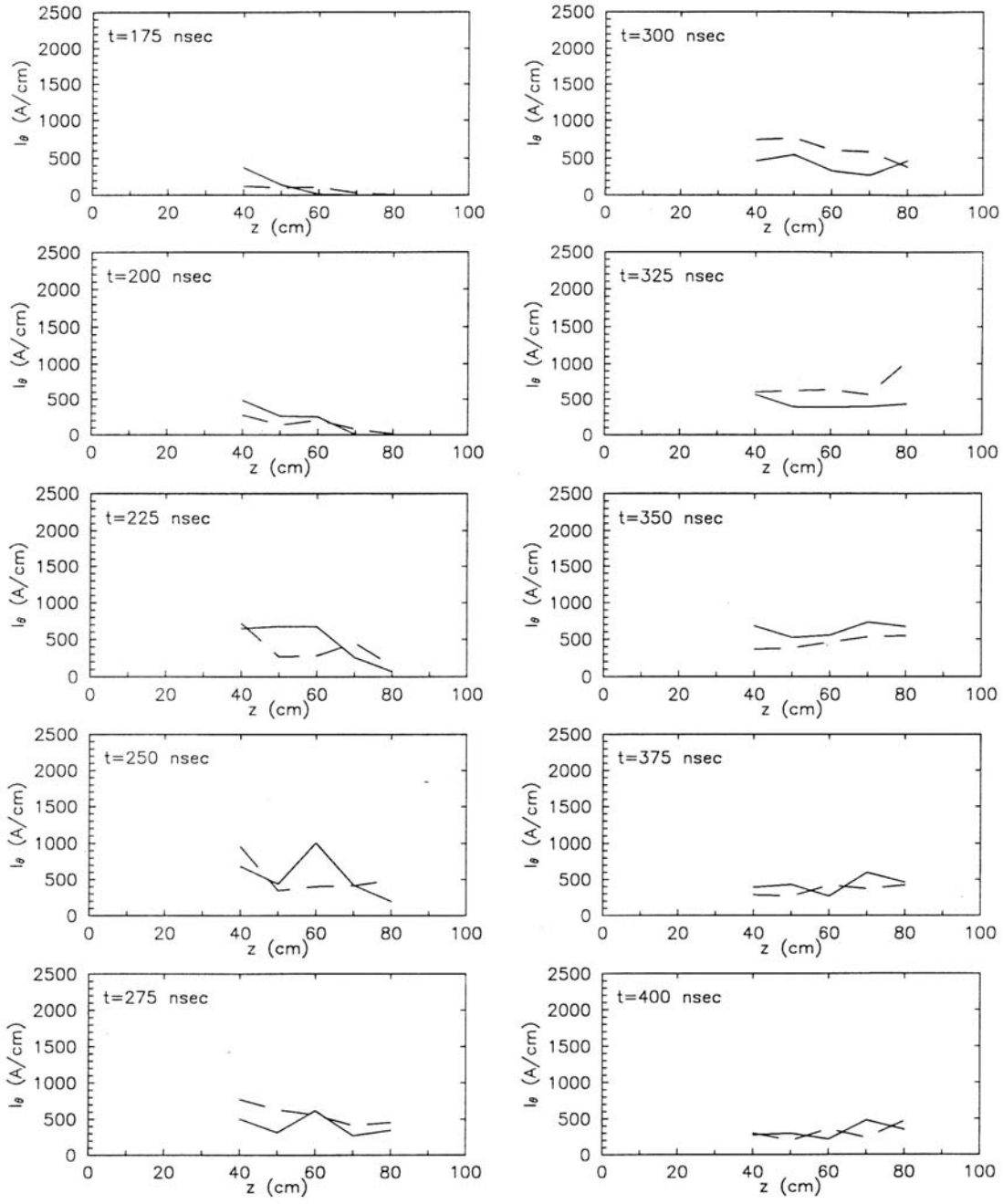

Figure 7. Comparison of 200 mTorr gas (dashed curves) with 2 mTorr preionized hydrogen (solid curves), as in Figure 6, but using collimated Faraday wands with less tendency to hole closure late in time.

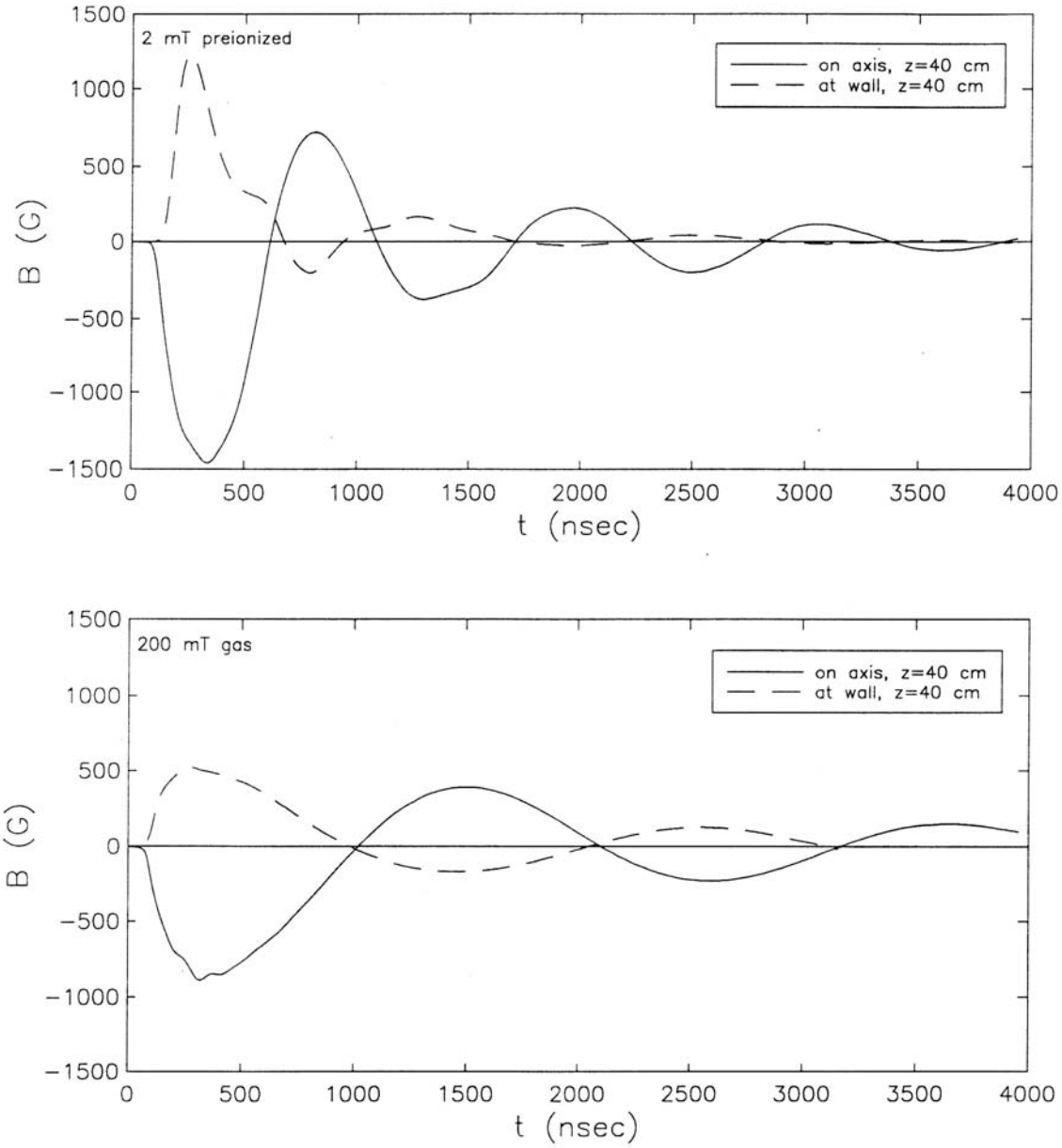

Figure 8. Ring diamagnetic signals in low (top) and high (bottom) density backgrounds, corresponding to the two cases in Table 1.

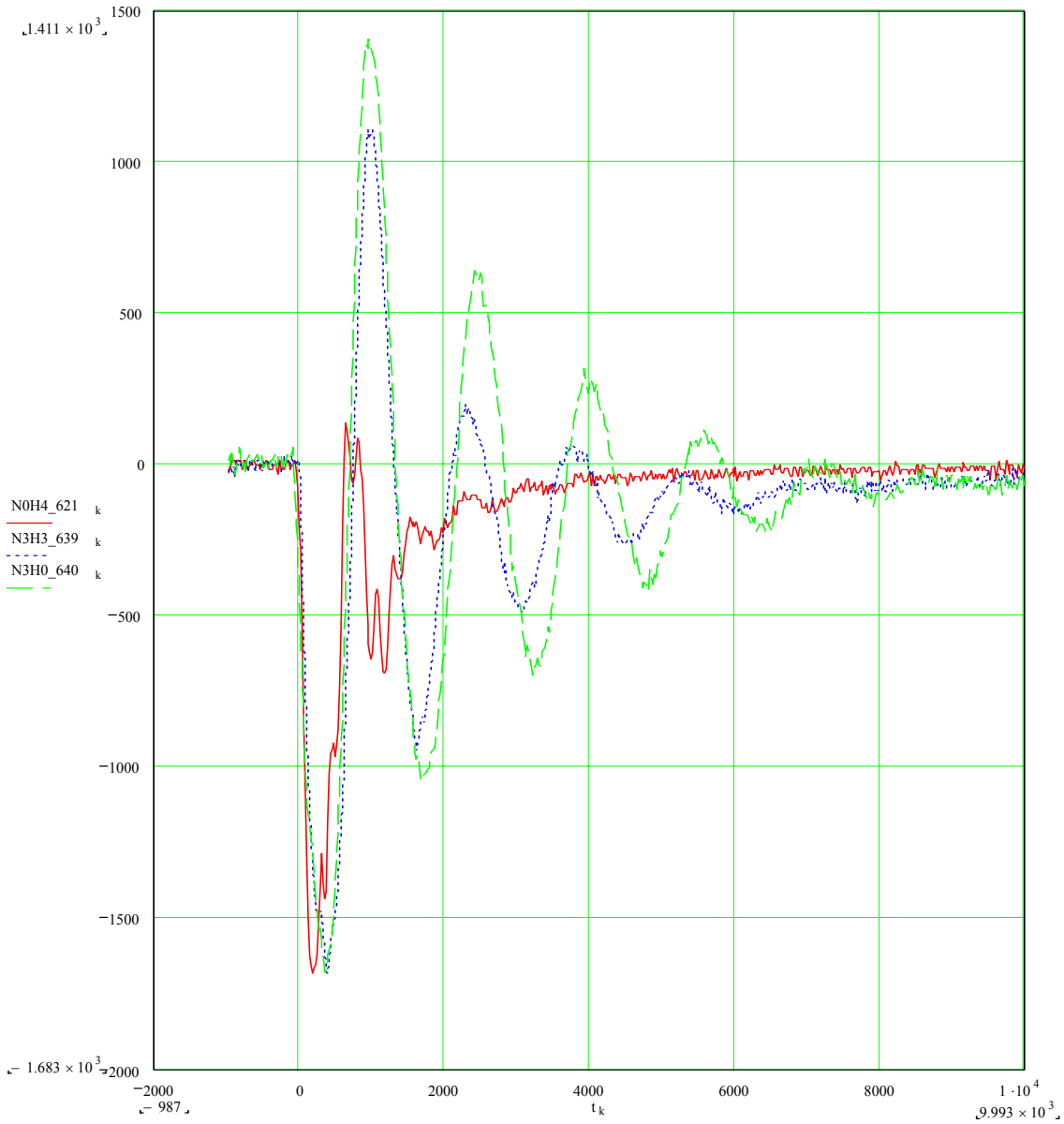

Figure 9. Comparison of magnetic field on axis at z=60 cm, for three pulses with similar injected ring current into preionized background plasma. Solid line is 4mTorr hydrogen, dotted line is 3 mTorr hydrogen plus 3 mTorr nitrogen, and dashed line is 3 mTorr nitrogen. The dominant low-frequency Alfven oscillation is damped most heavily in pure hydrogen, less heavily in the mixed fill, and least heavily in pure nitrogen. Higher frequency wave activity is more evident in pure hydrogen, an indication of the stronger instability in that background with the highest Alfven speed and lowest M_A of the ring.

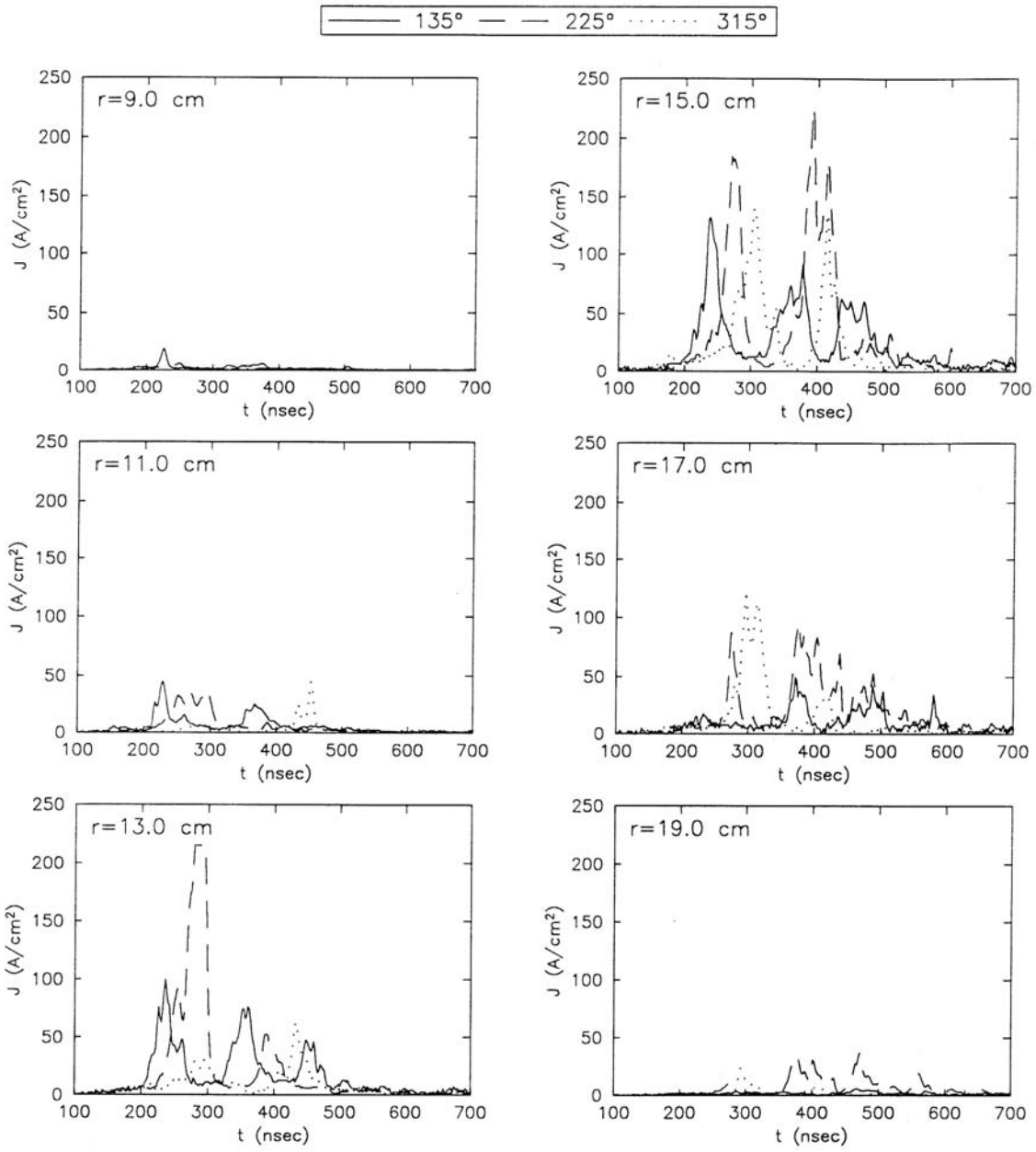

Figure 10. Azimuthal asymmetry of rings produced by the FIREX diode with the early coil design. Ion collector signals from three radial arrays at z=100 cm, separated azimuthally by 90 degrees. The ring rotates from the 135 to the 315 degree location.

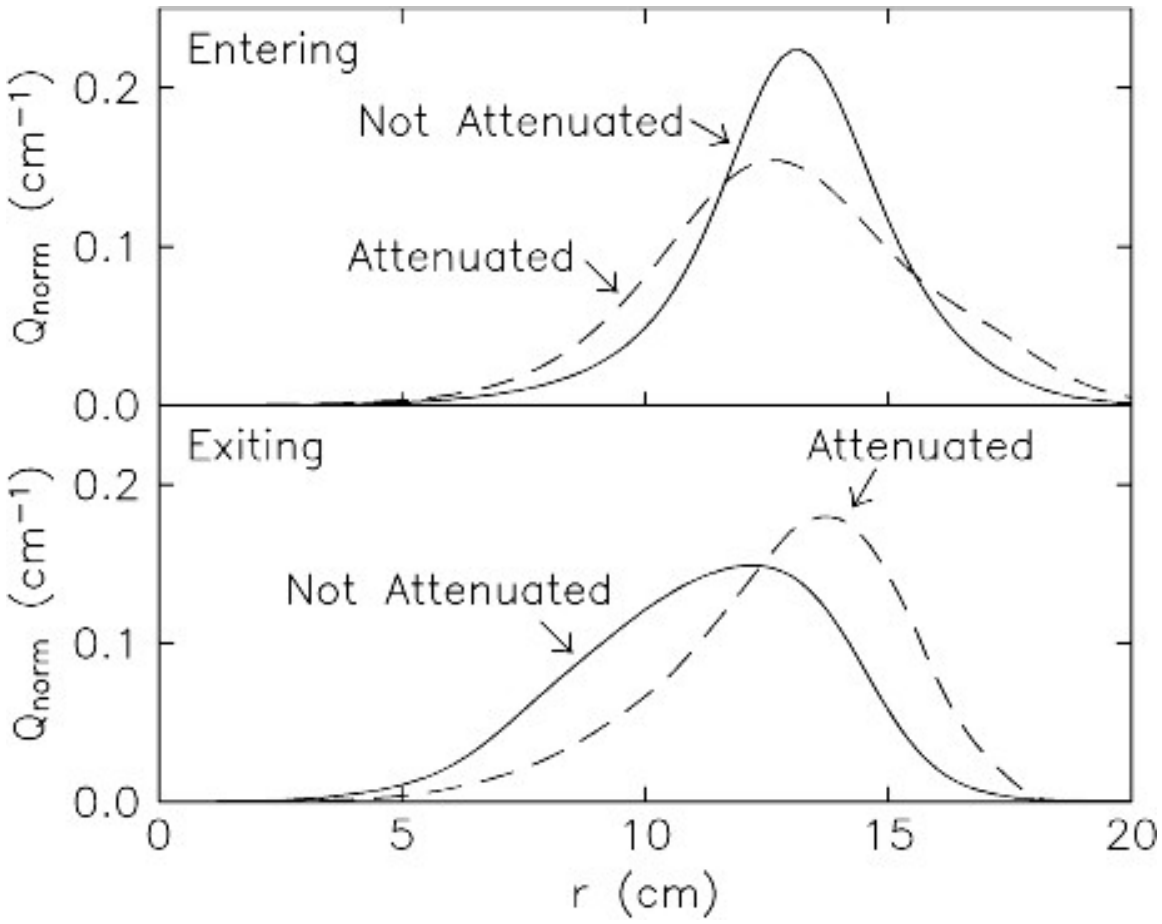

Figure 11. Comparison of the radial distribution of charge of the proton ring as it enters the solenoid with the radial distribution downstream, after the ring has interacted with the plasma. The figure compares data for typical strong rings with "attenuated beam" cases in which the ring is reduced in current by more than a factor of five. The data are normalized to the same total charge (integrated over radius and circumference) for comparison. Qnorm is in units of charge per cm of radius (integrated over the circumference). The incoming ring has essentially the same radial distribution for the full-strength and attenuated cases, the downstream profiles are different: the strong rings have moved radially inward compared with the weak rings. Mean radius of ring charge distribution is at 13.2 cm for the weak ring, 11.4 cm for strong ring.

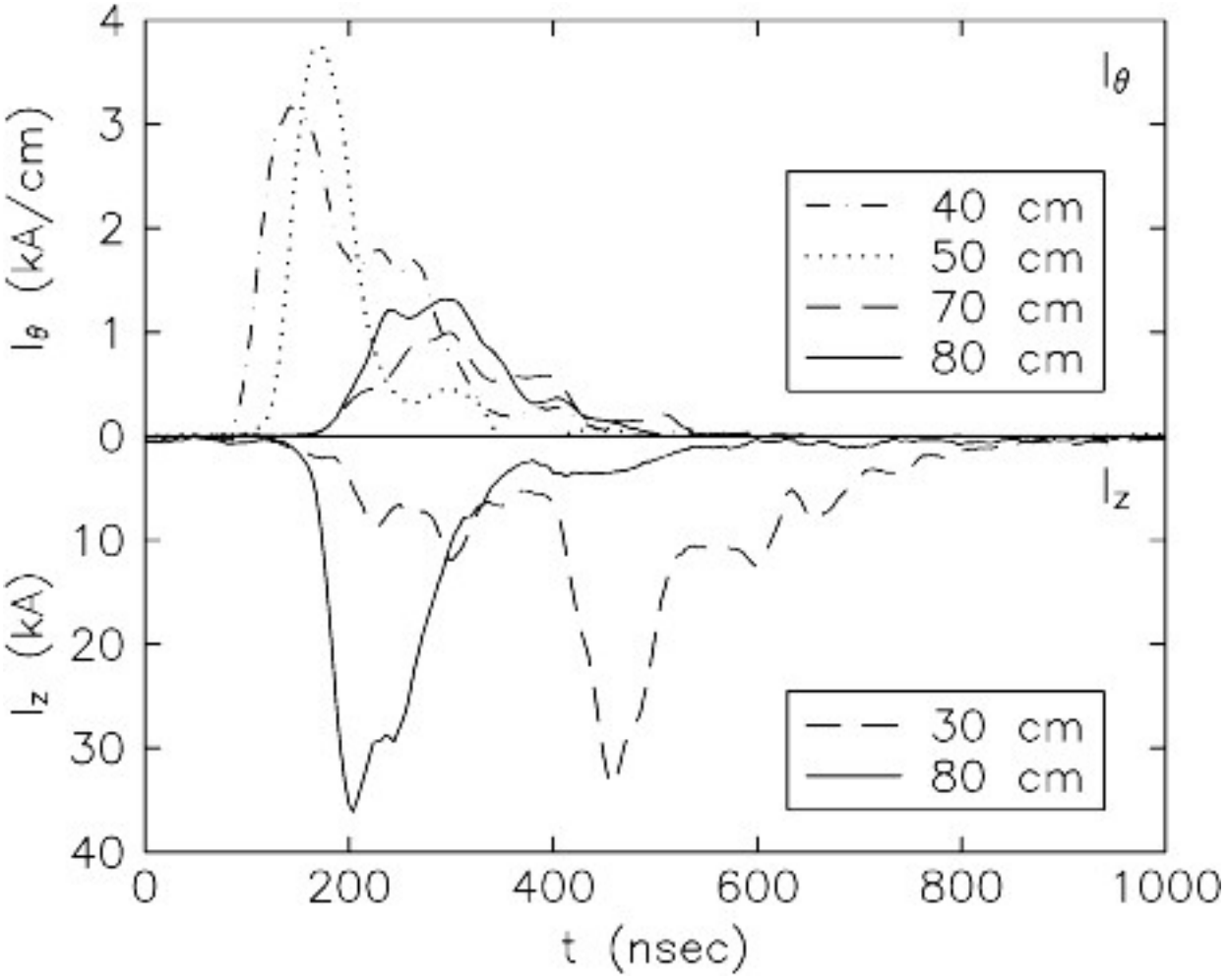

Figure 12. Data for a shot into 1 mTorr preionized hydrogen. The azimuthal and axial components of ring current density are shown, measured at the zxial locations indicated. The Iz diagnostics at the 30 and 80 cm locations are arrays of collectors oriented to measure ring protons that are leaving the solenoid in the upstream and downstream directions respectively.

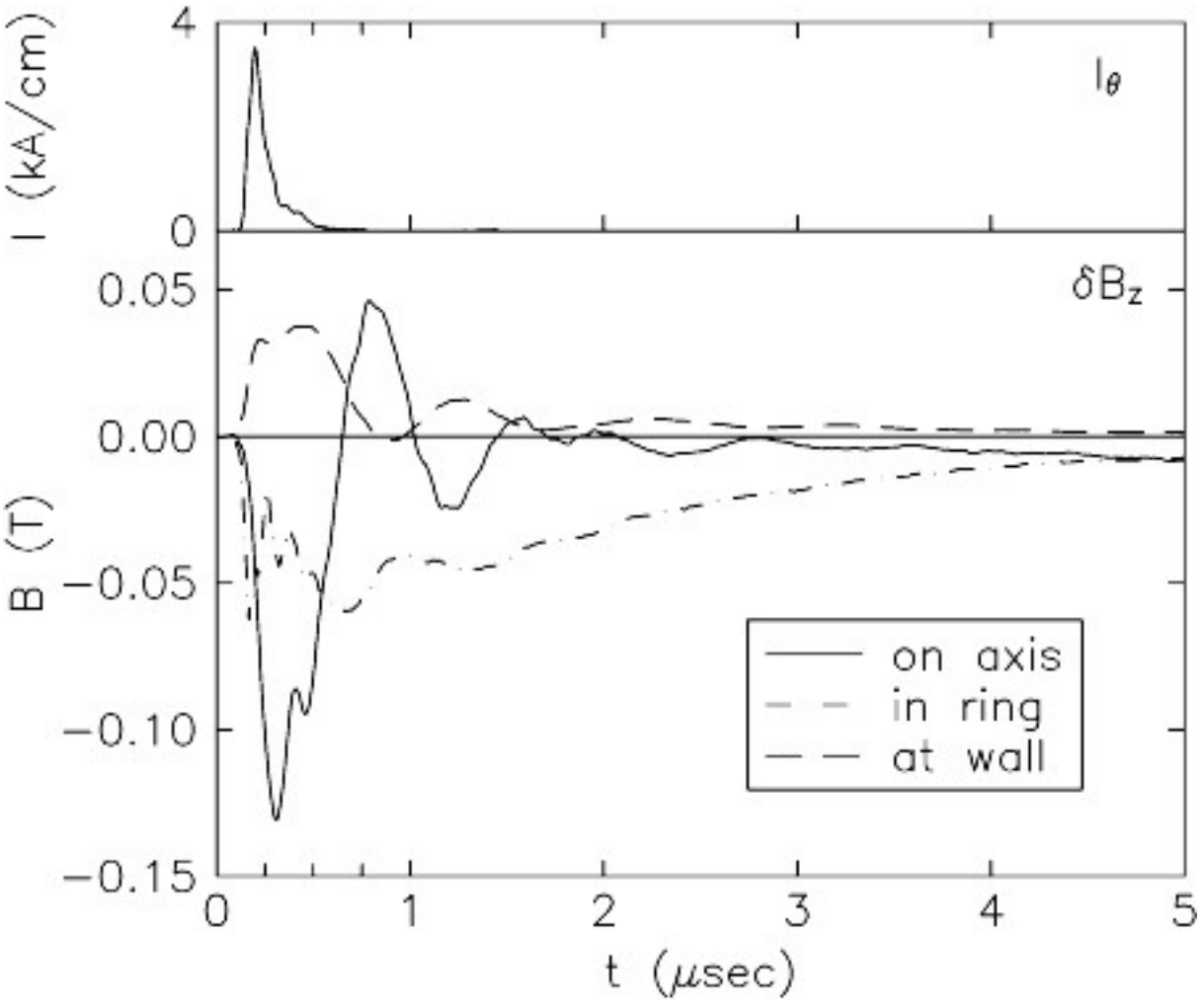

Figure 13. Typical data for strong FIREX ring. Upper trace: ring current density azimuthal component. Lower traces: ring diamagnetism on axis, in the ring annulus at 13 cm radius, and at the chamber wall. Note the much greater duration of the signal in the ring, and also the higher frequency components during the first 0.5 μs while the ring protons are present.

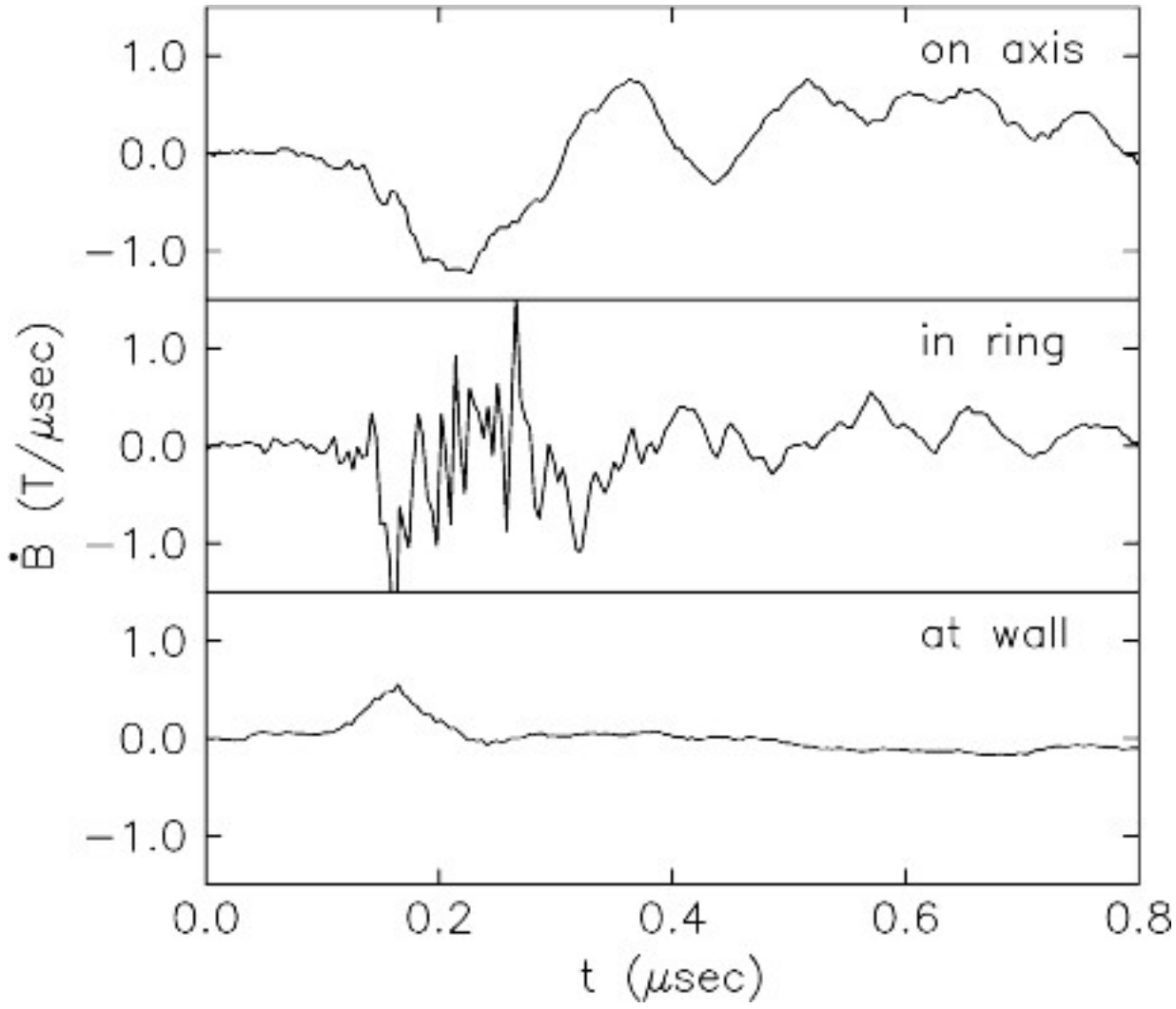

Figure 14. dB/dt sampled on axis, in the ring at 13 cm radius, and at the wall, to show more clearly the high-frequency content of the magnetic field changes in the ring. The spectrum in the ring is dominated by frequencies higher than the ion gyrofrequency (ion gyroperiod is 0.11 μs), while both inside and outside the ring annulus, the dominant frequency is the lowest radial Alfven mode of the column, which is somewhat less than the gyrofrequency.

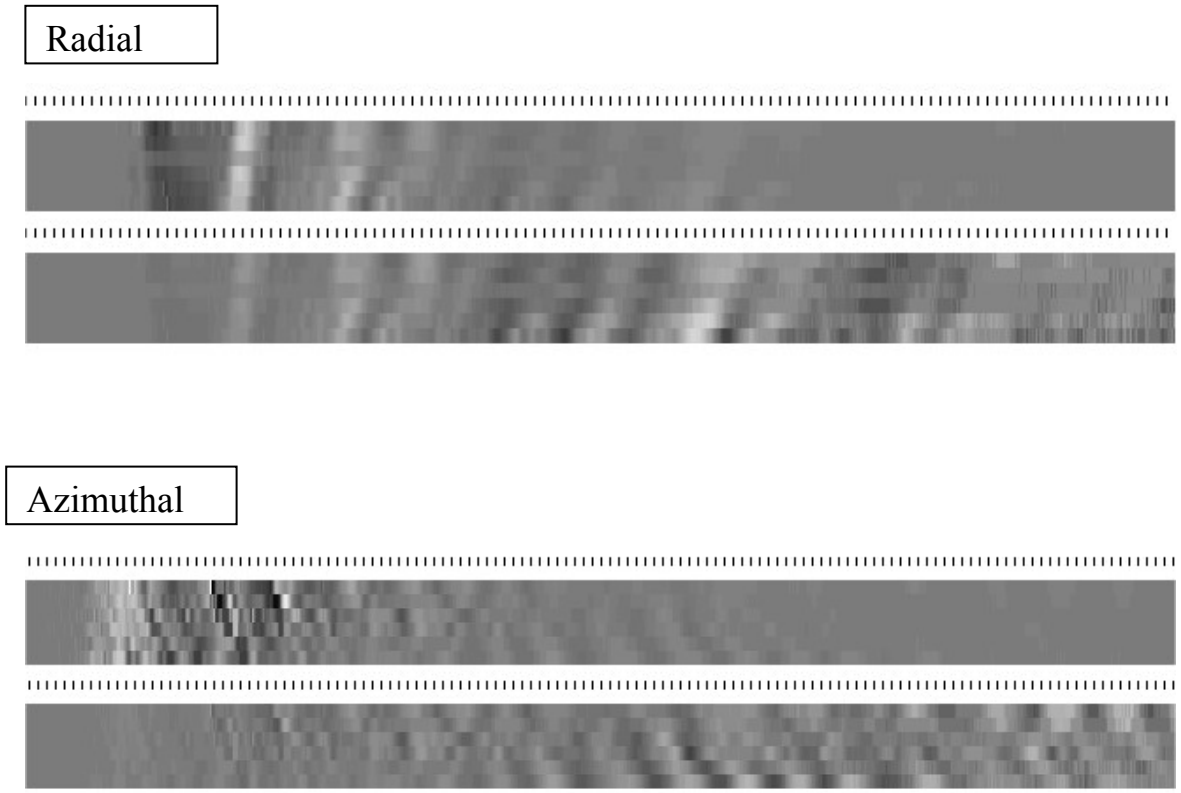

Figure 15. Visualizations of dB/dt data from closely-spaced (2 cm spacing) arrays of probes. Six probes were arrayed in the radial (upper pair of pictures) and azimuthal (lower pair of pictures) directions. The six stripes in each picture show the data from the six probes, with amplitude displayed as a greyscale. In each pair of pictures the lower one has its greyscale expanded exponentially in time to better show the small amplitude late in time. Time runs along the horizontal axis (small divisions are 10 ns). The different times of arrival of coherent wave structures as a function of position shows as a diagonal pattern in the amplitudes.

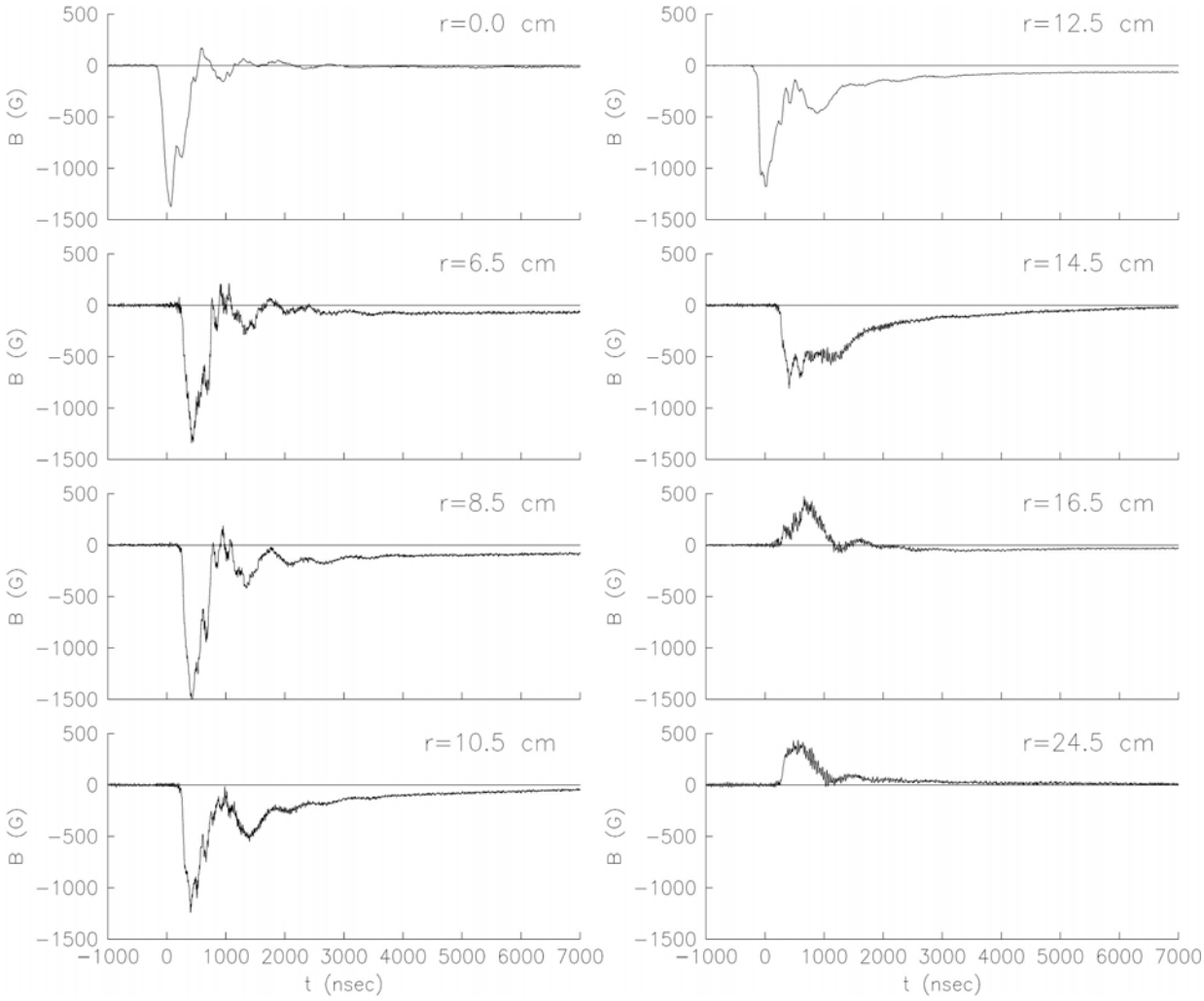

Figure 16. Data from a radial array of magnetic probes at the indicated radii, from axis to wall (25 cm). The probes at 10.5, 12.5 and 14.5 cm show slowly decaying signals consistent with plasma diamagnetism persisting after the ring has been lost.

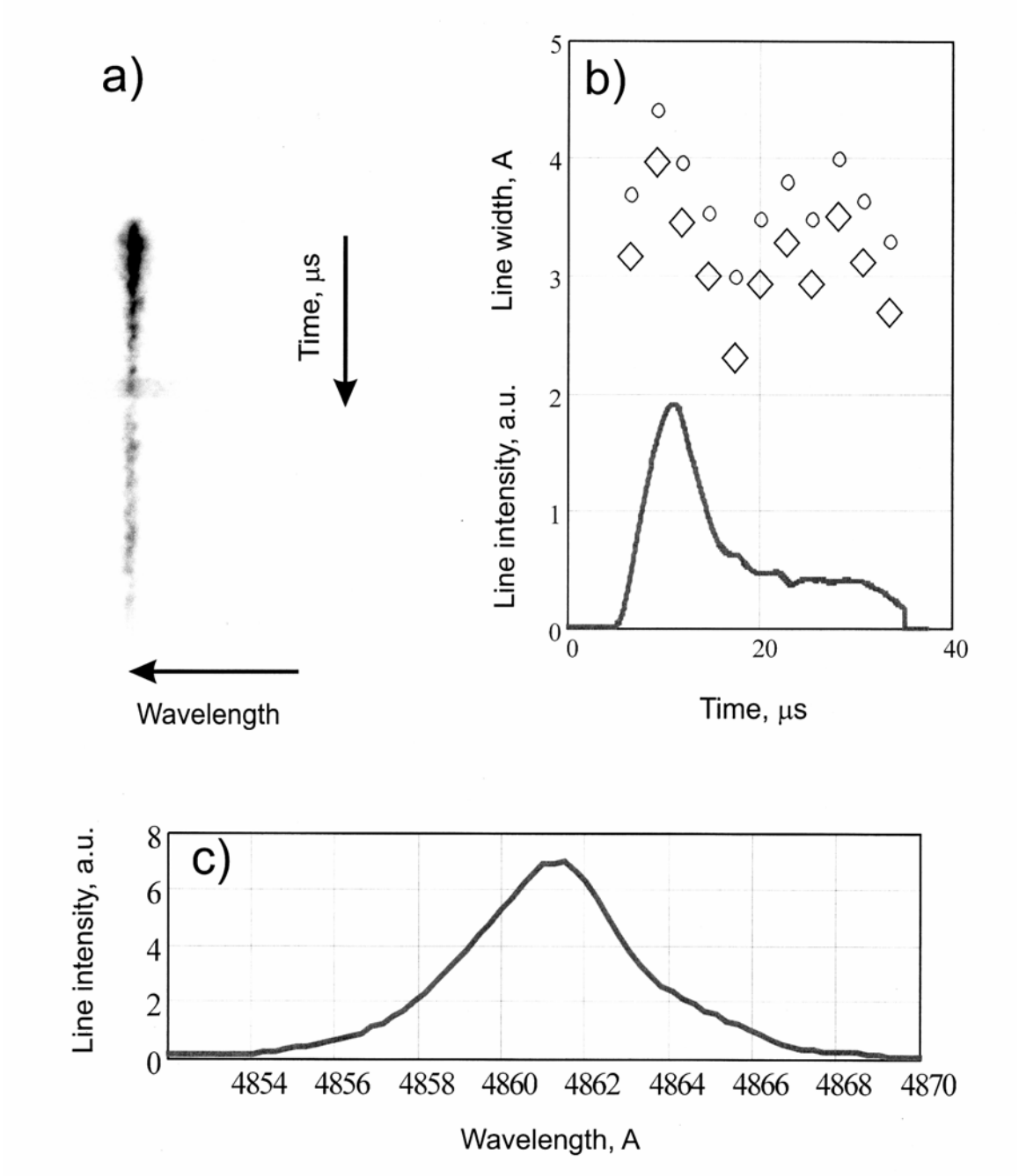

Figure 17. a) A streak of H_β lineshape as a function of time. b) from this streak image: measured line width in Angstroms (circles) and corrected for instrumental width (diamonds), and line intensity (arbitrary units). c) a sample of the line shape data from streak, at 9 μs , near peak width.

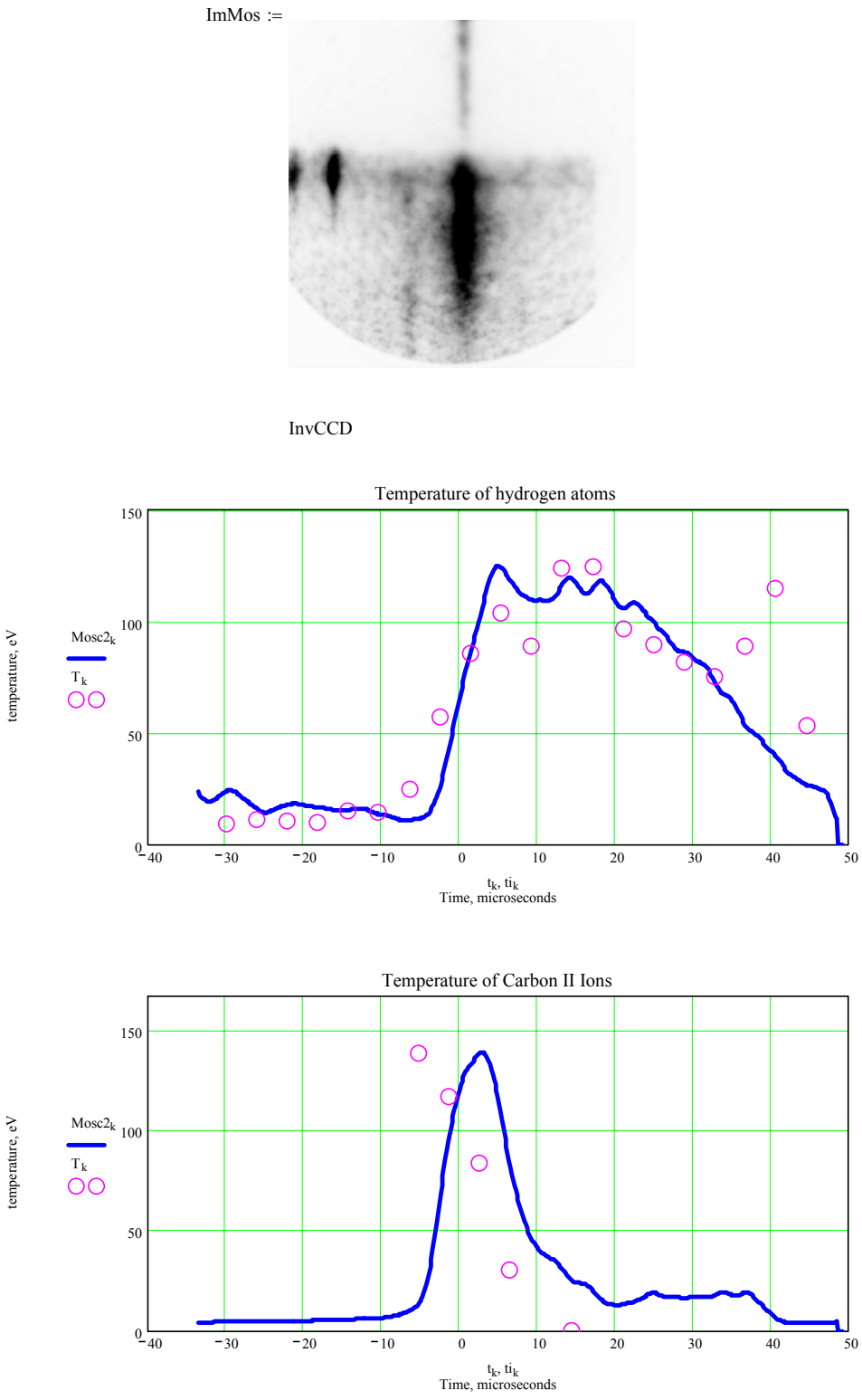

Figure 18. Typical spectroscopic data for ring injection into 1 mTorr hydrogen. Top: streak image. Upper plot: amplitude (line) and inferred temperature (circles) from Hb line. Lower plot: amplitude and inferred temperature for CII line. (time zero is arbitrary).

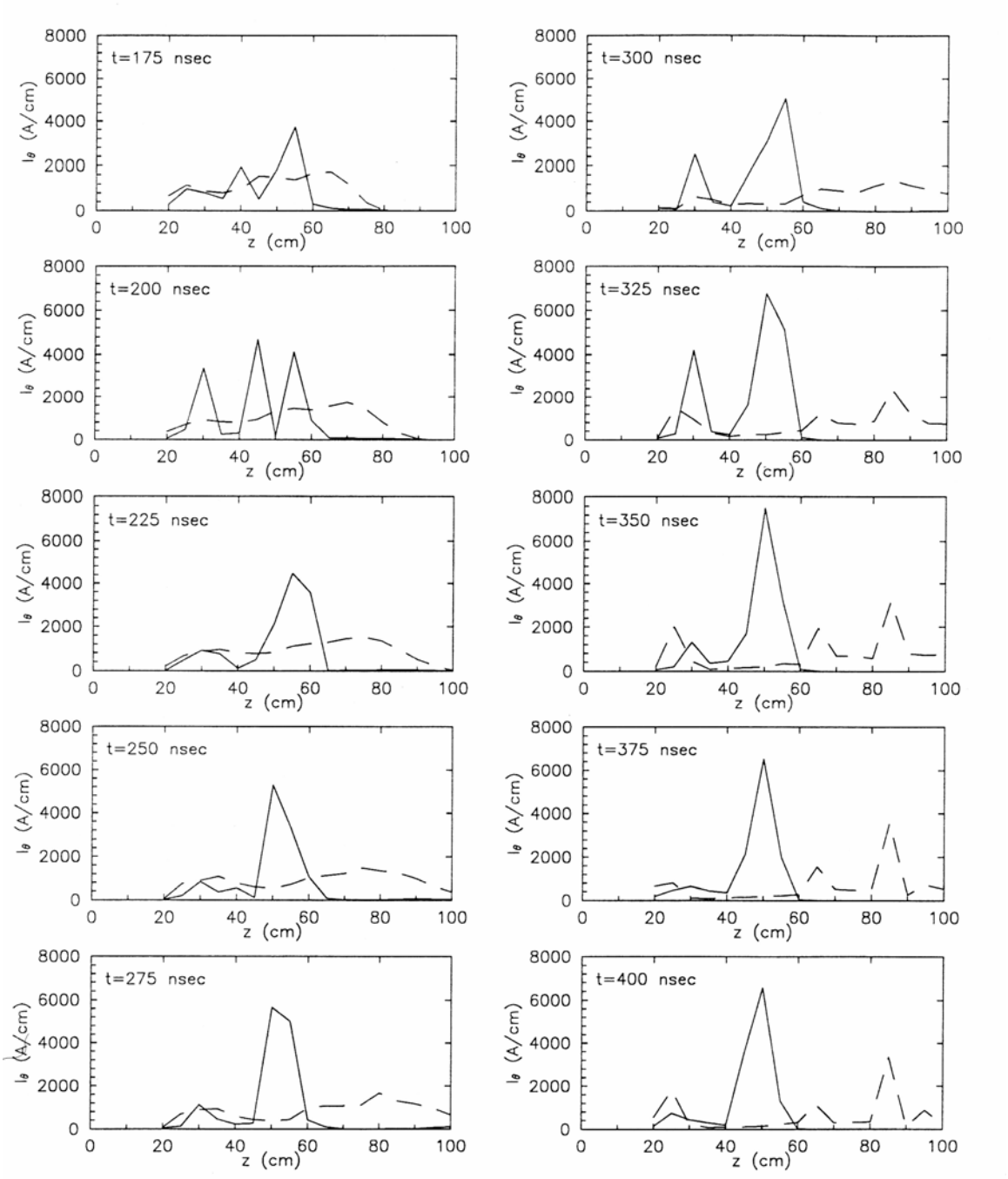

Figure 19. FIRE simulations. The dashed curves are for a uniform plasma density as estimated for conditions that apply in a shot into 200 mTorr hydrogen. The solid curves correspond to injection into fully-ionized 2 mTorr hydrogen. Compare with experimental data in Figures 6 and 7.

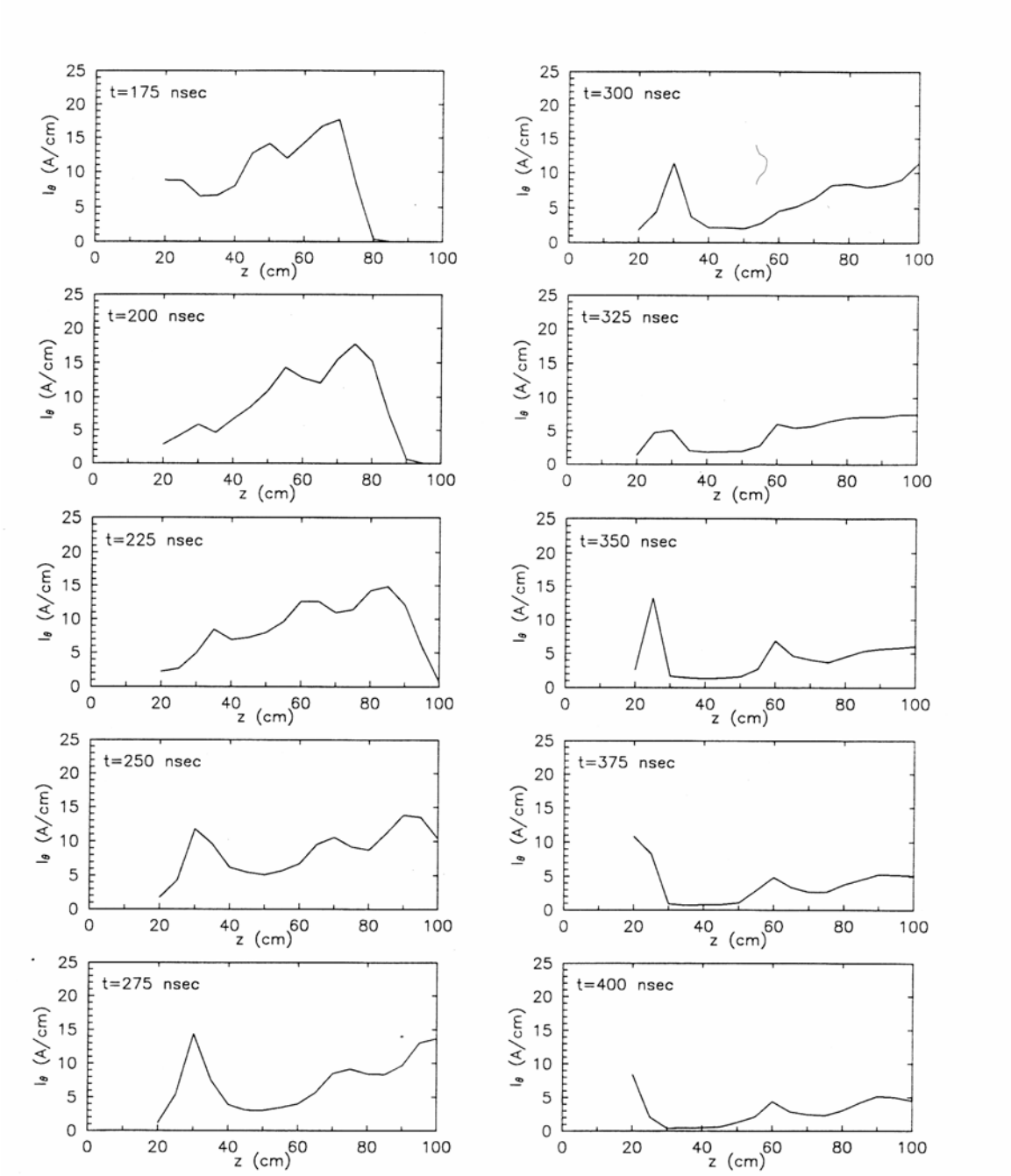

Figure 20. FIRE simulation of low-current ring injected into 2 mTorr preionized hydrogen. Compare with strong-ring case in Figure 19. In this case, except for a small component of the ring that stops at 20-30 cm and reflects, the ring does not stop, and exits downstream. Compare with experimental data of Figures 6 and 7.

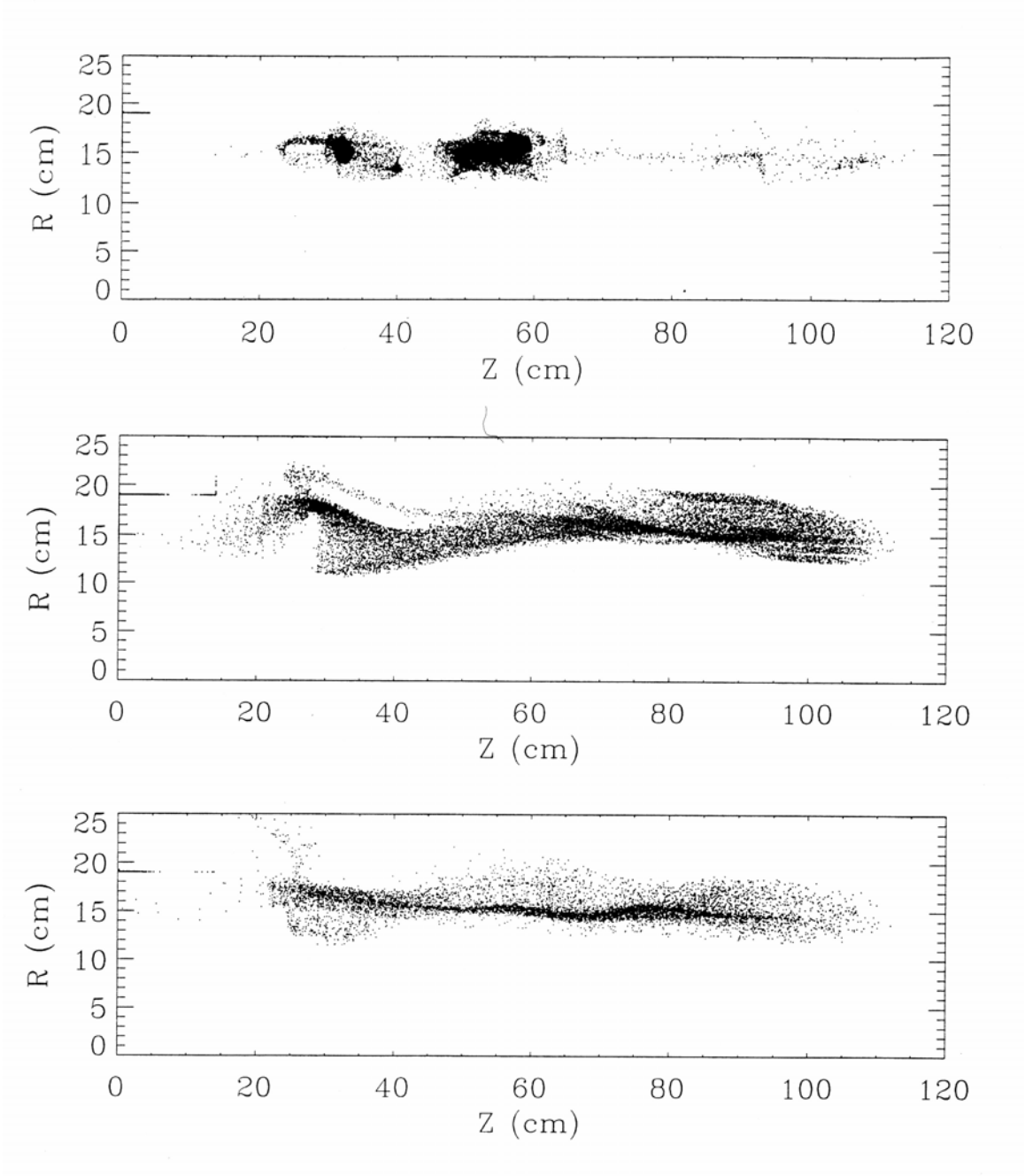

Figure 21. Snapshots of ring proton locations in (r,z) space from the FIRE simulations of Figures 19 and 20. Top: low density, strong ring case. Middle: high-density, strong ring case. Bottom: low-density, weak ring case. Stopping and ring axial self-confinement are evident in the strong ring, low-density case only.

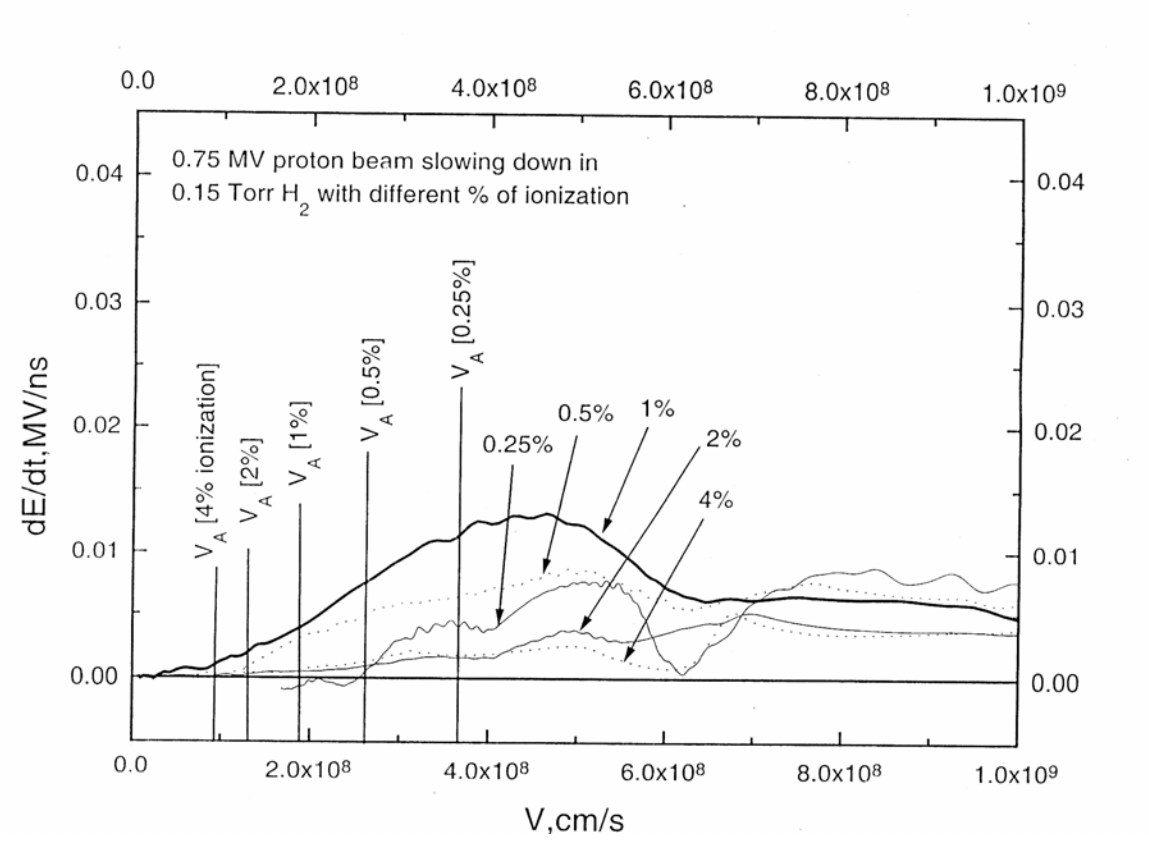

Figure 22. Axial energy loss rate for ring protons, in MeV/ns, as a function of ring axial velocity in different plasma densities. 4.4×10^8 cm/s is 100 keV energy for protons, the typical FIREX ring axial velocity. In all cases, the peak loss rate occurs for ring velocity above the Alfven speed, but the Alfven mach number of the peak dejpends upon the plasma density. The curves are parametrized by the percent ionization of a 150 mTorr hydrogen fill, and the corresponding Alfven speeds for the different cases are indicated along the velocity axis.

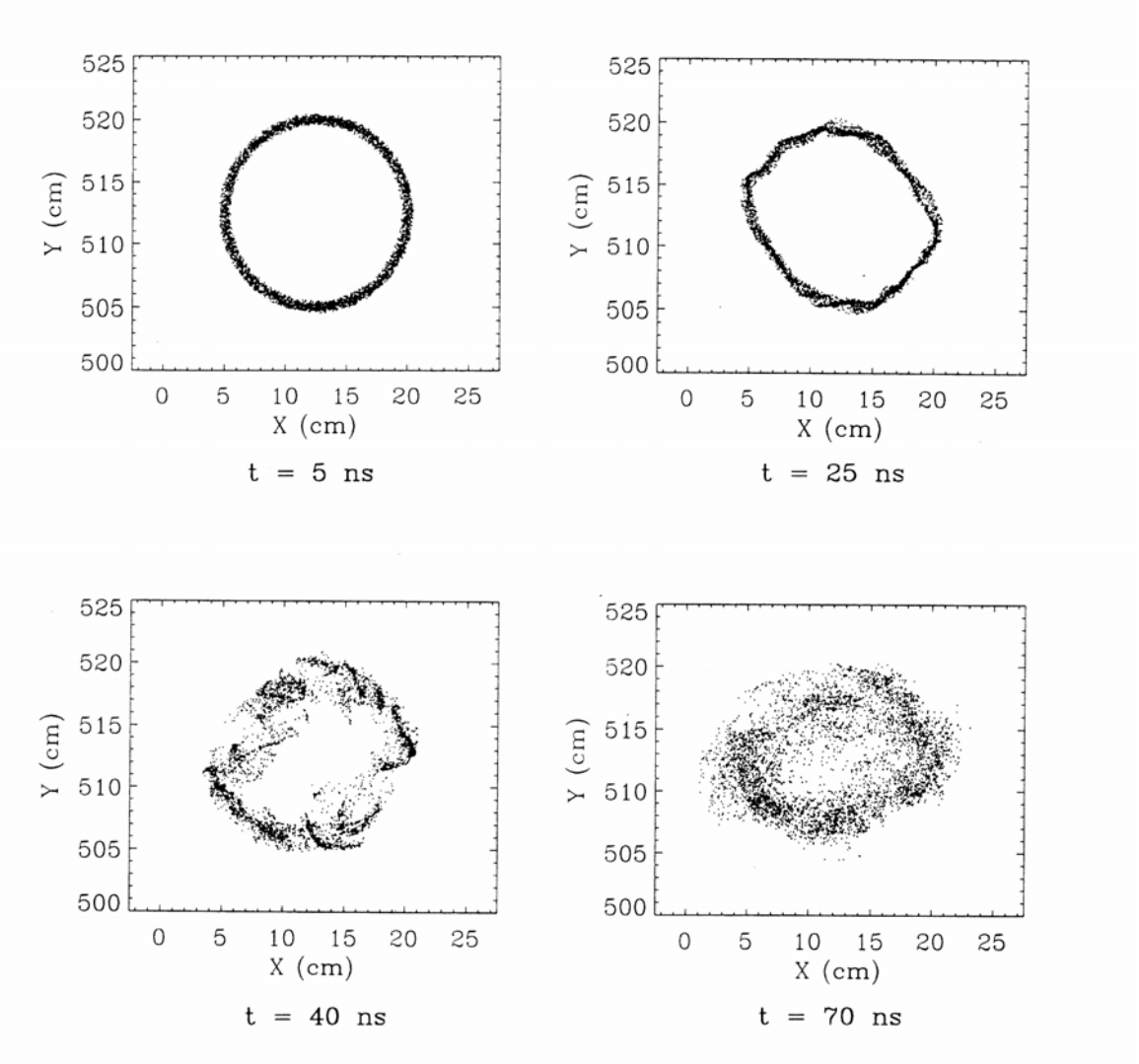

Figure 23. FIRE simulation in the (x,y) azimuthal plane of an initially thin ring in plasma, showing typical short-wavelength, high-order azimuthal modes growing unstably.

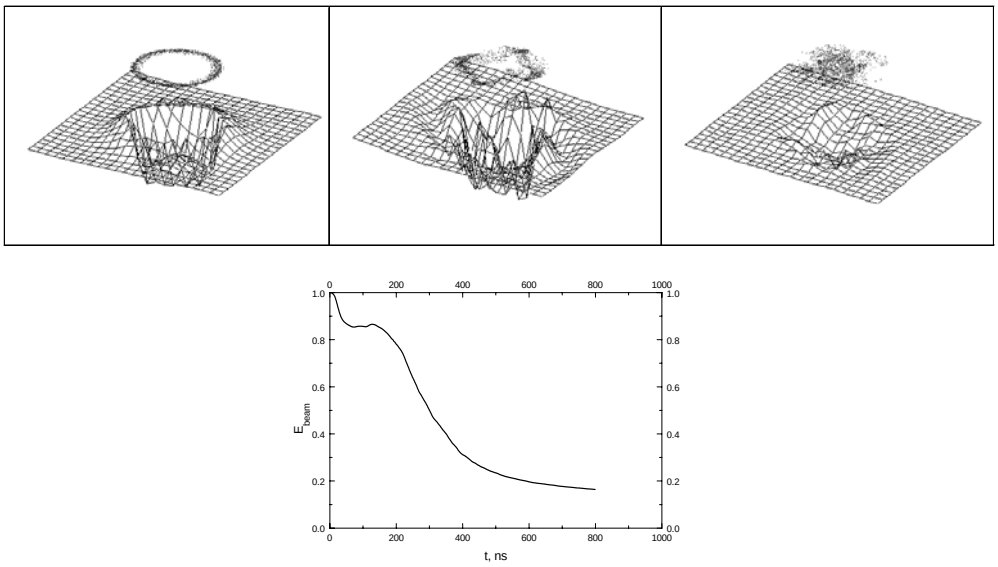

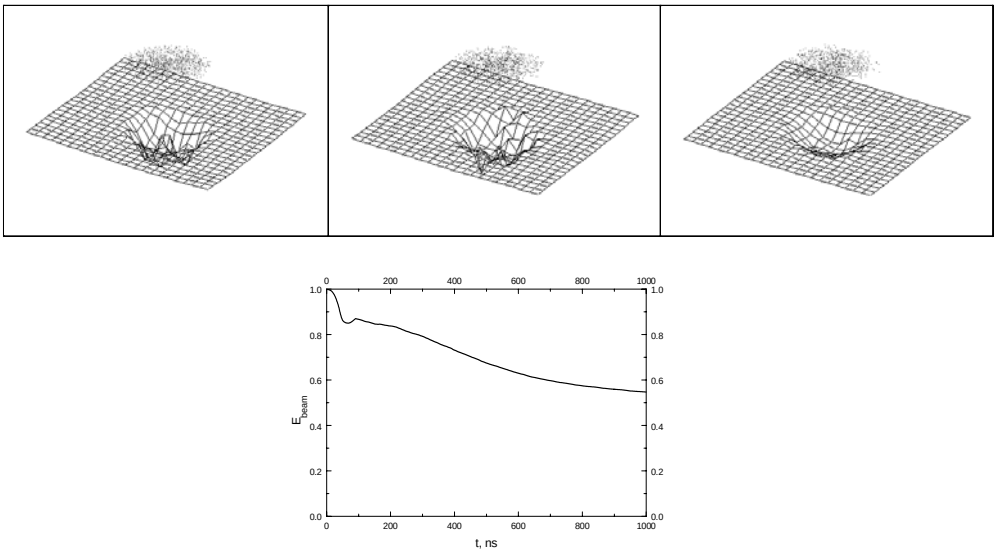

Figure 24. FIRE simulations of thin ring as in Figure 23 (upper) and of a radially thick ring with proton gyroradius about 1/2 of the ring radius (lower). The plots show ring energy versus time (ns). It is seen that the thick ring loses energy more slowly.

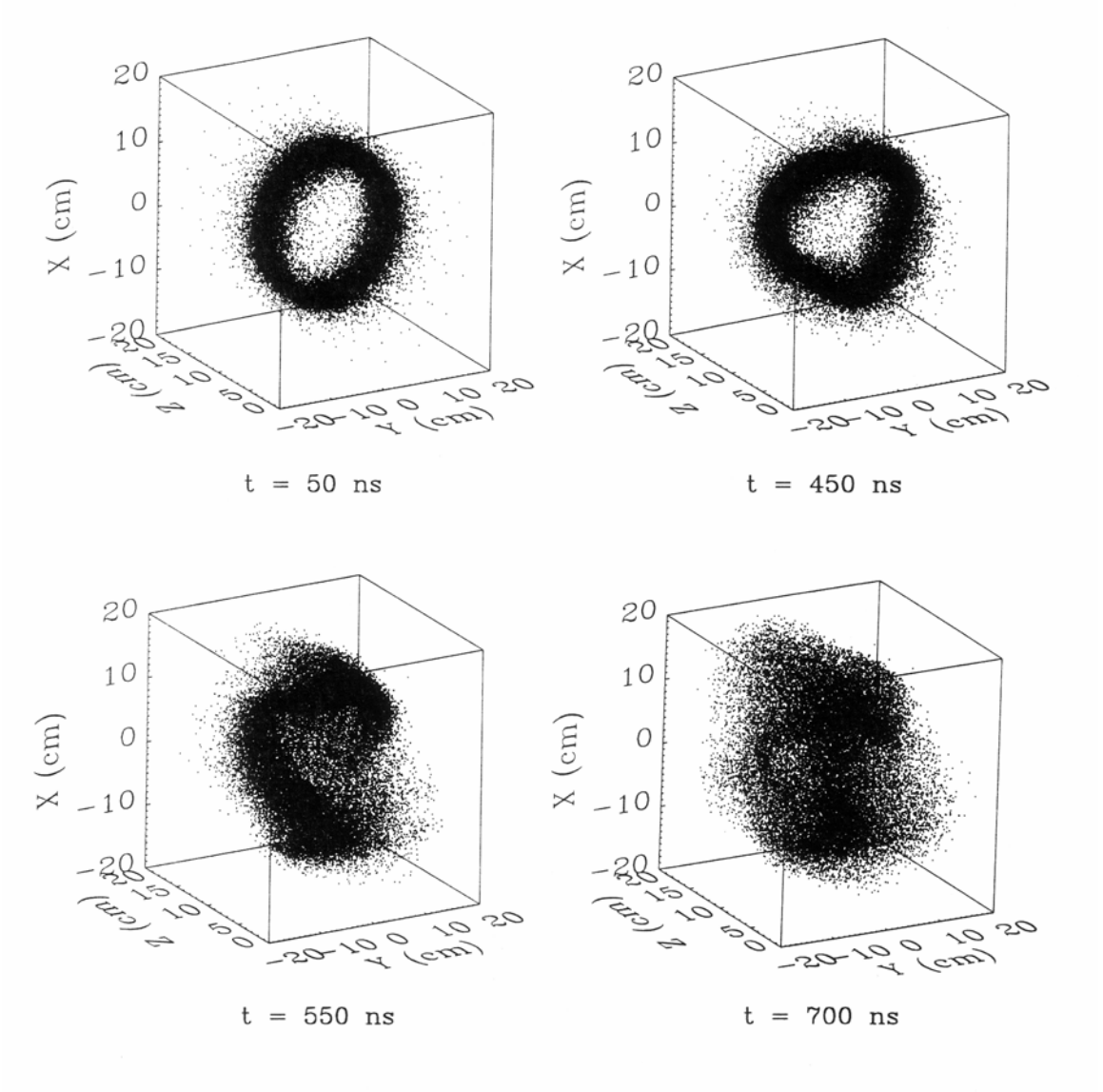

Figure 25. FLAME 3D simulations of a radially thin ring. The four lowest azimuthal modes were included in the spectral representation of that dimension in the code.

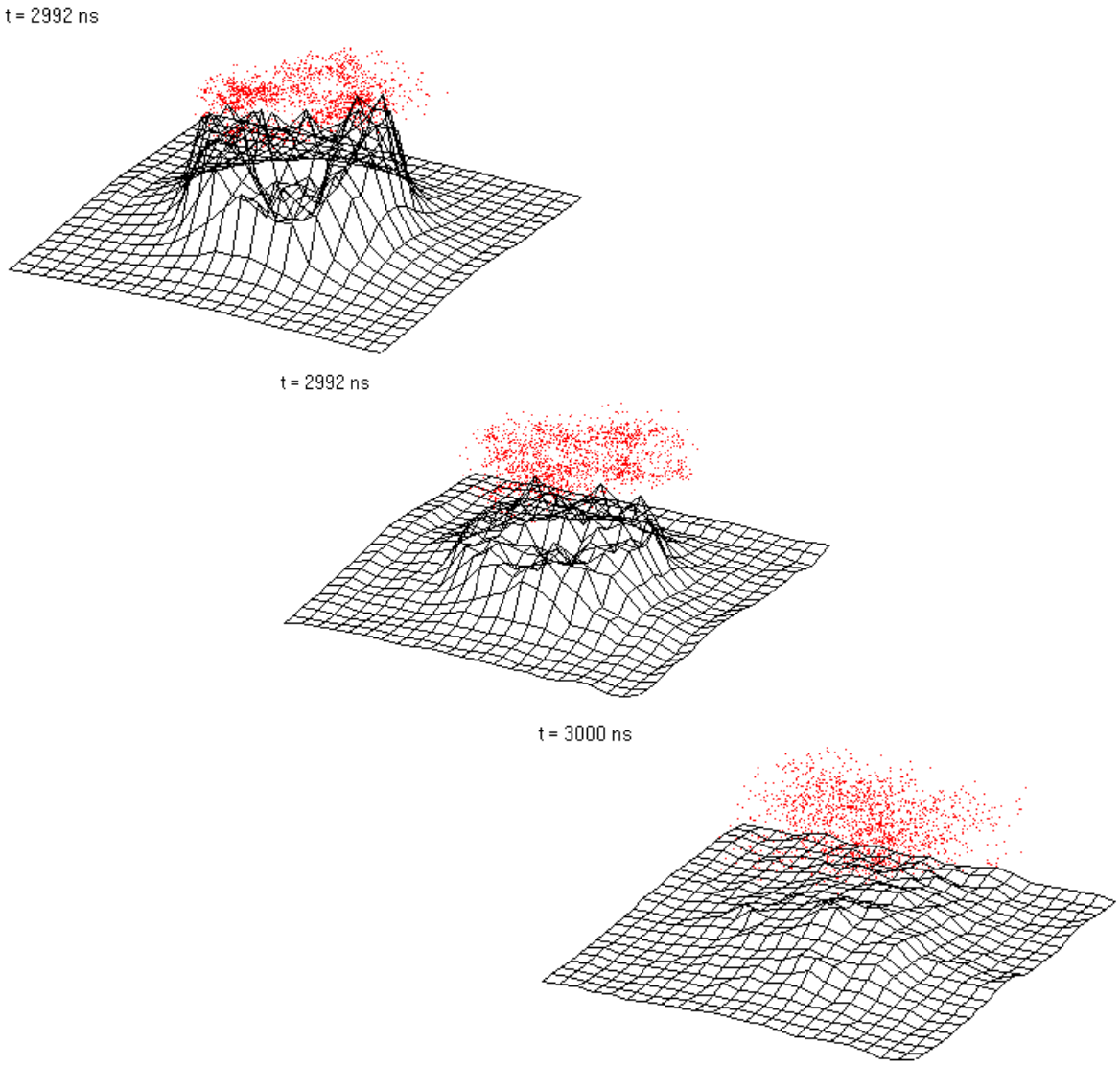

Figure 26. Ring particle distribution (dots) and plasma temperature distribution shown by grid, with increasing temperature above grid plane. FIRE simulation at t=3000ns. Three cases of differing plasma conductivity: $\sigma = 3*10^{11} s^{-1}$ (top), $\sigma = 10^{12} s^{-1}$ (middle), and $\sigma = 10^{13} s^{-1}$ (bottom)

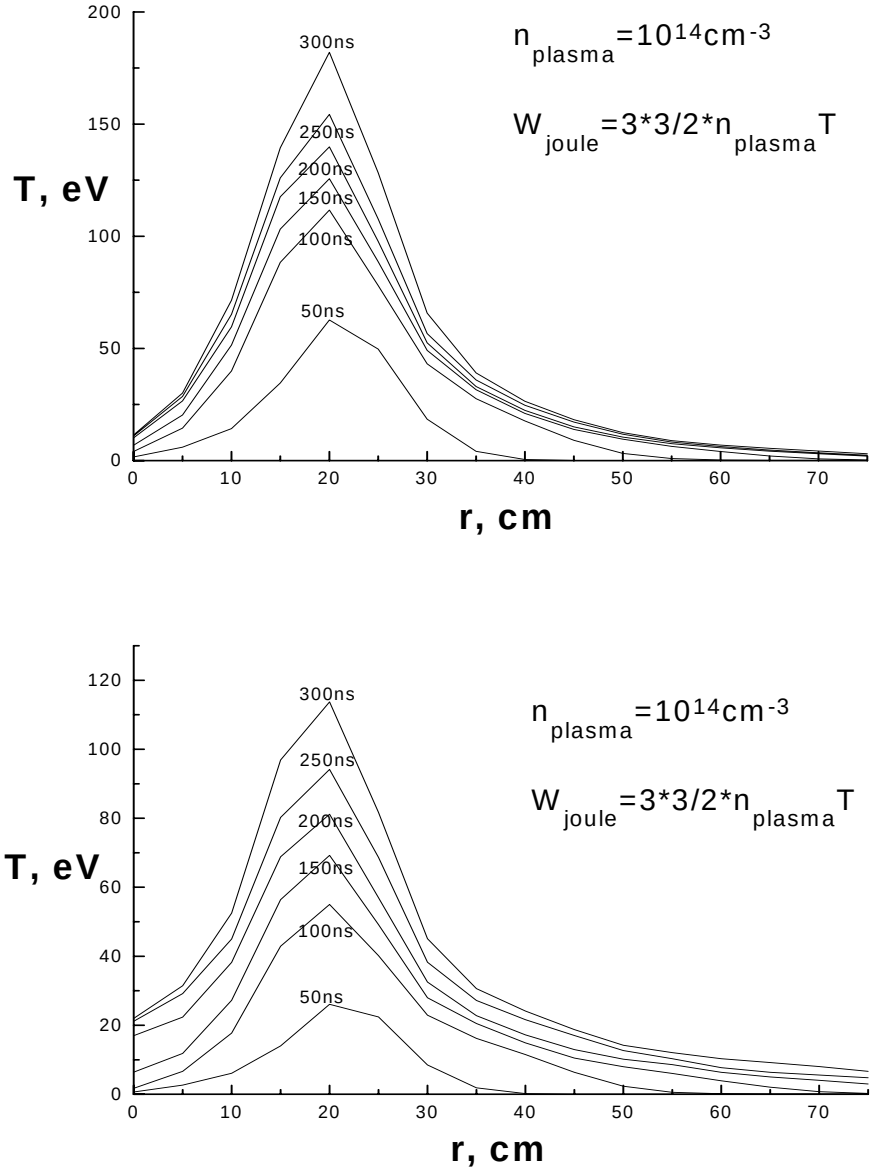

Figure 27. Radial plasma temperature profiles from FIRE simulations with different plasma conductivities: $\sigma = 3 * 10^{11} s^{-1}$ (upper), $\sigma = 10^{12} s^{-1}$ (lower).

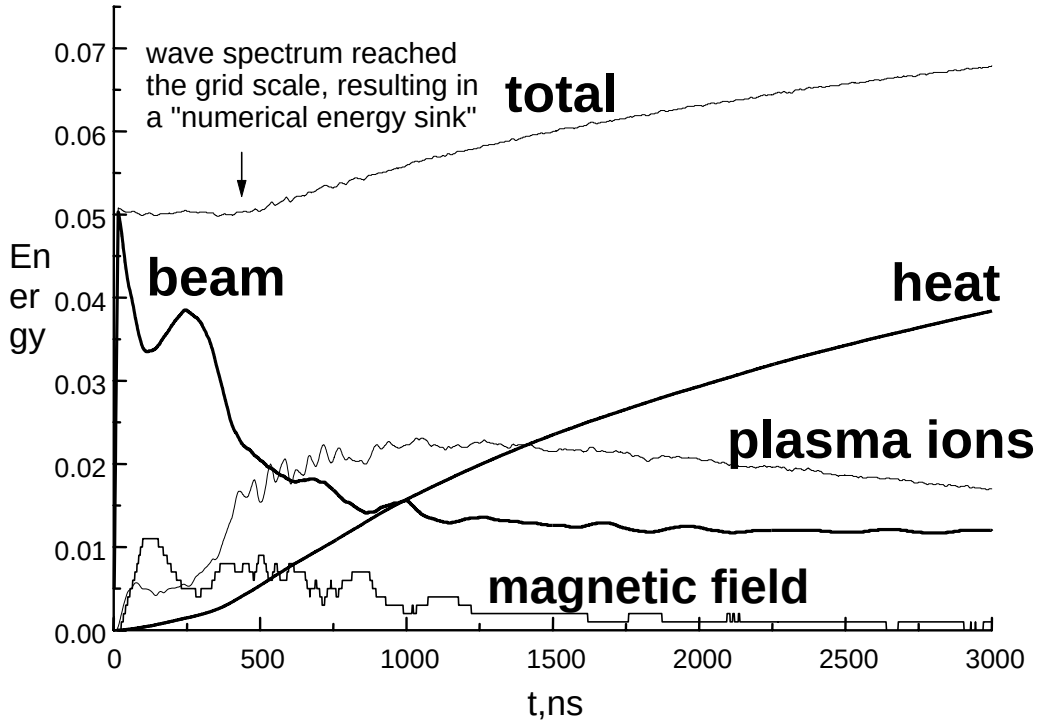

Figure 28. Energy balance for simulation with $\sigma = 10^{12} s^{-1}$. At t=500ns, wave energy spectrum reaches the grid scale, resulting in a "numerical energy sink."

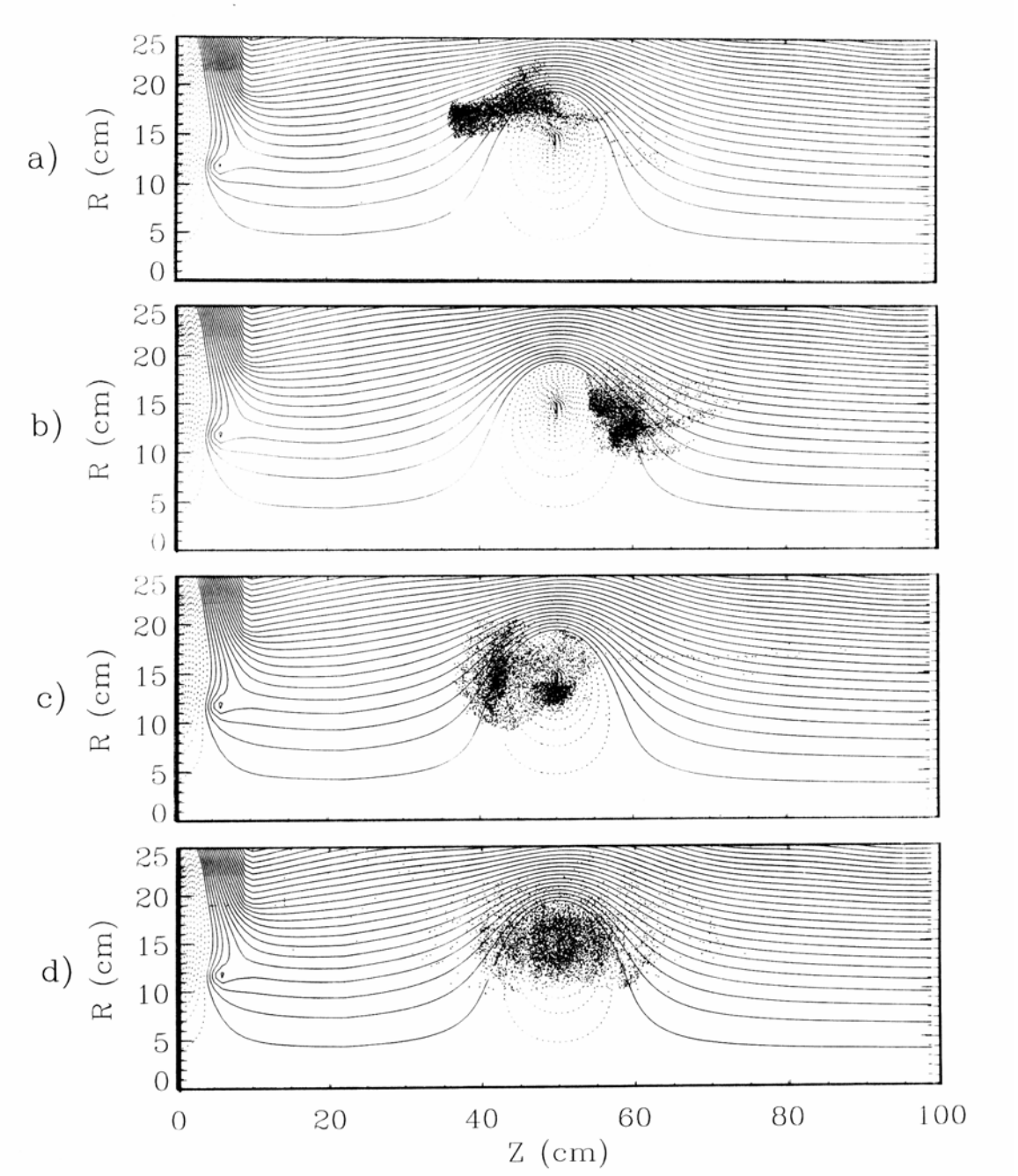

Figure 29. FIRE simulation of a ring injected into an FRC-like field. The ring transfers axial energy to waves strongly as it encounters the radial field at the end of the FRC and becomes trapped. A) t=100 ns, ring enters FRC. B) t=130 ns, ring bounces off downstream end of FRC. c) t=190 ns, reflected ring bounces off upstream end of FRC. d) t=400 ns, ring ions have sttled down into a stationary distribution in the FRC field.

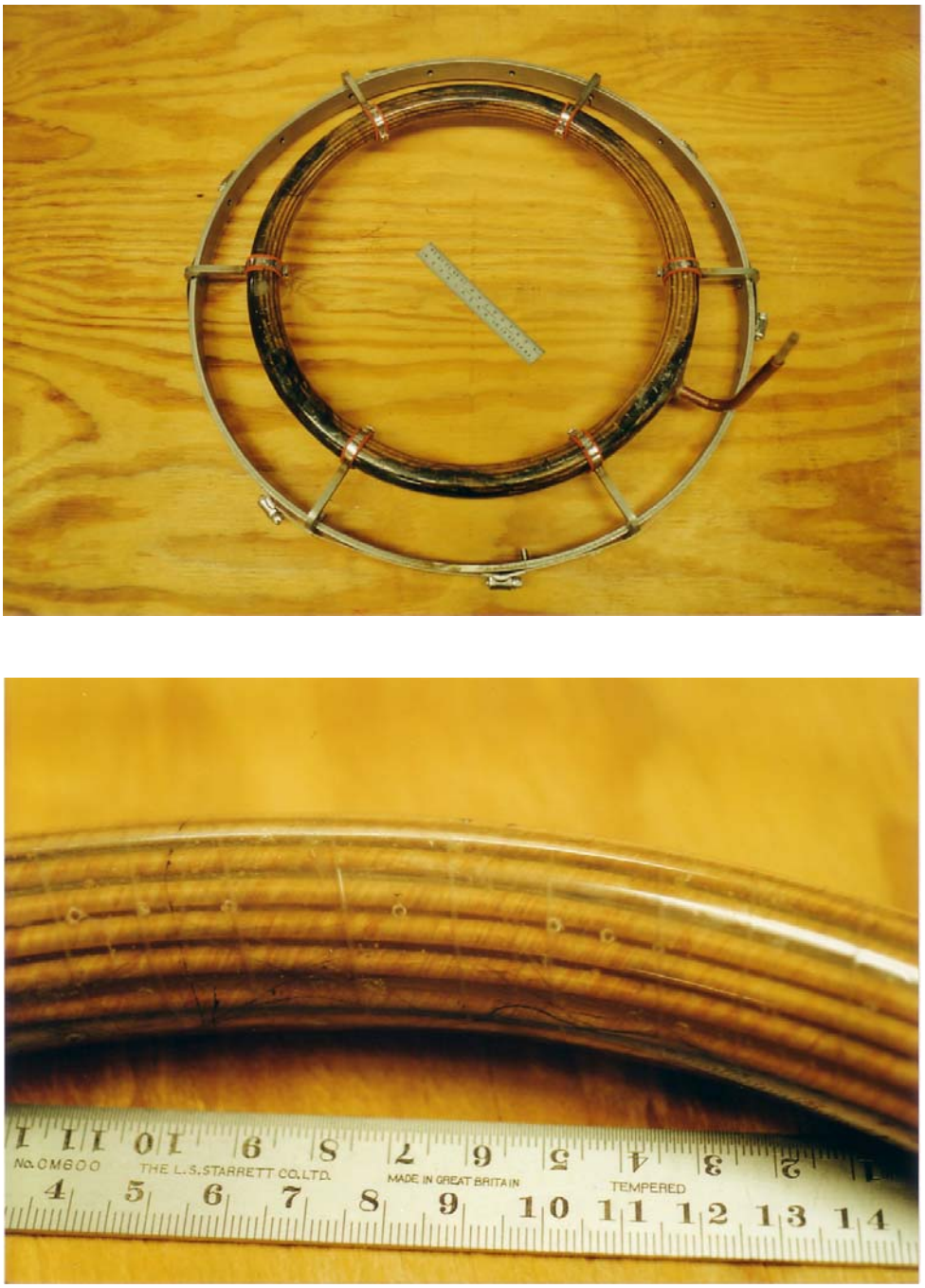

Figure 30. The FRC coil is wound as a hollow shell of 15 turns on the outside of a machined G10 form, reinforced outside with glass and carbon fiber windings, and vacuum-cast in epoxy. The scale is in cm.

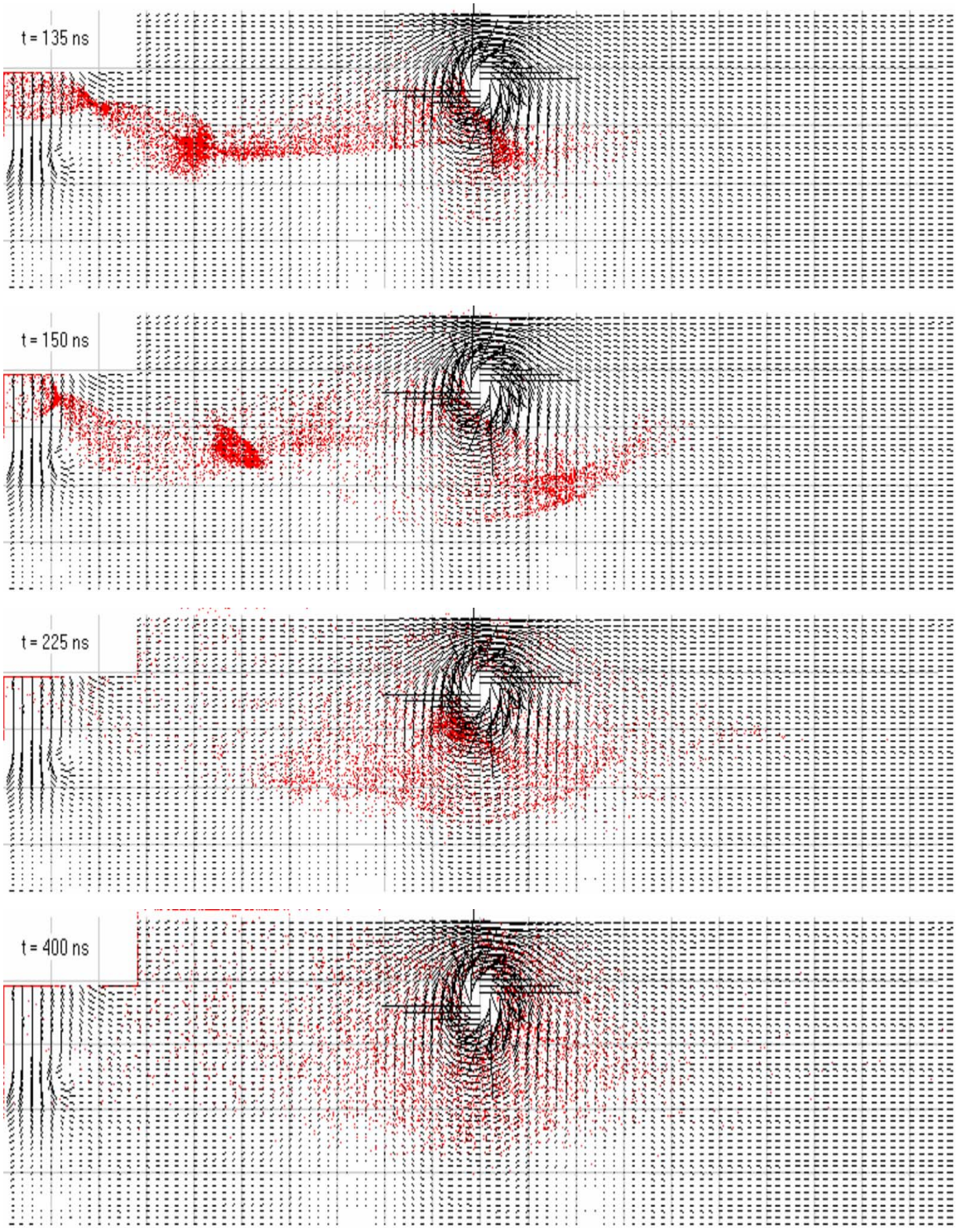

Figure 31. FIRE simulation of realistic FIREX ring injection into mock-FRC field. The strong field near the surface of the coil deflects the ring orbits and prevents collection on the coil surface. Simulation times are indicated.

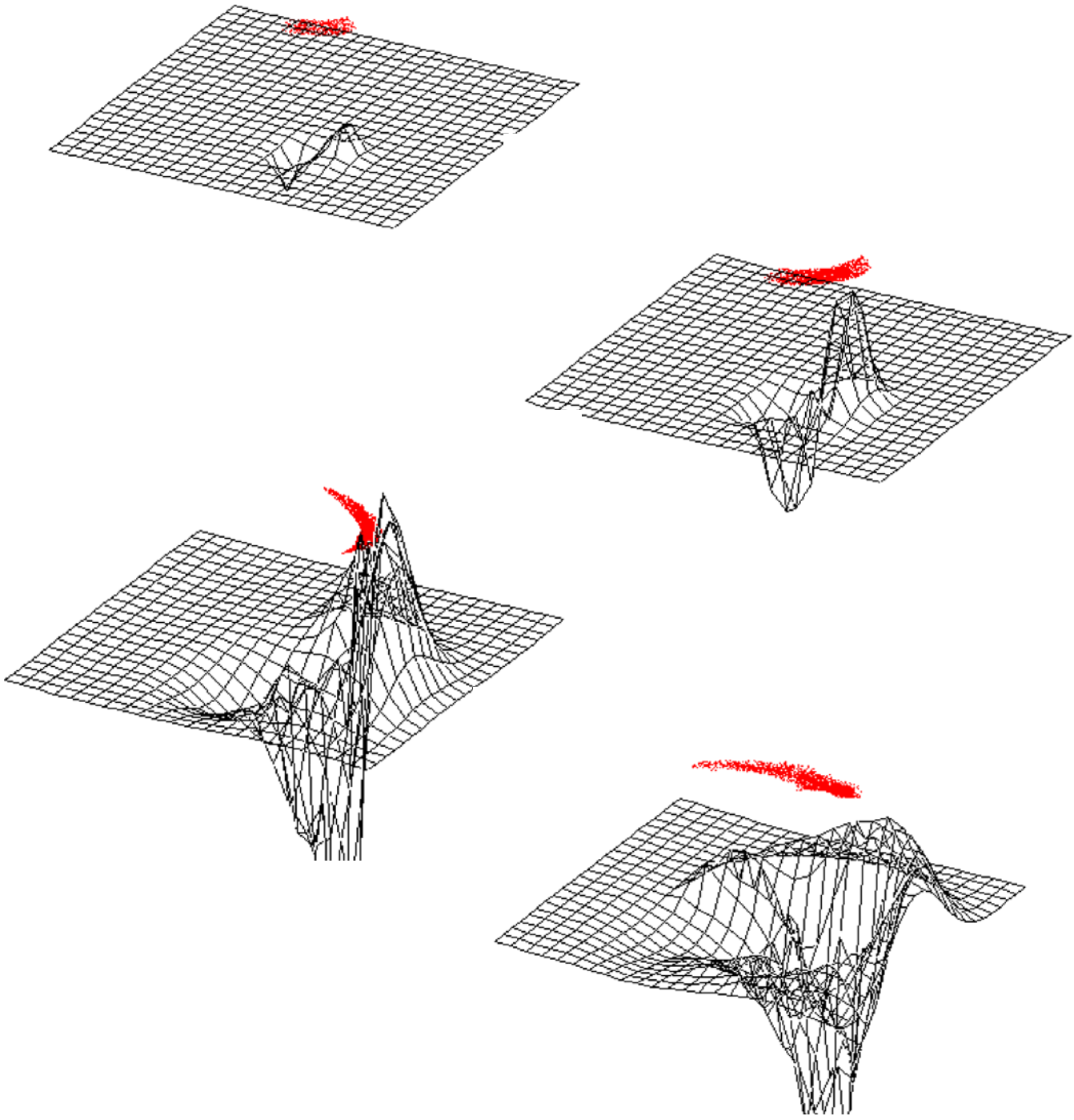

Figure 32. FIRE simulation of an isolated clump of ring charge (shown above the field grid) rotating in the applied field and plasma background. Time increases from top to bottom: the clump is rotating counterclockwise as seen from above. The grid shows magnetic field change, increasing magnitude is upward from the original applied field value defined by the plane of the unperturbed grid. Diffusive drag on the clump is apparent.

Appendix A. Coaxial ion diode and radial ion ring injection in the Cornell FIREX experiment, design and first results.

These experiments were carried out under the program, "Ion Rings for Magnetic Fusion" in the Laboratory of Plasma Studies, Cornell University, funded by USDOE grant #DE-FG02-93ER54221, with additional funding from Texas A&M University (TEES Project No. 61691 under Air Force Research Laboratory grant No. F08630-00-1-0004, CFDA#12.800).

I. Design considerations and advantages of radial injection over the standard FIREX axial cusp-injection configuration.

1) Electrical efficiency.

The radial injection scheme we describe here substantially increases the efficiency of conversion of electric current from the pulser to proton ring current, compared with the standard FIREX cusp-injection diode. The vacuum feed is a simple coaxial, bi-conic (tapered) MITL (self-magnetically-insulated transmission line), which at FIREX parameters is expected to transport up to 80% of the charge supplied at the vacuum interface. The diode is the natural, smooth termination of this feed, which should idealize the vacuum electron flow and give theoretical minimum electron current loss. The diode ion efficiency should therefore be capable, with careful optimization, of reaching the 80% level. The geometry is ideal for a MAP ion source that should produce above 95% of ions in the desired species. Thus a net ion efficiency of above 50% appears attainable if this design can be realized in practice, or a factor of five better than the cusp diode. Even if these expectations prove unrealistically optimistic though they are based on substantial experimental history, nevertheless a substantial increase in ring charge should still be obtainable.

2) ring stability:

In the FIREX cusp-injection geometry, a ring is produced which is very tightly-organized radially because all the injected ions are given nearly the same rotational energy. All the voltage variation during the pulse goes into axial velocity spread, making the ring difficult to trap axially: this axial velocity must be dissipated in order to bring the ring to a halt at a desired axial location. In contrast, if ions are injected radially into a solenoidal field to form a ring, they can have low axial velocity and all the pulse voltage variation goes into spread in rotational energy, producing a less tightly radially organized ring with a range of larmor radii, but a much better confined ring axially. Such a ring may be highly desirable for stability, both for magnetic fusion and for acceleration by magnetic compression. See Appendix B for the results of simulations of different ring distributions. In summary, rings with ion larmor radii of order half the radius of the ring (s~2), such as would be produced by radial injection, are found in simulations to be much more stable than standard s~1 FIREX rings with symmetric, axis-encircling orbits. These s~2 rings show initial instability but quickly reach a steady state which is only slightly spread from the initial state, with little ring energy loss. Essentially, this type of ring has much higher "temperature" than cusp-injected rings, is less tightly organized, and has much less free energy available to drive instability.

A basic parameter found in simulations to control ring stability is the Alfven mach number M_A. Rings with very high $M_A >>10$ were found to have much smaller growth rate and significantly less disruptive nonlinear stage of the azimuthal instability. In radial injection, parameters could be chosen to access this regime, but cusp injection is forced to use $M_A < 10$ in order to take advantage of the axial Alfven interaction to slow down and axially trap the ring, as has been demonstrated on FIREX.

Ring nonuniformity is a strong driver of the wave interaction that causes instability and energy loss, and limits ring lifetime. The surface breakdown ion sources used in the FIREX cusp diodes are always substantially nonuniform. Initially injected azimuthal nonuniformities in the ring are already far larger amplitude than the numerical noise

which seeds the instability in simulations; thus the drive for instability in the experiment is much stronger. By contrast, MAP ion sources have shown far better uniformity, giving the promise that when properly implemented in a radial injection scheme, the ring initial condition can be much more azimuthally uniform, reducing the drive for instability greatly.

To summarize, it appears that in the regime of background density and Alfven speed needed for rapid axial stopping of a radially thin, cusp-injected ring, azimuthal instability is also produced which reduces the ring lifetime. A radially injected, radially thick ring would avoid this conflict. First, by being formed with low axial velocity in a magnetic mirror, rapid axial slowing would not be required. Second, the wider distribution of larmor radii and radial thickness would tend to make the ring more inherently stable, and third, the inherently better uniformity would reduce the instability drive.

3) ring trapping:

Finally, with radial injection, the only axial velocity the ring ions will have is due to the self-field of the axial current in the diode, and this can easily be kept small enough that the ring will be "born trapped" in a magnetic mirror of reasonable strength. This means that the diode which emits the ring ions can be located within a mirrored solenoid, and the ions injected will have a ratio of rotational to axial energy large enough to be well-confined in a mirror ratio of order 1.5:1 or less.

II. FIREX radial injection experiments:

1) Design considerations.

The Cornell program, in our 1998 annal progress report to the USDOE, gave the first description of the scheme for radial injection which might develop a ring with the advantages we have described. In 1999 we designed and fabricated the components of

the current feed for this scheme. During 2000, S. Glidden of Applied Pulsed Power, Inc (APP), and J.B. Greenly of Cornell developed and tested the MAP ion source for this configuration.

The FIREX program at Cornell began collaboration with Texas A&M University (TEES Project No. 61691 under Air Force Research Laboratory grant No. F08630-00-1-0004, CFDA#12.800) because of our mutual interest in the radial injection scheme. Funding ($20,000) from Texas A&M was contributed in 2000 to help fund development of the plasma source for this diode at APP. This source was a direct application of a type of source developed by Cornell and APP for several other applications. The main issue for this application is the rather strong (5-8 kG magnetic field in which the source must operate. The source uses an inductive breakdown of a localized hydrogen gas puff to produce a nearly pure proton plasma, which streams out to form the anode plasma as described. In tests in up to 2.5 kG applied solenoid field on a test stand outside of FIREX at APP, the plasma moves at several cm/μs axially, has excellent azimuthal uniformity, and has density in the $10^{14}/cm^3$ range, which should be more than adequate for the anode plasma of this diode.

In the period January, 2001 to March, 2001 a first series of experiments was conducted on FIREX with this configuration, which is shown in Figure A1. The coaxial, bi-conic feed reduces the diameter of the FIREX vacuum feed to 5 cm, with a 1 cm radial feed gap. The ion diode, in coaxial geometry, is the direct termination of this feed. The MAP plasma source is located inside the anode cone. Observed scaling of the source behavior with the applied field up to the 7 kG level on FIREX was straightforward, and is now well-understood. The source operation is based on producing, with the current in the inductive loop that powers the source, enough magnetic field opposed to the ambient solenoidal field to produce a field null within the volume of gas to be ionized. The breakdown originates at and propagates from this x-type null. Operation of the source clearly did depend on this condition being met, and the design is adequate to produce it at the 8 kG level desired for ring formation in FIREX.

In FIREX, the ion source produces a proton plasma that is allowed to stream out of the cone at about 1-2 cm/μs, along the solenoidal field, forming the anode of the diode. The solenoid field also acts as the magnetic insulating field for the diode gap, as well as being the confining field for the ion ring. The "virtual" cathode is formed by electron space charge transported as vacuum flow in the MITL feed, as well as that emitted from the tip of the cathode cone, as in all magnetically-insulated diodes. The axial length of the diode is thus determined by the time allowed for the anode plasma to spread out along the field away from the conical electrode. Approximately 40-50 cm length was used in the first experiments. Increasing length increases the diode area and proton current, lowering the diode impedance. The optimal value would be 1-2 ohms for the FIREX pulser.

It is useful to describe this diode configuration in the context of other experimentally successful magnetically insulated diodes. In that sense, this configuration may be called an inverted "barrel" diode with single-sided feed and a MAP anode. It is an inverted barrel diode in that it is coaxial like the barrel diodes developed at Sandia National Laboratories for light-ion inertial fusion drivers, but the anode is on the inside and ions are accelerated outward, the inverse of the Sandia arrangement. Current is fed at one end, thus the single-sided feed. The anode is a Magnetically-confined Anode Plasma (MAP) with no backing solid surface. Extensive experience with these devices indicates the following. First, the barrel geometry is an excellent one with a continuous electron drift path (azimuthal) and has operated at very high ion efficiency. The inverse arrangement is the same in that respect. The MAP anode is the only ion source for magnetically-insulated ion diodes that provides an essentially pure and very spatially uniform proton beam, and has shown impedance characteristics far superior to surface sources, producing flat or even rising voltage pulses. The single-sided feed means that electrons will have a drift component axially away from the cathode edge, analogous to the inward radial drift component in the present FIREX diode, but in this radial diode there is no solid anode structure for the electrons to be lost to downstream in the axial direction. All these

features are attractive and apparently synergistic, but no diode has been previously tried which combines them all. Thus this is a high-risk, high-payoff diode concept.

Expectations of characteristics of the rings formed by radial injection from this diode also have many unknowns. Single-particle orbits from this diode would not encircle the axis, since the proton velocity would be purely radial at the 5 cm diode gap radius, as shown in Figure A1. If axisymmetry were strictly maintained, these orbits would not encircle the axis in a strong ring either, and it is not clear how their radial distribution would evolve to produce field reversal on axis. If the diode is able to couple charge into the proton beam with good efficiency, the current in these initially off-axis proton orbits will be large enough in the experiment to exclude all (or more) of the magnetic flux of the applied field. We anticipate that full three-dimensional dynamics will be needed to produce a physically reasonable picture of the evolution of such a ring, and that transient symmetry-breaking may be important. If dissipative or symmetry-breaking dynamics occur, these orbits would tend to fall together into their mutual self-magnetic radial well, and form a strongly diamagnetic ring, with the accompanying complex physics of magnetic reconnection. If this happens, the radial distribution of the ion orbits would certainly not be radially narrow as in the FIREX cusp injection. This radially "hot" ring could be expected from our present understanding to be much more stable than the cusp-injected rings.

Another issue in this configuration, in which the diode and its insulating field is immersed in the ion ring formation region, is that the applied field at the diode gap must not be disrupted by the ring field during the injection pulse. The diode insulating field will be maintained at least until Alfven waves propagate inward from the outer ring radius to the gap radius. If this time is similar to the present experiments, this condition will be satisfied.

Despite the radial injection, we point out that axial dynamics are not negligible in this configuration. This is because the current is fed to the diode axially from the electrodes, and produces an azimuthal self-magnetic field. The ion radial velocity interacting with this field component gives a downstream axial kick to the protons. The question is again

where and when this field appears radially. It is initially expected to be excluded by the plasma outside the diode gap, but can propagate into the plasma as an Alfven mode. Again, its radial propagation timescale would be comparable to or longer than the diode pulse length. If the azimuthal field is confined to the diode gap, a maximum of about 100 keV axial energy of the protons would result in FIREX at full current. This largest axial kick would be felt by protons at the upstream (current feed) end of the diode, near the end of the pulse at peak diode current. The axial kick would vanish at the downstream end because the axial diode current goes to zero there. Thus the ring would tend initially to come together axially near the downstream end of the diode, which could be advantageous in tightly confining the ring. The result of the spread in axial velocity would be to increase the axial "temperature" of the ring, and therefore act as a limit on the minimum equilibrium axial length of a ring formed in this configuration, thereby limiting the maximum field reversal with a given total ring charge.

2) FIREX radial injection results.

The FIREX first results, though far from being optimized, have established positive conclusions about the basic features of the radial injection scheme. First, the biconic MITL feed is efficient in delivering power and charge to the diode. Second, the MAP ion source produces a pure proton plasma adequate to establish an effective plasma anode confined radially by the solenoidal field. Third, the resulting magnetically-insulated diode gap is able to form a virtual cathode with low electron current loss and good impedance history, coupling power efficiently from the MITL to the diode over the full FIREX pulse length. Fourth, the diode produces a radially-directed proton beam with high ion efficiency, and excellent axial uniformity over a 40 cm or longer axial length. Initial measurements indicate proton current and total charge in excess of that produced with the optimized standard cusp injection.

To illustrate these points, Figures A2-A5 show results from one of the FIREX pulses with highest ion current obtained in this first run. Figure A2 shows current delivered to the vacuum interface, and current reaching the diode at the end of the biconic MITL power

feed ("feed" current). The peak feed current varies from 70% to 80% of the interface current, and this represents the efficiency of the MITL transmission of charge to the diode. This performance was reproducible, and showed the characteristic MITL scaling that the more current drawn by the diode, the higher the MITL efficiency became; conversely, on pulses with no ion beam when the plasma source was not energized, the MITL efficiency was as low as 30%. Essentially all the current loss is in the final 5 cm length of the biconic electrodes, just upstream of the diode.

Figure A3 shows the diode voltage inductively corrected from the water-vacuum interface monitor, the feed current, and the resulting, calculated, diode impedance. The inductive correction through a MITL is known to be a poor measure, because especially early in the pulse the MITL inductance is not constant, and EM transmission line effects are important throughout the pulse. The apparent rapid excursions in the corrected voltage are not real. An attempt to provide a more reliable inductive monitor at the load was not successful in thie first run, but probably can be implemented in the future. In any case, ring ion energy diagnostics will be used to determine the injected proton energies dierctly. In Figure A3, the peak voltage of about 700 kV is probably fairly accurate, and the pulse duration shows the full 150 ns FIREX pulse is being coupled to the diode. The impedance is, as with all high-power ion diodes, decreasing with time, and is above the optimum 1.5-2 ohms for much of the pulse. Optimizing diode performance to improve this impedance history will be a major objective of future experiments, both to couple more current to the diode, and especially to reduce the peak voltage, as discussed below.

Figure A4 shows ion current density signals from magnetically-insulated ion collectors located at 8 cm radius, 5 and 15 cm from the end of the electrode gap oriented to collect radially outward flowing ion current. Peak ion current densities of 70-100 A/cm^2 were reproducibly observed. The ion current density rose very rapidly at the start of the voltage pulse, indicating the presence of the plasma anode already formed before the pulse, and continued throughout the pulse length, indicating that the plasma was not being significantly depleted by ion beam extraction.

Figure A5 shows the interface voltage (uncorrected) and the signals from four radially integrating, magnetically-insulated ion collector arrays. These arrays sample the azimuthal (rotating) component of ion ring current density from 10 cm to 19 cm radius in the chamber (the wall is at 25 cm radius). In these diode proof-of principle pulses, no plasma background was introduced into the chamber, and the propagation of the radially injected beam is almost certainly disrupted by space charge; nevertheless, about 600 A/cm axial length of ring current was measured by the arrays. The relatively slow risetime of the array signals in Figure A5 compared with the collectors looking directly at the diode, in Figure A4, may be evidence of beam disruption by space charge in this injection across magnetic field in vacuum.

The remarkable axial uniformity of the ion beam produced by the diode and MAP ion source is evident in Figure A5. The timing with respect to the voltage illustrates a time lag from interface voltage to the start of beam current which is a combination of MITL self-insulation delay and ion propagation time to the ion diagnostics. The ion current signals persist beyond the interface voltage because the diode voltage is actually positive after the interface voltage reverses, and also at the end of the pulse as the voltage falls, the ion transit time grows longer. Arrays beyond the 40 cm shown did see about half this current density at 50 cm, a small amount at 60 cm, and none beyond that, indicating the axial extent of the drifting anode plasma at the time of the pulse. This axial length was controllable by varying the drift time before the pulse was applied.

The results of this first run give the following accounting of the total injected proton charge. In the best pulses, a beam was produced in 50cm of axial length, with an average proton current density above 50 A/cm^2, measured by the collectors at 8 cm radius. This gives a proton current greater than 2.5 kA/cm axial length, or >125 kA total proton current in the solenoid for the 150 ns pulse length, giving more than 19 mC (1.2×10^{17}) protons injected. This compares with 8 mC (5×10^{16}) in the strongest ring ever produced by the optimized standard FIREX cusp injection.

It must be emphasized that this charge has not yet been formed into a lasting, rotating ring. The ring ion current density signals in Figure A5 last only about 200 ns because the rings produced in all these pulses intersected the wall and were lost there. Most of the protons were lost to the vacuum wall in their first orbit because their energies and larmor radii were too large. Thus, the operation of this new type of ion diode and radial injection of very large total proton charge have been successfully demonstrated; formation of this charge into a well-organized ring would be the next task. To accomplish this, a plasma background in the solenoid would certainly be needed to provide good charge neutralization and eliminate space-charge disruption of the ring. To confine the orbits within the wall, lower voltage, higher magnetic field or larger chamber radius would be required.

The first run was terminated because the MAP ion source was subject to frequent breakdowns. The basic source design criteria were given to APP by Cornell, and specified that the source not be totally hermetically sealed. The exposed high voltage at the source electrical components in the vacuum broke down in the FIREX plasma environment. The unsealed design was chosen because it was expedient in producing a cheap, simple and easily modifiable source for first tests. It proved very convenient for the quick modifications that were made in investigating its operation and scaling with magnetic field in FIREX, and it was adequate to produce a few successful FIREX pulses to establish the basic viability of the concept. However, breakdowns made many of the FIREX pulses unproductive of useful diode data. After several attempts at temporary fixes on FIREX, it was decided to terminate the experiments. The requirements for the electrical design parameters were met by the first version of the source. After several minor modifications during the run, the source chamber, gas puff valve and inductive driving loop configuration were clearly adequate. It would be straightforward to keep these features while upgrading to a fully-sealed high voltage design, to make a source which should have more than adequate performance.

With the successful results of the first FIREX experimental run of the coaxial diode and radial injection, it can be argued that substantially more proton charge can indeed be

injected into the solenoid with this scheme than in the standard FIREX cusp configuration. How much of this charge can be organized into a ring, and what the ring configuration will look like, are as yet still matters for speculation. At best, the first results indicate that this could indeed be the most efficient way of using the FIREX pulsed power to produce a ring. The results also make it highly likely that a new experimental regime would be accessible, allowing investigation of a strong and possibly field-reversed ring with very different radial and axial dynamics than the cusp-injected rings.

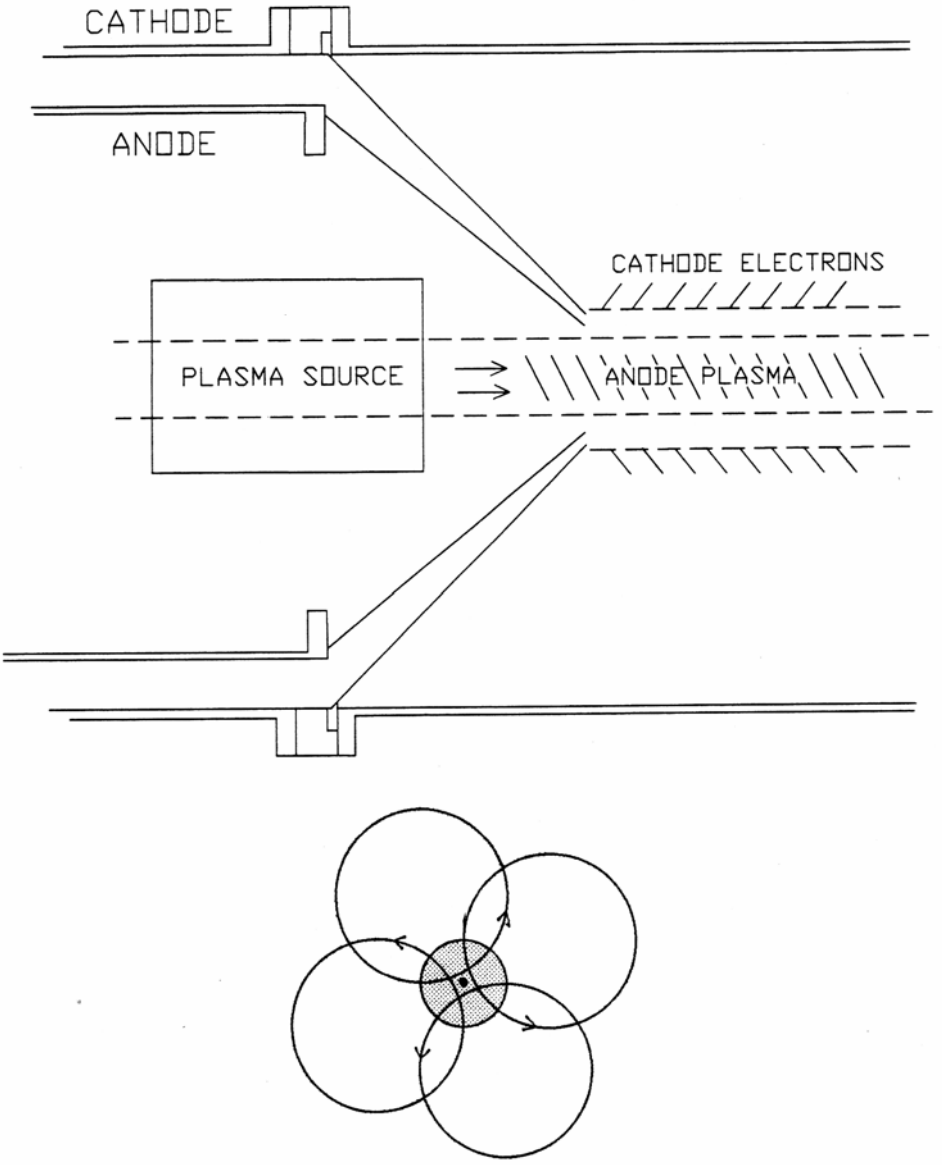

Figure A1. Diagram of the FIREX radial-injection diode. The upper diagram shows the bi-conic coaxial MITL power feed from the water-vacuum interface of the FIREX pulser (off the left edge of the figure). The MAP plasma source supplies proton plasma which drifts axially along the applied solenoidal magnetic field to form the anode plasma as shown. The lower sketch is an end (axial)view of the anode plasma (shaded region) and indicates idealized single-particle orbits of protons that are accelerated across the gap from the outer boundary of the plasma.

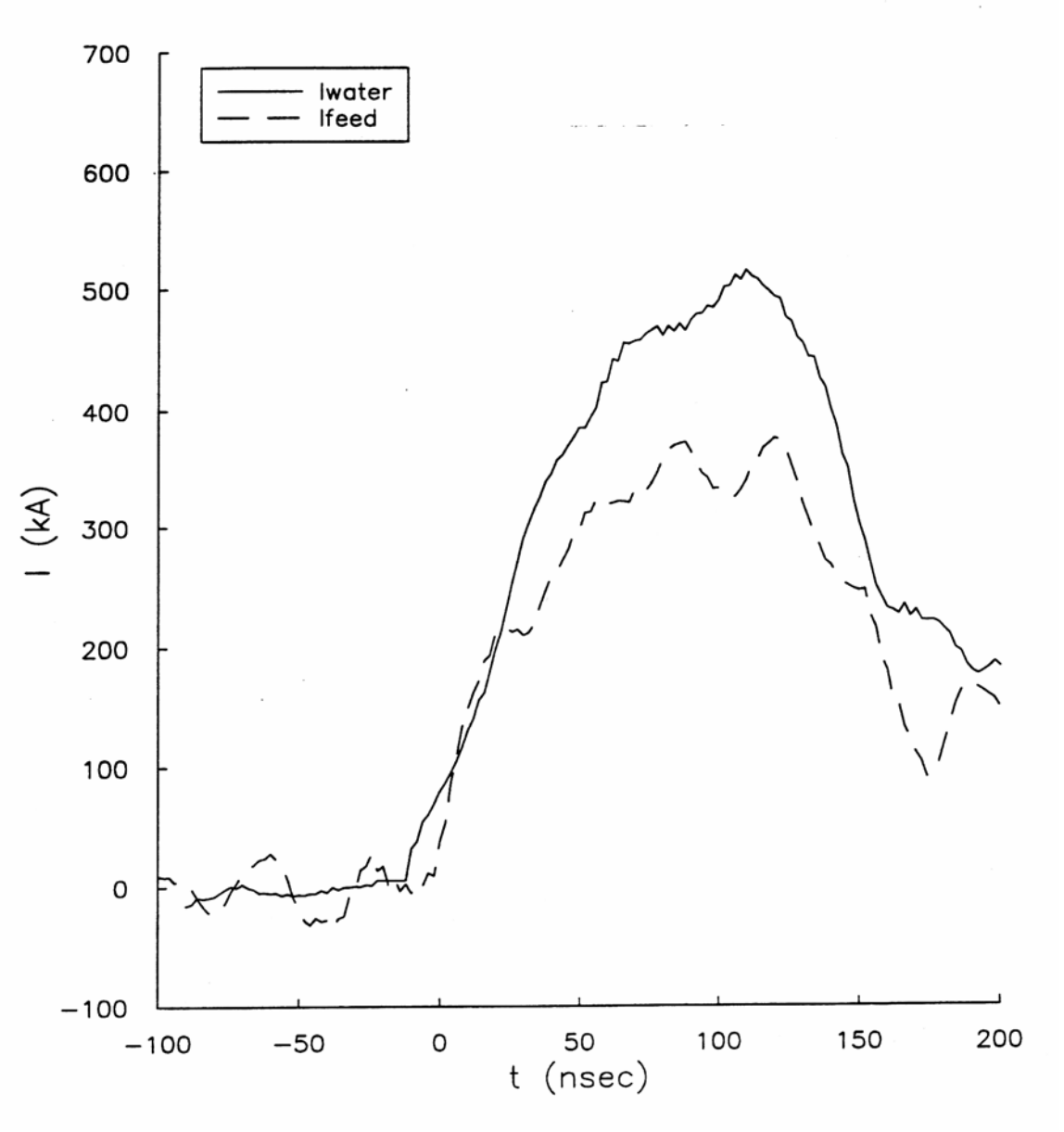

Figure A2. Current at the water-vacuum interface (Iwater) and just upstream of the radial diode (Ifeed).

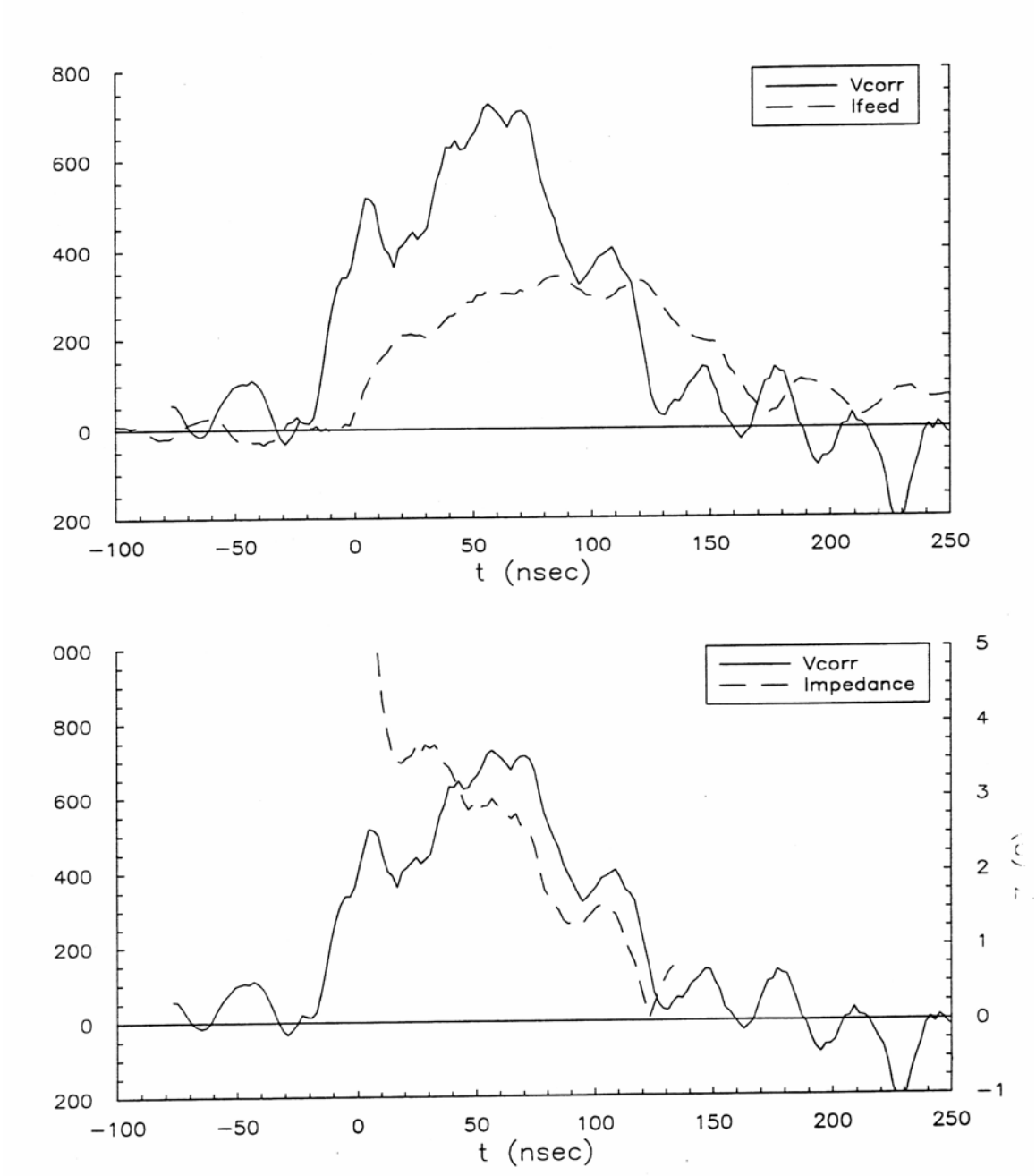

Figure A3. Inductively-corrected diode voltage (Vcorr), Ifeed, and calculated diode impedance (in ohms, right-hand scale) for the same pulse as Figure A2.

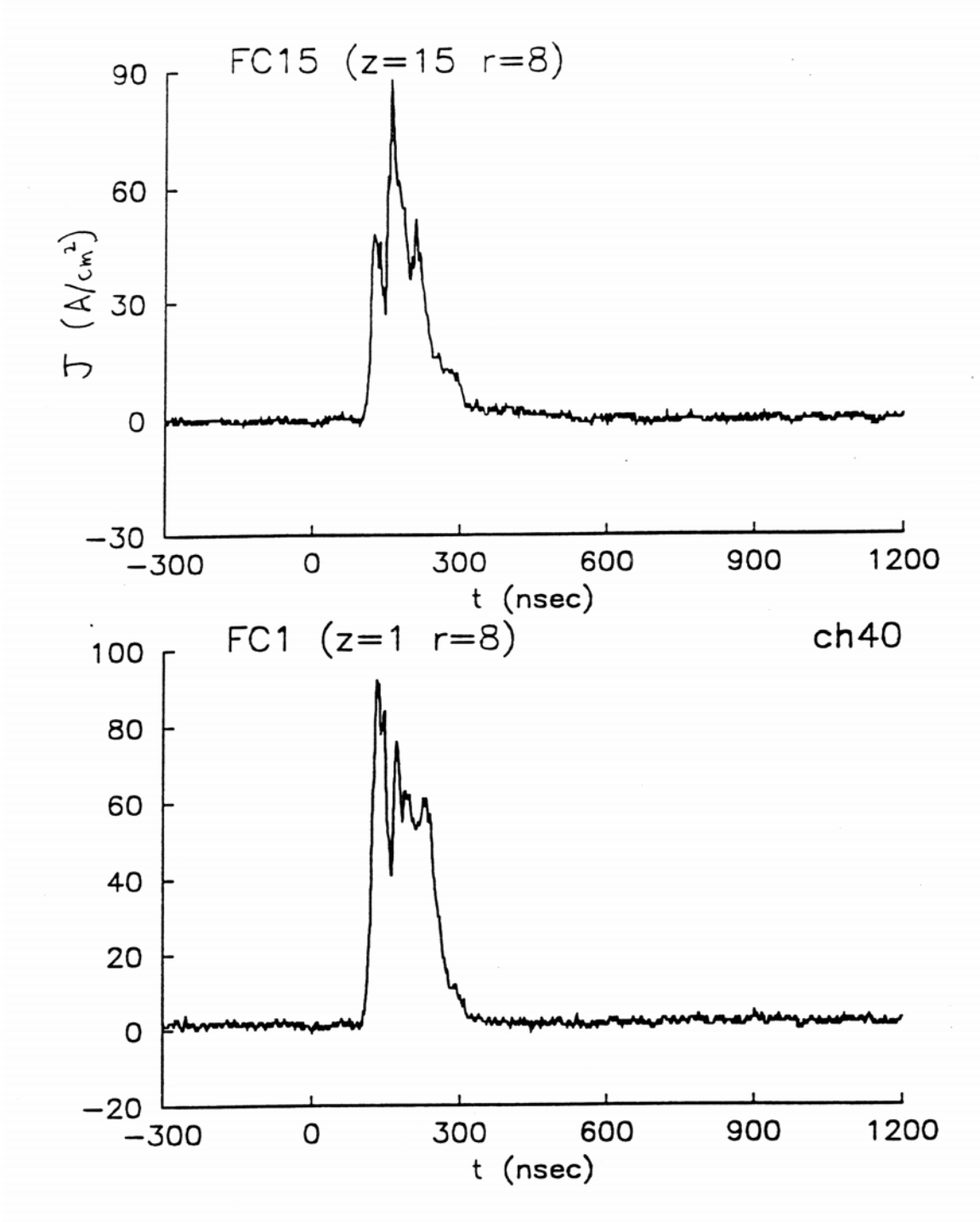

Figure A4. Signals from two magnetically-insulated proton current collectors located at 8 cm radius, at 1 cm and 15 cm axial positions. Collectors are oriented to collect the positive radial (outward) ion current component.

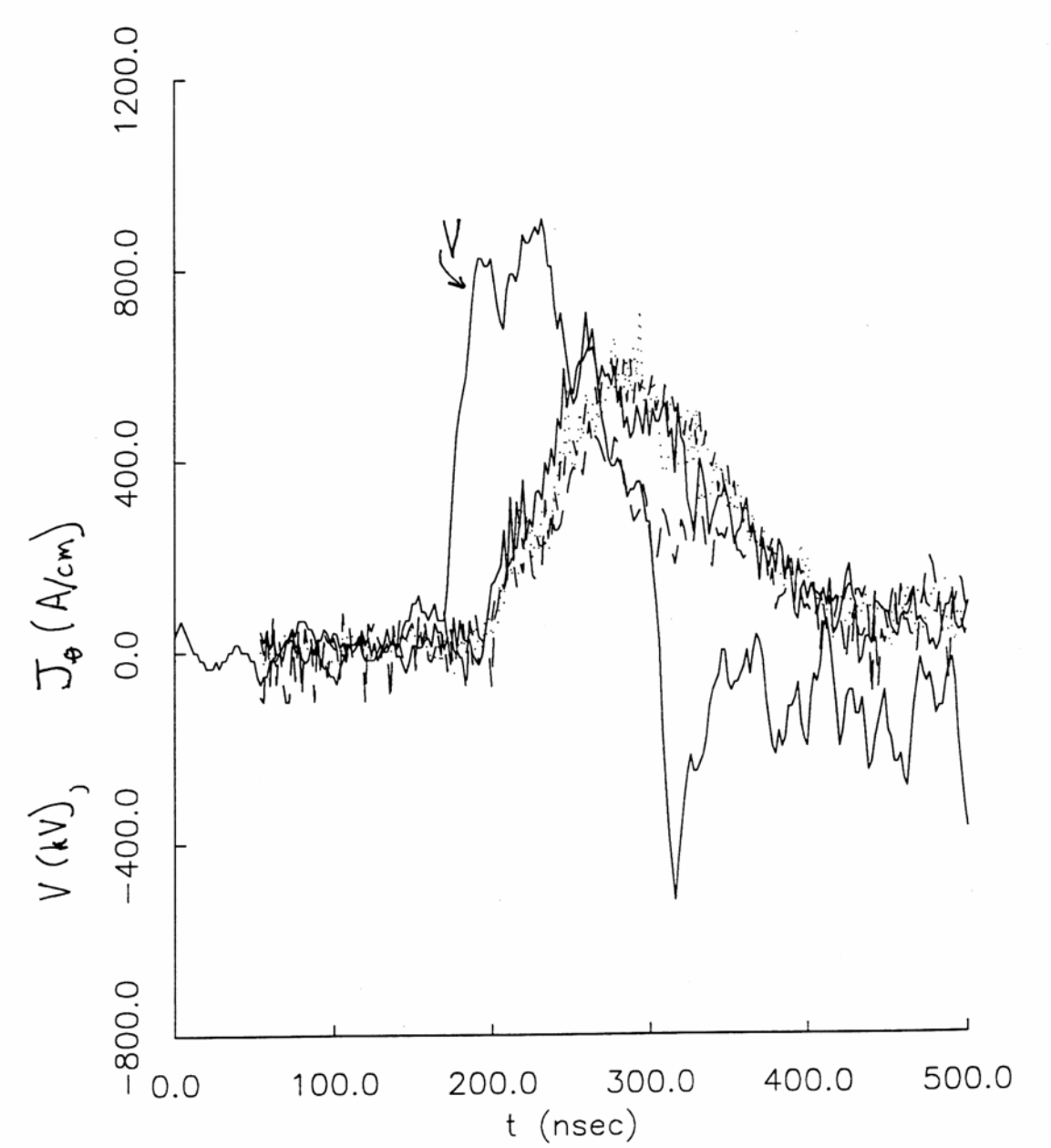

Figure A5. Uncorrected voltage at the water-vacuum interface ("V"), and signals from four radially-integrating Faraday wand collectors (hence unit of current density per unit axial length, A/cm) of the rotating (azimuthal) component of proton current between 10 and 19 cm radius. Solid line is collector at 10 cm axial distance from the end of the diode electrodes, dashed is at 20 cm, dot-dash is at 30 cm, and dotted is at 40 cm.

Appendix B. Ion Ring - Alfven Wave Instability: theory and simulation results.

The FIREX program has demonstrated that even at ion ring currents below that required for field reversal, large magnetic fluctuations are generated, accompanied by rapid energy loss by the ring ions. Numerical simulations and simple linear theory show that ion ring stability is controlled by the interaction of the ring beam with compressional Alfven waves in the background plasma. Sensitivity of the growth rate and the character of the nonlinear stage of the ion ring instability to the parameters of the ring and background plasma is analyzed in two-dimensional (r,θ) simulations with the FIRE code. This Appendix presents these results. The simulations reveal that in FIREX-like ring-plasma systems collective interaction of the ring current with compressional Alfven waves in the plasma indeed generate extremely large-amplitude (>0.1 T) magnetic fluctuations and rapid ring energy loss. Stable configurations may nevertheless exist, and these results indicate possible regimes of stability for further study. It is clear that a successful FRC-ion ring reactor design must find such a regime.

Most of the early theoretical work on ion ring azimuthal stability has been focused on the low-frequency phenomena, not involving wave excitation in the background plasma (see review by Finn and Sudan [B1]). Systematic consideration of low-frequency ion ring dynamics started with works by Sudan and Rosenbluth [B2,3] and Lovelace [B4,5]. Sudan and Rosenbluth used a generalized energy principle, treating plasma in the MHD, double adiabatic, or small-gyroradius drift approximation, while treating ring ions exactly by the Vlasov equation. The energy principle became popular in the analysis of low-frequency ring stability. Lovelace [B4,5,6] applied it to investigate the kink instability of thin, "bicycle-tire" rings. Furth [B7] predicted unstable precession of a ring about its cylindrical axis using the rigid-ring approximation. Berk and Sudan [B8] showed that the approximation is only valid for frequencies much lower than the axial betatron frequency of the ring. Rutchi and Lovelace [B9] have studied tilt stability of ion rings with arbitrary aspect ratio and found the stability criterion $w_z > k\Omega$, where w_z is the mean axial

betatron frequency, Ω is the mean toroidal circulation frequency, and k=0.7..1. They have also suggested that the unstable rings would evolve to stable shapes through increase of the axial ion temperature if in the initial formation process they are axially short.

Fewer theoretical works considered higher-frequency effects, involving possible wave emission. One of the earliest of them, by Berk and Sudan [B8] considered the case when ring precession is coupled to compressional Alfven waves in plasma. Gerver and Sudan [B10] used the WKB approximation to study stability of a field-reversed ion layer in the slab geometry. Because of the approximation used, the results were mostly applicable to short-scale wave packets in the layer and were only marginally relevant for wavelengths comparable with the layer thickness. In the latter case, the estimate for the largest growth rate was $\gamma \propto V_A / a$, where V_A is the Alfven velocity, and a is the layer thickness. Friedman, Sudan, and Denavit [B11] used a linearized 3D hybrid code to study ion ring linear stability. The most stable ring configuration they found was a moderately thick ring with aspect ratio on the order of 4:1. For such a ring, the l=1 MHD precession mode was observed to be stable. The l=1 tilt mode as well as radial and axial kink modes (l=2) and the l=3 were found to be unstable. The structure of various unstable modes was found to range from near rigid to very complicated. Omelchenko and Sudan [B12] used a 3D hybrid code, in which both the ring ions and the background plasma ions were treated as particles, to study formation and stability of ion rings. The simulations used only a small number of azimuthal modes and did not reveal noticeable ring instability.

A number of theoretical works were devoted to the study of the stabilizing effect of an energetic ion component for magnetic confinement configurations. It has been shown that ion rings could stabilize low-frequency modes of compact torus configurations (Sudan and Kaw [B13]; Litwin, Sudan, and Turnbull [B14]; Turnbull and Sudan [B15]; Litwin and Sudan [B16]). In one of the most recent works, Barnes and Milroy [B17] demonstrated that ion beam injection provides an optimal way of adding the required kinetic effects to maintain a stable FRC.

In this work, we move the focus of the consideration towards high-frequency effects. We present results of the (r,θ) simulations of the ring and the background plasma dynamics using the code FIRE. FIRE is a 2-D hybrid, time-dependent, Particle-in-Cell (PIC) code,

developed in our Laboratory by Dr. Omelchenko and described in detail in [B18]. In FIRE, the ion beam is injected into partially ionized gas, which maintains charge-neutrality throughout the simulation. The ion beam and the background plasma ions are treated as macro-particles, and the plasma electrons as a drifting, cold, massless fluid. The massive background neutral component is assumed motionless and experiences no further ionization during the simulation, contributing only to the electron collisions. All processes are assumed slow in comparison with the speed of light, which is reflected in neglecting of the displacement current in Maxwell equations. The field solver uses a time and space centered finite-difference scheme. The particle advance algorithm uses a standard leap-frog scheme. The code is written in C and runs on a HP J282 workstation as well as on a fast PC under Linux.

The simulation results presented here emphasize the role of the interaction between an ion ring and magnetosonic waves. Let us illustrate that role by considering linear stability of a thin ion ring layer circulating in the magnetic field. We will only consider perturbations of much longer wavelength than the layer thickness, but much shorter than the Larmor radius of the beam. The latter condition allows us to use slab geometry for the beam (Figure B1). The mechanism of the instability is simple: perturbations of the beam density result in the emission of magnetosonic waves, which, in turn, leads to further growth of the perturbations. If $V(x,t)$ is the beam azimuthal velocity and $N(x,t)$ is the beam density per unit length (the coordinate x is looking in the azimuthal direction), then the equations for the beam dynamics and the fields are

$$M(V_t^{'} + VV_x^{'}) = eE_x,\ N_t^{'} + (NV)_x^{'} = 0,\ B|_{y=+0} - B|_{y=-0} = 4\pi I / c,\ I = eNV,\ B_t^{'} = -c\nabla \times E.$$

Perturbations of the beam current I will generate magnetosonic waves propagating away from the beam: $\delta B \propto \exp(ikx + i\kappa|y| - iwt)$, where $w = V_A(k^2 + \kappa^2)^{1/2}$, and $V_A = B/(4\pi M n_p)^{1/2}$. Linearized equations for the beam and the fields are

$$M(ikV - iw)\delta V = e\delta E_x,\ (ikV - iw)\delta N + ikN\delta V = 0,$$

$$\delta B|_{y=\pm 0} = \pm 2\pi / c \cdot (N\delta V + V\delta N),\ -iw\delta B = -c\nabla \times \delta E$$

Let us consider the strongly supersonic limit $V >> V_A$. In that limiting case,

$$-iw\delta B|_{y=\pm 0} = -c\nabla \times \delta E \approx \pm i\kappa c\delta E_x,\ \kappa \approx w/V_A$$

and we arrive at the dispersion relationship

$$(w-kV)^2 = -i2\pi e^2 NwV_A / Mc^2$$

Assuming $w = kV + \delta w$, $\delta w << kV$, we find

$$\delta w = i^{1/2}(2\pi e^2 NkVV_A / Mc^2)^{1/2},$$

which corresponds to the growth rate

$$\tau^{-1} = w_{Bi} 2^{-3/2} \cdot (\delta B / B)^{1/2} \cdot (c / w_{pi}\lambda)^{1/2},\ w_{pi} = (4\pi e^2 n_p / M)^{1/2},\ k = 2\pi/\lambda,\ \delta B = 4\pi I / c$$

Figure B2 shows simulation results illustrating different stages of this instability in a radially thin ring, with the magnetic field reversal factor $\delta = B_{ring} / B_{external} \approx 0.2$ and Alfven Mach number $M_A = V_\theta / V_A \approx 2$ (Case 1). One can see that, in contrast with the approximations used in earlier ion ring stability theories, the dominating modes are the high-order ones: $l = 10..20$. As the instability develops, ring particles lose a large fraction of their energy and the ring spreads and fills in toward the axis as particle Larmor radii decrease.

We have performed a series of simulations to find the parameters affecting the growth rates as well as the nonlinear stage of the instability. In accordance with the simple theory presented above, the important parameters that control ring stability were found to be the azimuthal ion speed/Alfven speed ratio M_A and the ring field reversal factor $\delta = B_{ring} / B_{external}$. Rings with orbital velocity much larger than the plasma Alfven

velocity as well as weaker rings with smaller δ were found to have a smaller growth rate and a significantly less disruptive nonlinear stage of the azimuthal instability. Figure B3 shows ring particle distribution and the magnetic field profile for (M_A=10, $\delta = 0.2$, Case 2), (M_A=10, $\delta = 0.4$, Case 3), and (M_A=2, $\delta = 0.4$, Case 4). One can see transition from relatively stable behavior to violent instability as δ goes up and M_A goes down. Figure B4 shows ring evolution and sample orbits for the case M_A=2, $\delta = 0.4$ and times t=100ns, t=500ns, t=1000ns. One can see drastic de-centering of the orbits and ion energy decrease as a result of the instability.

Plasma resistivity was found to be another important parameter. It affects the excitation and propagation of Alfven waves, thus affecting the magnetic perturbation felt by the ring and determining its dynamics. Figure B5 shows ring azimuthal instability for different background plasma conductivity: $\sigma = 10^{11}$ s^{-1} (Case 5) and $\sigma = 10^{12}$ s^{-1} (Case 6). One can see how the character of the interaction between beam particles and plasma determines the wavelength of the instability. In the more resistive regime, the interaction is mostly limited by diffusion of the magnetic field, which results in small-scale rippling of the beam in the azimuthal direction and no substantial Alfven dynamics of the magnetic field. In the more conductive regime, the interaction is mostly limited by the Alfven propagation, which makes the instability wavelength determined by the geometric effects and comparable with the ring radius. In this case, the instability is accompanied by strong Alfven wave radiation that becomes the main channel through which the beam loses its energy.

Another factor affecting stability was found to be the ring geometry. For radially thick rings, simulations showed less violent instability. We have also found that ring distributions that are less highly singular but rather are quasi-thermal, show much greater stability against energy loss than the standard FIREX rings. Such distributions would be produced by orbits that do not symmetrically encircle the ring axis, for instance rings in which the injected ions have larmor radius in the initial field that is half or less of the ring radius. These rings show only very little initial instability and reach a steady state which is only slightly spread from the initial state, with little ring energy loss. Figure B5 also compares ring dynamics of a singular ring with that of a somewhat “thermalized” ring, with Larmor radius equal to one half of the ring radius (Case 7).

The table below summarizes the results of the simulations:

Case number	Dominating Modes	Growth Rate	Nonlinear stage
1	*l=10..20*	$10^8\ s^{-1}$	*Extremely violent*
2	*l=2*	$3\ 10^5\ s^{-1}$	*Medium*
3	*l=2*	$5\ 10^6\ s^{-1}$	*Medium*
4	*l=2,4*	$1.2\ 10^7\ s^{-1}$	*Violent*
5	*l=7..9*	$10^7\ s^{-1}$	*Mild*
6	*l=4*	$1.1\ 10^7\ s^{-1}$	*Violent*
7	*l=2,4*	$4\ 10^6\ s^{-1}$	*Mild*

We have performed a set of simulations, to determine the scaling features of the instability growth rate as a function of the perturbation wavelength as well as the plasma and the ring parameters. Figure B6 shows the dynamics of the modes for M_A=1, $\delta = 0.3$ (top), M_A=5, $\delta = 0.3$ (middle, base case), and M_A=10, $\delta = 0.3$ (bottom). For low mode numbers *m*, the growth rate increases almost linearly with *m*. At M_A>>1, the growth rate is roughly proportional to $M_A^{-0.5}$, and strongly peaks at M_A=1. Figure B7 shows the dynamics of the modes for M_A=5, $\delta = 0.1$ (top), M_A=5, $\delta = 0.3$ (middle, base case), and for M_A=5, $\delta = 0.3$, and a four times radially thicker ring (bottom). One can see an approximately linear increase of the growth rate with the ring strength, and its peaking at the wavelength equal to the ring's radial thickness. Figure B8 shows the dynamics of the modes for two highly resistive cases: M_A=5, $\delta = 0.3$, $\sigma = 2*10^{11}\ s^{-1}$ (top), and M_A=5, $\delta = 0.3$, $\sigma = 6*10^{11}\ s^{-1}$ (bottom). The growth rate peaks at the wavelength 3-4 times larger than the ring's radial thickness and increases roughly as $\sigma^{-0.5}$ as the plasma resistivity increases.

The described (*r,θ*) 2D simulations do not address fully three-dimensional (*r,z,θ*) effects that can come into play when the ring axial thickness becomes comparable with its radius: excitation of the oblique Alfven and whistler waves and the effect of the betatron motion of the ring particles. Our next step will be performing a series of three-

dimensional runs with codes FLAME, and FLEX3D (recently provided to us by University of Washington), for analyzing such effects. Adequate modeling will require a large number of modes for the code to be capable of resolving the small-scale structure that we now know from the 2D simulations to play an important role in the ring evolution.

References.

[B1] J. Finn, R.N. Sudan, Nucl. Fusion 22, 1443 (1982)

[B2] R.N. Sudan, M.N. Rosenbluth, Phys. Rev. Lett. 36, 972 (1976)

[B3] R.N. Sudan, M.N. Rosenbluth, Phys. Fluids 22, 282 (1979)

[B4] R.V. Lovelace, Phys. Rev. Lett. 35, 162 (1975)

[B5] R.V. Lovelace, Phys. Fluids 19, 723 (1976)

[B6] R.V. Lovelace, Phys. Fluids 21, 1389 (1978)

[B7] H.P. Furth, Phys. Fluids 8, 2020 (1965)

[B8] H.L. Berk, R.N. Sudan, Plasma Phys. 6, 413 (1971)

[B9] C.B. Rutchi, R.V. Lovelace, Phys. Fluids 27, 1789 (1984)

[B10] M.J. Gerver, R.N. Sudan, Phys. Fluids 22, 686 (1979)

[B11] A.Friedman, R.N. Sudan, J. Denavit, Plasma Phys. 29, 3317 (1986)

[B12] Yu. A. Omelchenko, R.N. Sudan, J. Comp. Phys. 133, 146 (1997)

[B13] R.N. Sudan, P.K. Kaw, Phys. Rev. Lett. 47, 575 (1981)

[B14] C. Litwin, R.N. Sudan, A.D. Turnbull, Phys. Fluids 27, 2791 (1984)

[B15] A.D. Turnbull, R.N. Sudan, Phys. Fluids 29, 1923 (1986)

[B16] C. Litwin, R.N. Sudan, Phys. Fluids 31, 423 (1988)

[B17] D.C. Barnes, R.D. Milroy, Phys. Fluids B3, 2609 (1991)

[B18] Yu. A. Omelchenko and R. N. Sudan, Phys. Plasmas 2, 2773 (1995).

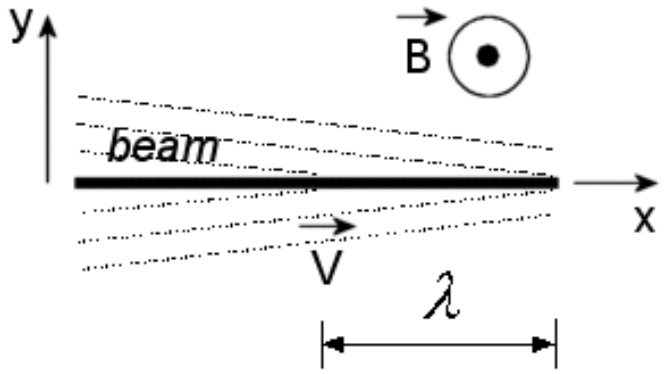

Figure B1. Slab geometry approximation for the linear stability theory.

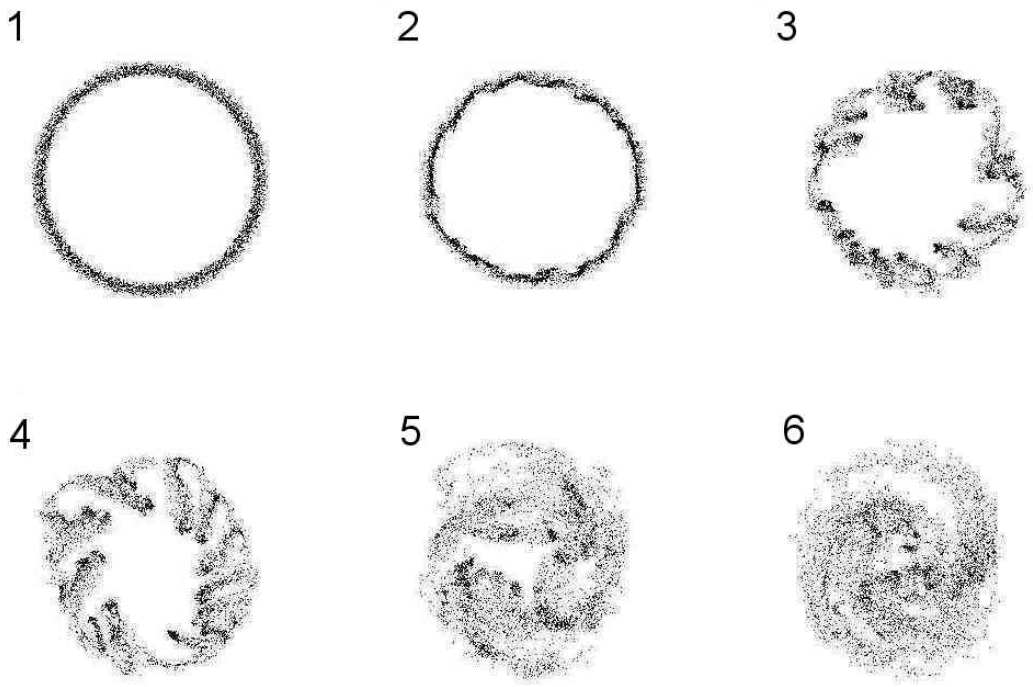

Figure B2. Stages of azimuthal instability of a radially thin ring

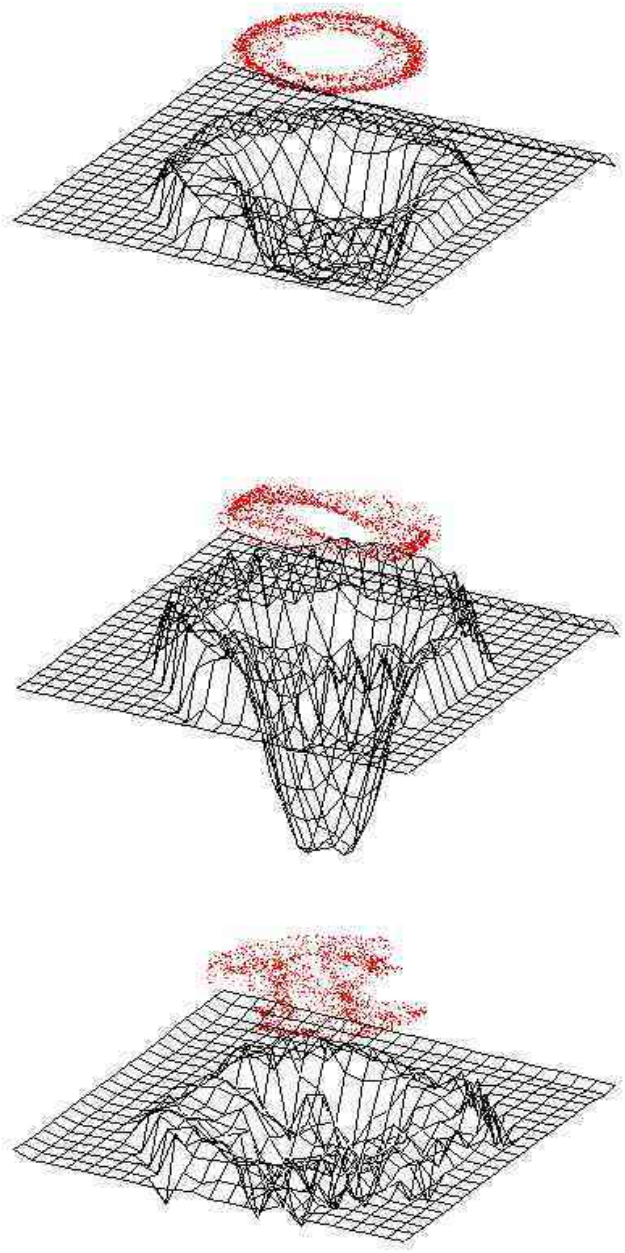

Figure B3. Ring particle distribution and the magnetic field profile at $t = 1\mu s$ for M_A=10, $\delta = 0.2$ (top), M_A=10, $\delta = 0.4$ (middle), and M_A=2, $\delta = 0.4$ (bottom). One can see transition from relatively stable behavior to violent instability as δ goes up and M_A goes down.

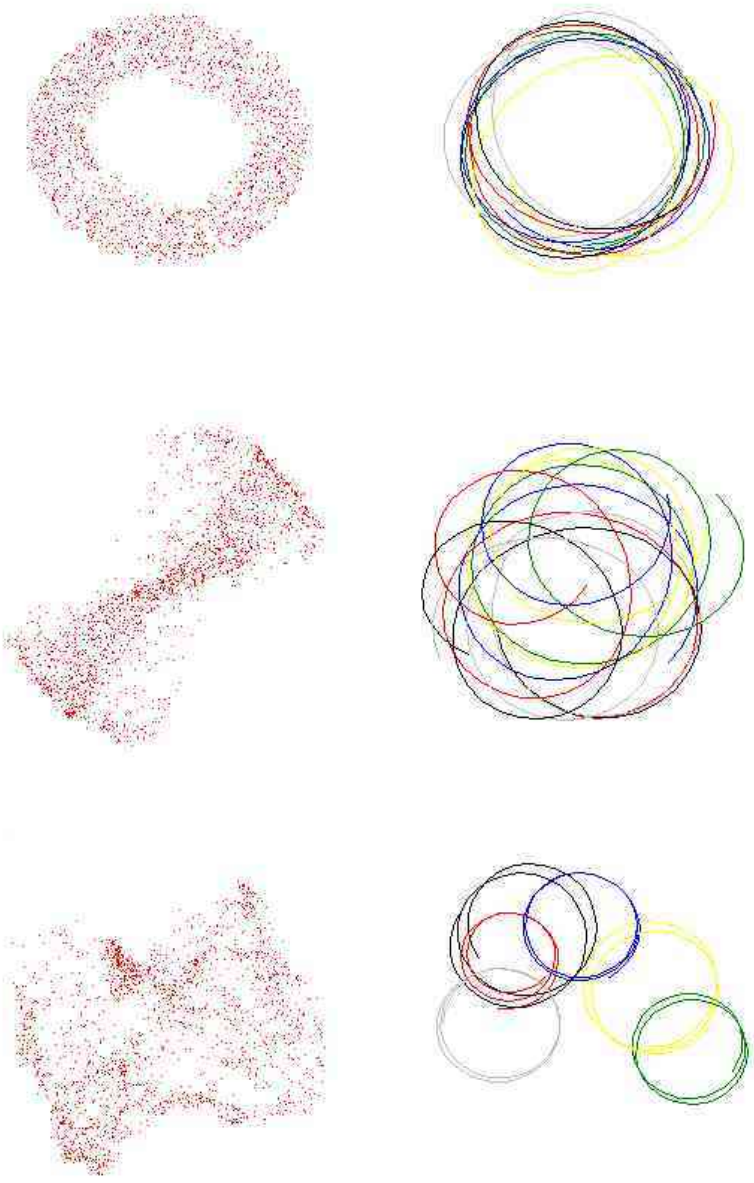

Figure B4. Ring evolution and sample for M_A=2, $\delta = 0.4$ and times t=100ns (top), t=500ns (middle), t=1000ns (bottom). One can see de-centering of the orbits and ion energy decrease as a result of the instability.

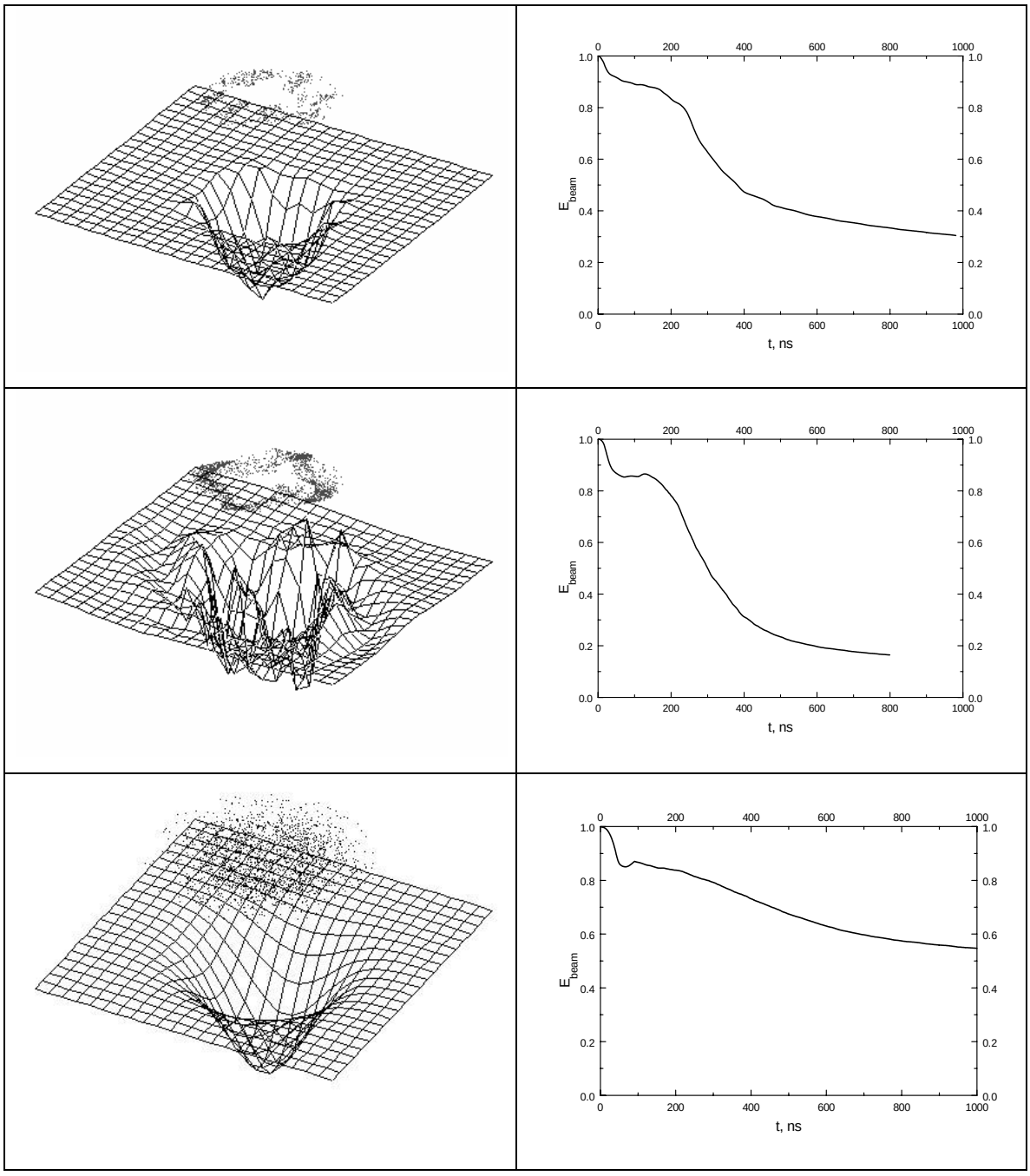

Figure B5. Ring density, magnetic field distribution, and beam energy losses for $\sigma = 10^{11}$ s^{-1} (top), $\sigma = 10^{12}$ s^{-1} (middle), and a "thermalized" ring, with $\sigma = 10^{12}$ s^{-1}, and Larmor radius equal to one half of the ring radius (bottom). The "thermalized" ring shows little initial instability and reaches a steady state which is only slightly spread from the initial state, with little ring energy loss.

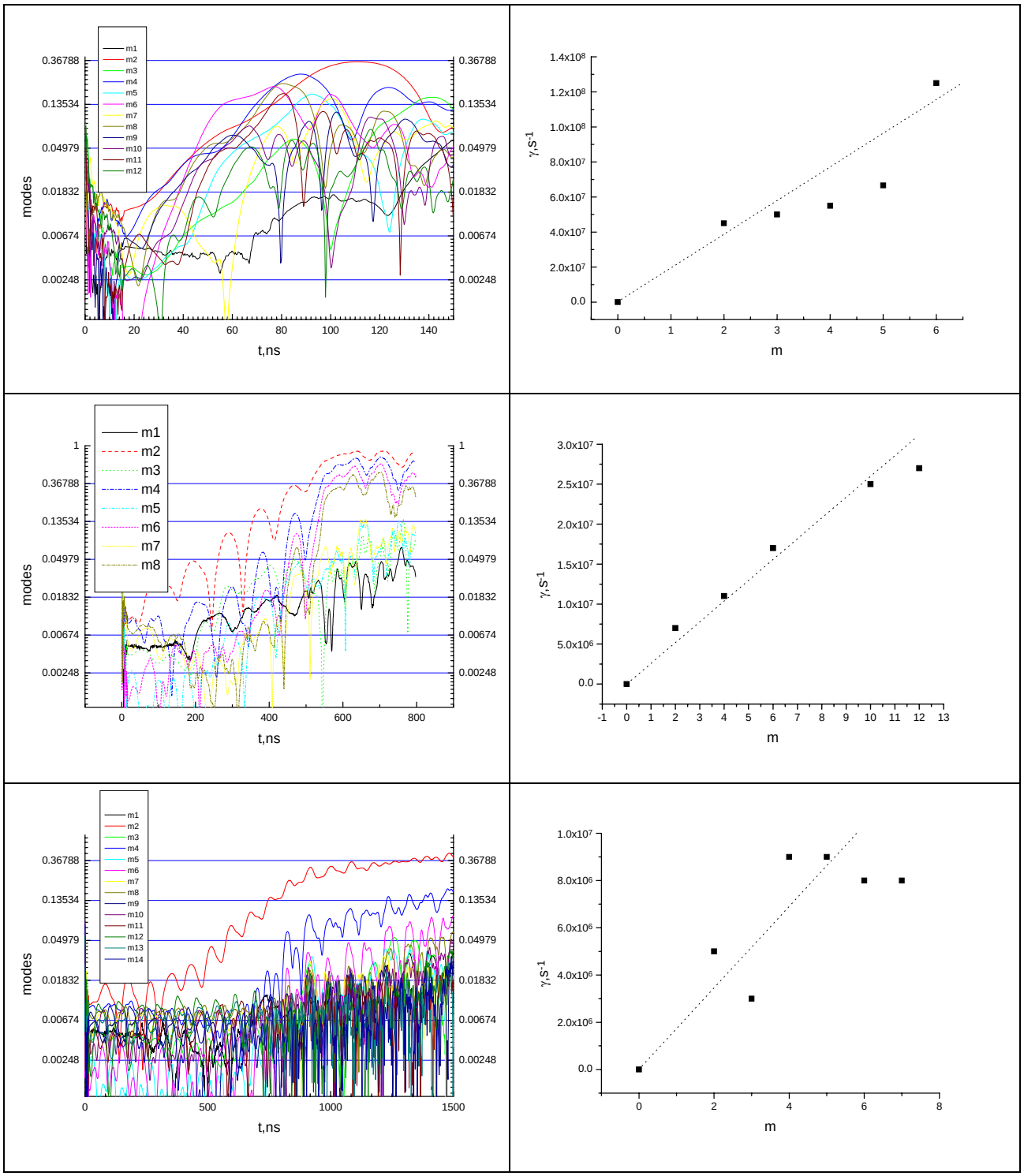

Figure B6. The dynamics of the modes for M_A=1, $\delta = 0.3$ (top), M_A=5, $\delta = 0.3$ (middle, base case), and M_A=10, $\delta = 0.3$ (bottom).

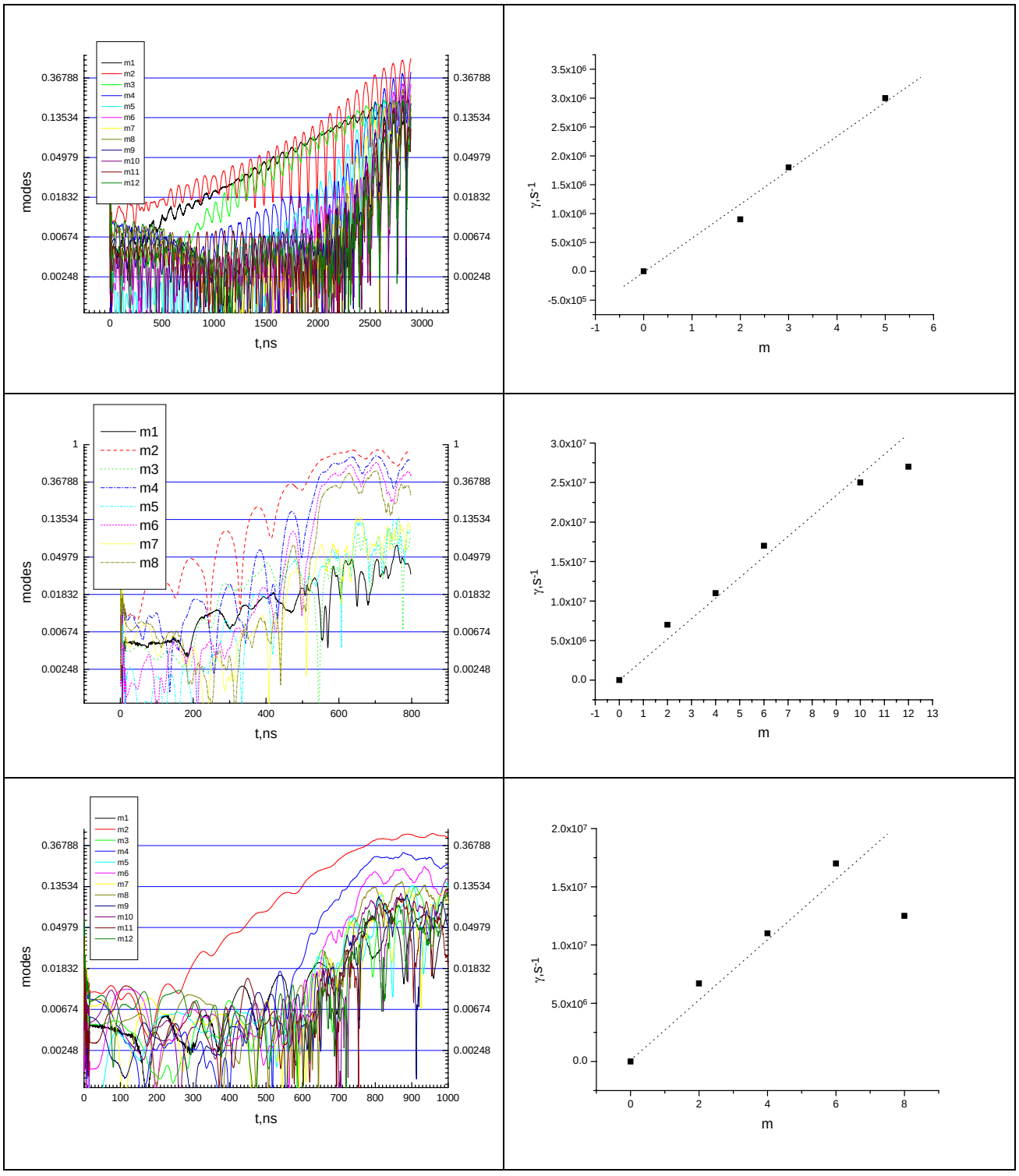

Figure B7. The dynamics of the modes for M_A=5, $\delta = 0.1$ (top), M_A=5, $\delta = 0.3$ (middle, base case), and M_A=5, $\delta = 0.3$, and a four times radially thicker ring (bottom).

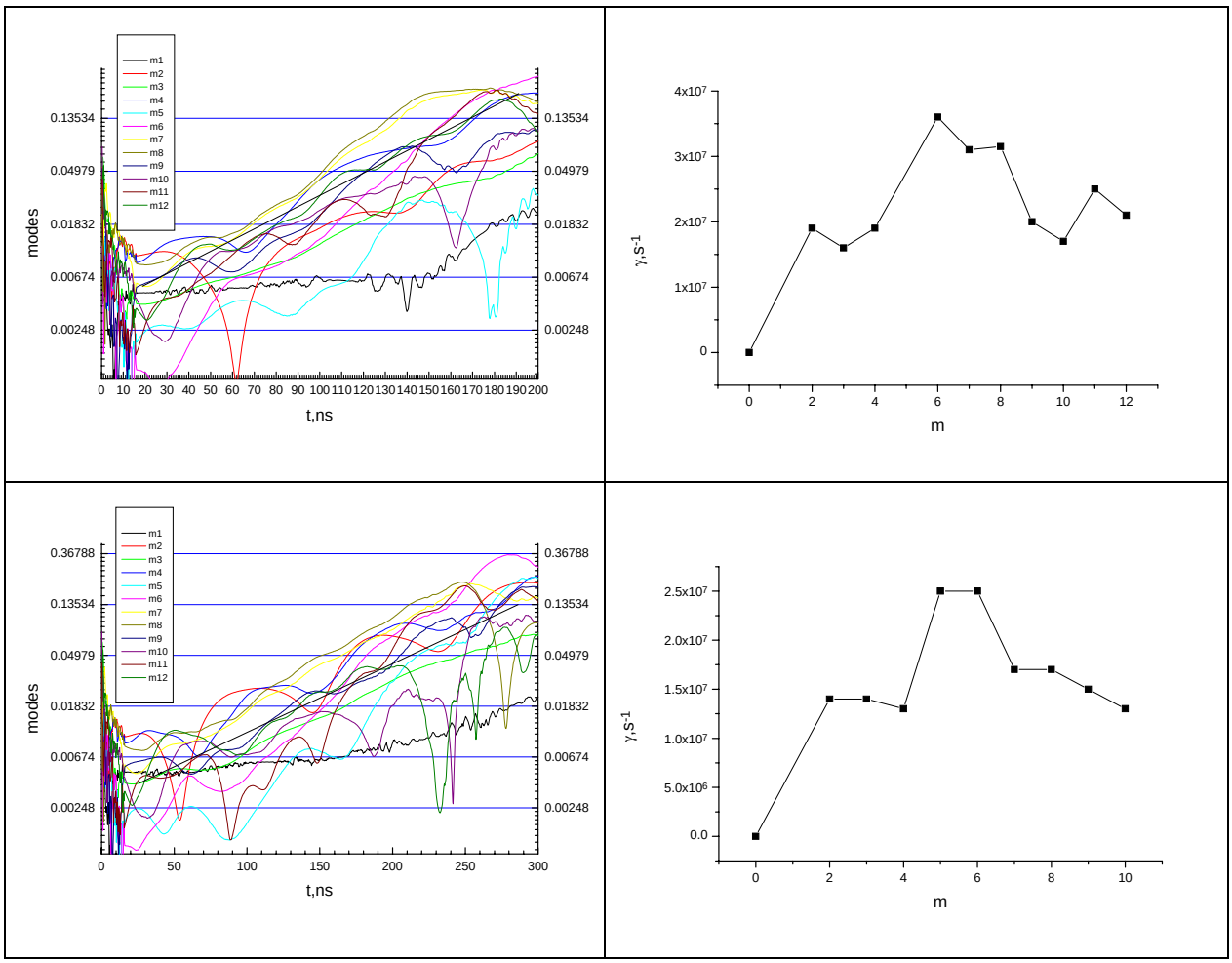

Figure B8. The dynamics of the modes for two highly resistive cases: M_A=5, $\delta = 0.3$, $\sigma = 2*10^{11}$ s^{-1} (top), and M_A=5, $\delta = 0.3$, $\sigma = 6*10^{11}$ s^{-1} (bottom).